DYNAMIC RESPONSE OF OFFSHORE STRUCTURES

Annual Technical Report
Research Supported by the U.S. Geological Survey,
Department of the Interior

Under USGS Contract No. 14-08-0001-20665
Period of Contract and Report:
September 1, 1981 to August 31, 1982
Contract Amount $112,000

Prof. J. Kim Vandiver
Massachusetts Institute of Technology
Room 5-222
Cambridge, Massachusetts 02139

August 31, 1982

Introduction

The research described in this report is primarily directed at measuring and predicting the dynamic response properties of offshore structures. This report covers the most recent year in a project which has spanned five years of effort. In the recent year, the research has focussed on the dynamic response of offshore platforms to wave excitation and on the vibration responses of long flexible cylinders, such as cables and marine risers, to vortex shedding.

The format of this report is a sequence of professional papers which have been published or presented in the last year. To aid the reader in assessing the content of these papers, an abstract of each paper is presented immediately following the Acknowledgements section.

Acknowledgements

The author wishes to thank Mr. John Gregory, the U.S.G.S. program manager for his thoughtfulness and support over the several years of this research program. This program has supported many graduate students in Ocean Engineering at M.I.T. The U.S.G.S. Branch of Marine Oil and Gas Operations and more recently the Minerals Management Service research program for activities on the Outer Continental Shelf is one of the few sources in this country of university research support in ocean engineering. This program has made a substantial and identifiable impact on the preparation and training of engineers going to industry. Without such support, the future supply of adequately prepared ocean engineers is in jeopardy.

The SENSITIVITY OF FATIGUE LIFE ESTIMATES TO VARIATIONS IN STRUCTURAL NATURAL PERIODS, MODAL DAMPING RATIOS, AND DIRECTIONAL SPREADING OF THE SEAS

by Prof. J. Kim Vandiver

Abstract

Structures with natural periods in the range of four to ten seconds will be susceptible to hi cycle-low stress fatigue damage due to resonant structural response in commonly occurring sea conditions. It is shown that the computed fatigue life of a structure is extremely sensitive to the designer's estimate of the natural period - varying by as much as the natural period raised to the minus eighteenth power. A 10% error in the estimated natural period may result in a factor of six error in computed fatigue life. Damping ratio estimates are very prone to error. Fatigue life is shown to vary as approximately the square of the estimated damping ratio.

A MATHEMATICAL BASIS FOR THE RANDOM DECREMENT VIBRATION SIGNATURE ANALYSIS TECHNIQUE

by Prof. J. Kim Vandiver, A.B. Dunwoody, R.B. Campbell, and M.F. Cook, MIT

The mathematical basis for the Random Decrement Technique of vibration signature analysis is established. The general relationship between the autocorrelation function of a random process and the Randomdec signature is derived. For the particular case of a linear time invariant system excited by a zero-mean, stationary, Gaussian random process, a Randomdec signature of the output is shown to be proportional to the autocorrelation of the output. Example Randomdec signatures are computed from acceleration response time histories from an offshore platform.

This paper was published in the Journal of Mechanical Design, 1982.

THE SENSITIVITY OF FATIGUE LIFE ESTIMATES TO VARIATIONS IN STRUCTURAL NATURAL PERIODS, MODAL DAMPING RATIOS, AND DIRECTIONAL SPREADING OF THE SEAS

by J. Kim Vandiver
Associate Professor of Ocean Engineering
Massachusetts Institute of Technology
Cambridge, Massachusetts

SUMMARY

Structures with natural periods in the range of four to ten seconds will be susceptible to hi cycle-low stress fatigue damage due to resonant structural response in commonly occurring sea conditions. It is shown that the computed fatigue life of a structure is extremely sensitive to the designer's estimate of the natural period - varying by as much as the natural period raised to the minus eighteenth power. A 10% error in the estimated natural period may result in a factor of six error in computed fatigue life. Damping ratio estimates are very prone to error. Fatigue life is shown to vary as approximately the square of the estimated damping ratio.

It is known that directional spreading of wave energy has a mitigating effect on fatigue damage. This is quantified in a parameter variation study. A new wave spreading model is proposed that as a result of informal communication is already being adopted by oceanographers for the description of observed sea states.

NOMENCLATURE

A	constant of proportionality
b, c	constants of the SN fatigue life curve
C_x	factor which accounts for spreading of waves
$D(\theta)$	spreading function
E	Young's modulus
e	eccentricity
$F(\ )$	rate of fatigue damage accumulation
g	acceleration of gravity
$H_{\eta s}(\ )$	stress transfer function
K_x	modal stiffness
m_x, M_x	modal mass
N	number of cycles
$R_r(\omega)$	radiation damping
$R_T(\omega)$	total damping
$S_{max}(\omega)$	Krogstad upper bound wave spectrum
$S_\eta(\omega)$	point wave amplitude spectrum
$S_\eta(\omega,\theta)$	directional wave amplitude spectrum
$S_s(\omega)$	stress spectrum
γ	Wirsching correction factor
$\Gamma(\ )$	Gamma function
$\delta(\ )$	Delta function
ν_o^+	average zero upcrossing frequency in Hz
ω	frequency in radians per second
ω_p	frequency of the peak of the wave spectrum
ω_x	natural frequency of mode x
ξ	modal damping ratio
ρ_w	density of water
σ_d^2	mean square dynamic response
σ_q^2	mean square static response
σ_s^2	mean square stress
σ_x^2	mean square deflection for mode x
θ	angle of wave incidence

INTRODUCTION

The purpose of this analysis is to investigate the sensitivity of fatigue life calculations to variations in natural frequencies, modal damping ratios, and directional spreading of the wave spectrum. The results of such an analysis may be used to reveal the extent to which uncertainties in the estimates of such parameters will affect the estimated fatigue life of offshore structures excited by waves.

This analysis does not consider the uncertainties in material properties or the fatigue damage accumulation models themselves. This area is left to the materials specialists. This study also leaves to others the analysis of the uncertainties associated with the description of the sea states to be encountered by the structure.

The influence of wave spreading is considered for a given wave spectrum, and a new single parameter spreading function is introduced. A structural model and its idealization are selected and one method of wave force estimation is used. The wave force model assumes that drag exciting forces are negligible and that finite wave amplitude effects are not significant. In any specific application these two assumptions can and should be checked. However, for the computation of high cycle-low stress fatigue damage on large deepwater structures these assumptions are usually valid.

For the case that drag excitation cannot be neglected, the results of some recent research at MIT are mentioned. With these results the second order statistics of response may be estimated including non-linear drag exciting forces.

The exclusion of finite wave amplitude effects is probably valid for large deepwater structures in low to moderate seas, which contribute the most to high cycle-low stress fatigue damage. The governing non-dimensional parameter is likely the ratio of wave amplitude to water depth for slender bottom mounted structures. However, this is an area in which some additional research is justified.

THE FATIGUE ACCUMULATION MODEL

For the purpose of this study the assumed form of the fatigue damage accumulation model is that used by Crandall and Mark, 1973, when the stress history is assumed to be described by a narrow band random process. This formulation implicitly assumes a Palgren-Miner rule for damage accumulation. Equation (1) describes the mean rate of accumulation of the fatigue damage index for a location β in the structure due to a directionally spread random sea with mean direction θ_o.

$$F(\beta,\theta_o) = \frac{\nu_o^+}{c} (2^3\sigma_s^2)^{b/2}\Gamma(1+b/2) \qquad (1)$$

$F(\beta,\theta_o)$ = the mean rate of accumulation of the fatigue damage index at position β, due to a wave field with nominal direction of propagation θ_o.

σ_s^2 = the mean square stress at position β.

ν_o^+ = the average zero upcrossing rate of the stress process in Hz.

$\Gamma( )$ = the Gamma function

b, c = constants of the S-N fatigue curve of the material as defined by Equation (2), where N is the number of cycles to failure with a stress range S.

$$NS^b = c \qquad (2)$$

This model, and the material constants b and c are assumed fixed. This leaves ν_o^+ and σ_s^2 as variables to be considered.

ν_o^+ depends on the frequency content of the wave spectrum as well as the wave amplitude to stress transfer function for the structure. If the structure has no natural frequencies in the region of significant wave force, then the response is generally quasi-static in nature and ν_o^+ is governed primarily by the frequency content of the wave spectrum. When the stress is primarily due to the response at a natural frequency, then ν_o^+ is strongly dependent on the natural frequency.

In both of the cases the response is approximately narrow band and the use of Equation (1) is appropriate. In the case that the response spectrum is composed of significant quasi-static and dynamic response peaks then it may be necessary to modify the above equation. One such modification is the use of a final correction factor, such as proposed by Wirsching, 1979, in which rain flow cycle counting procedures are used to obtain a correction factor to account for

broad band stress spectra. The use of such a correction factor is assumed to be valid here.

The task is then to investigate the sensitivity of the mean square stress σ_s^2 and the average zero upcrossing frequency, ν_s^+, to variations in structural natural frequency and modal damping.

QUASI-STATIC AND DYNAMIC CONTRIBUTIONS TO MEAN SQUARE STRESS

In this study, it is assumed that mean square stress at a point in a structure may be approximated by the sum of a quasi-static component due to low frequency waves and a dynamic component due to the damping controlled response of natural modes of the structure excited by the higher frequency components of the wave spectrum. This is comparable to the procedure of supplementing a full static finite element solution with the dynamic contributions of the significantly responding natural modes.

In this analysis the response is assumed to be quasi-static up to within one half power bandwidth of the lowest natural frequency of the structure. Furthermore, the lowest natural frequency is not allowed to be less than the peak frequency of the wave spectrum. The computation of the mean square stress is then accomplished by summing the mean square static component with the dynamic contributions.

The quasi-static component of stress at a specific location is assumed uncorrelated with the dynamic components. However, for closely spaced natural frequencies, correlation between the stress components of two or more natural modes may have to be considered. The partitioning of static and dynamic contributions to the total stress is illustrated in Figure 1, a stress spectrum with a quasi-static stiffness controlled peak and one damping controlled resonant peak.

The quasi-static mean square stress σ_q^2, is obtained by integrating the stress spectrum up to $\omega_c = \omega_1(1-2\xi)$ where ω_1 is the lowest natural frequency and ξ is the modal damping ratio of that mode.

$$\sigma_q^2 = \int_0^{\omega_c} S_s(\omega)d\omega \tag{3}$$

where $S_s(\omega)$ is the stress spectrum.

For a complex structure σ_q^2 could be computed from a static finite element model. The calculation of the static mean square stress may include the influence of drag forces, in which an equivalent linearization procedure has been used or a more accurate non-linear wave force spectrum has been computed using the results of Dunwoody, 1981. Drag forces are neglected in the examples of this report.

This static approximation does neglect any dynamic amplification at frequencies below the cut off.

The average zero upcrossing frequency of the static component of stress is computed from the zero and second order moments of the truncated spectrum.

$$\omega_q^2 = \frac{\int_0^{\omega_c} \omega^2 S_s(\omega)\, d\omega}{\int_0^{\omega_c} S_s(\omega)\, d\omega} = \frac{1}{\sigma_q^2} \int_0^{\omega_c} \omega^2 S_s(\omega)\, d\omega \tag{4}$$

σ_q^2 and ω_q^2 for the example calculations are assumed to be provided for the purposes of the remaining discussions.

The dynamic or damping controlled contributions to the mean square stress are computed separately. The area under the stress spectrum as shown in Figure 1 for $\omega_1(1-2\xi) \leq \omega \leq \omega_1(1+2\xi)$ is defined as the mean square dynamic response for mode 1.

There may be more than one mode which has significant dynamic response. The dynamic contribution of each must be separately evaluated. In this report the mean square dynamic response of all significant modes will be computed using techniques described by Vandiver, 1980. In this reference it is shown that the mean square dynamic response of an individual mode x is given by:

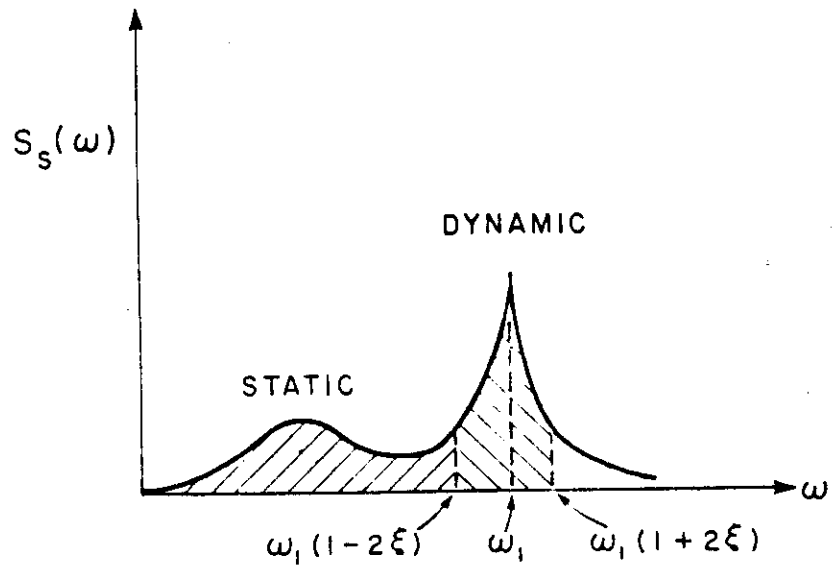

Figure 1. The partitioning of stress into static and dynamic components.

$$\sigma_x^2 = \frac{2.5C_x\rho_w g^3}{m_x\omega_x^5} \; S_\eta(\omega_x) \; \frac{R_r(\omega_x)}{R_T(\omega_x)} \tag{5}$$

where:

σ_x^2: mean square dynamic deflection of the xth normal mode

m_x: modal mass

ω_x: natural frequency

$S_\eta(\omega_x)$: wave amplitude spectrum evaluated at ω_x

ρ_w: density of water

g: acceleration of gravity

$\frac{R_r(\omega_x)}{R_T(\omega_x)}$: ratio of the radiation (wave making) to total modal damping evaluated at ω_x

This result is valid for lightly damped modes excited by linear wave forces. The constant C_x depends on structural geometry and wave spreading and is assumed to have been evaluated as as described in Vandiver, 1980. Through knowledge of the mode shape and structural details, the mean square stress at a specific location can be related to σ_x^2.

If there is more than one mode contributing in a significant way to the dynamic response then the stress at any specific location in the structure will depend upon the superposition of stresses from each mode. If the natural frequencies of each responding mode are different, (at least so that their damping controlled peaks as defined in Figure 1 do not overlap), then the stresses contributed by each may be assumed to be uncorrelated and the total mean square stress will be the sum of the mean square stresses due to each individual mode. This is a consequence of the fact that waves and hence wave forces of different frequencies are uncorrelated. If two peaks overlap then the correlation between stress components must be included.

The mean zero upcrossing frequency for mode x is simply $\omega_x/2\pi$. The mean upcrossing frequency for the combined static and dynamic stress history may be computed as a weighted sum of the

individual contributions as shown below for a system with a single dynamic component.

$$\nu_o^+ (H_z) = \frac{1}{2\pi}\left[\frac{\omega_q^2\sigma_q^2 + \omega_1^2\sigma_{d1}^2}{\sigma_q^2 + \sigma_{d1}^2}\right]^{1/2} \tag{6}$$

where ω_q^2 and σ_q^2 reflect the static response and ω_1^2 and σ_{d1}^2 are the natural frequency and mean square dynamic stress contributed by mode 1.

THE EFFECT OF NATURAL FREQUENCY ON FATIGUE

If the fundamental flexural natural period of a steel jacket structure was taken to be 3.5 seconds for the purpose of fatigue life computation, and the as-installed natural period turned out to be 4.0 seconds, how much would the estimated fatigue life be reduced? Recalling equation (1) and adding γ, a Wirsching type correction factor to account for broadbanded spectral effects, yields

$$F = \gamma\frac{\nu_o^+}{c}(2^3\sigma_s^2)^{b/2}\Gamma(1 + b/2) \tag{7}$$

Assuming that wave spreading effects have been taken into consideration, then a variation in the estimated natural period of a mode will influence three parameters in the above equation: γ, ν_o^+, and σ_s^2. σ_s^2 will change because its dynamic component will change. This is because the wave spectrum is a rapidly changing function of frequency, and as can be seen in Equation 4, the mean square dynamic response is proportional to the wave spectrum divided by the natural frequency raised to the fifth power. ν_o^+ will change as can be seen in Equation 6 because it depends on the natural frequency as well as on the mean square dynamic stress; γ may change because the broadbandedness of the stress spectrum may change. If an asterisk is used to denote the result with a shifted natural frequency, then the ratio of fatigue damage between two cases may be expressed as:

$$\frac{F^*}{F} = \frac{\gamma^*}{\gamma}\left(\frac{\nu_o^{+*}}{\nu_o^+}\right)\left(\frac{\sigma_s^{2*}}{\sigma_s^2}\right)^{b/2} \tag{8}$$

The two extreme cases are simple to evaluate. The first is when the estimated and actual natural periods are so short that the dynamic component of σ_s^2 is negligible. This is true for most structures when the lowest natural frequency corresponds to a period of 2.4 seconds or less. In this case $F^*/F = 1.0$.

The more interesting extreme is when σ_{d1}^2, the dynamic component of stress of a single natural mode is assumed to be much larger than the static component. This may not always be the case, but provides a useful upper bound on the variation of fatigue with natural frequency. One way to estimate this case is through the ratio of fatigue damage at two different natural frequencies.

$$\frac{F^*}{F} = \frac{\nu_o^{+*}}{\nu_o^+}\left(\frac{\sigma^*_{d1}}{\sigma_{d1}}\right)^b = \frac{\omega_1^*}{\omega_1}\left(\frac{\sigma_{d1}^*}{\sigma_{d1}}\right)^b \tag{9}$$

Because the process is narrow banded, the Wirsching correction factor reduces to 1.0 for both cases, and the upcrossing frequency reduces to the natural frequency divided by 2π.

$$\nu_o^+ = \frac{\omega_1}{2\pi} \tag{10}$$

The only remaining step is to evaluate the frequency dependence of σ_{d1}^2, the mean square stress from dynamic response of the mode. This is quite easy and may be estimated directly from Equation (5), with one minor modification. In normal mode formulations, the product of the modal mass and the natural frequency squared is simply the modal stiffness.

$$M_1\omega_1^2 = K_1 \tag{11}$$

If the natural frequency varies because the modal stiffness is different than expected then the effect on mean square stress should be evaluated using equation (5). However, if the modal mass varies, then the effect on mean square stress should be evaluated after substituting Equation (11) into Equation (5), as follows.

$$\sigma_1^2 = \frac{2.5C_1\rho_w g^3}{K_1\omega_1^3} S_\eta(\omega_1) \frac{R_r(\omega_1)}{R_T(\omega_1)} \tag{12}$$

If it is assumed for small variations in natural frequency that the ratio between mean square modal deflection and mean square stress at a location of concern remains constant, then the frequency dependence of the mean square stress is the same as that for mean square deflection as given in Equations (5) or (12). This is essentially an assumption that the mode shape does not change, which is not true, but is adequate here for the purpose of a simple check on sensitivity to changes in natural frequency. Therefore stress and deflection may be related as shown.

$$\sigma_{d1}^2 = A^2\sigma_1^2 \tag{13}$$

If there is any substantial wave spreading, such as cosine squared, then C_1 is only weakly dependent on frequency and is assumed not to vary. Similarly the ratio of radiation to total damping is assumed constant in comparison to other sources of variation. Lumping all constant quantities into A^2 in Equation (13), two expressions for σ_{d1}^2 result, depending on whether the source of change was mass or stiffness.

$$\sigma_{d1}^2 = \frac{A^2}{M_1} \frac{S_\eta(\omega_1)}{\omega_1^5} \quad (\text{stiffness changes}) \tag{14}$$

$$\sigma_{d1}^2 = \frac{A^2}{K_1} \frac{S_\eta(\omega_1)}{\omega_1^3} \quad (\text{mass changes}) \tag{15}$$

It remains only to evaluate the frequency dependence of the wave spectrum.

Krogstad, 1979, has presented evidence that wind driven wave spectra may be modeled at frequencies higher than the frequency of the peak in the wave spectrum as given below:

$$S_{max}(f) = 1.62 \times 10^{-3} \; f^{-4.6} \; m^2 - sec \tag{16}$$

This is the upper bound curve for spectral values, but possesses the frequency dependence characteristic of the high frequency side of wind driven wave spectra.

Expressed as a function of ω, Equation (16) takes the form

$$S_{max}(\omega) = \frac{1}{2\pi} \times 1.62 \times 10^{-3} \left(\frac{\omega}{2\pi}\right)^{-4.6} \tag{17}$$

Assuming all of the constants in this spectrum are absorbed into the constant A^2 in Equations (14) or (15) yields

$$\sigma_{d1}^2 = \frac{A^2}{M_1} \frac{1}{\omega_1^{9.6}} \quad (\text{stiffness changes}) \tag{18}$$

$$\sigma_{d1}^2 = \frac{A^2}{K_1} \frac{1}{\omega_1^{7.6}} \quad (\text{mass changes}) \tag{19}$$

Substituting each of these expressions into Equation (9) and setting the slope, b, of the S-N curve equal to 4.1 for welded tubular joints yields

$$\frac{F^*}{F} = \left(\frac{\omega_1^*}{\omega_1}\right)^{-14.6} \quad (\text{mass changes}) \tag{20}$$

$$\frac{F^*}{F} = \left(\frac{\omega_1^*}{\omega_1}\right)^{-18.7} \quad (\text{stiffness changes}) \tag{21}$$

Therefore, if the natural frequency is 10% greater than predicted, then the fatigue life will be increased by a factor of 4.02 or 5.94 depending on the source of the error.

These examples were upper bound situations in which the quasi-static contributions to mean square stress were assumed small. In most cases of practical interest both contributions will be of importance and the sensitivity to natural frequency variation will not be so extreme.

THE EFFECT OF DAMPING ON FATIGUE

A variation in the estimated damping of a normal mode influences the mean square dynamic contribution to the total stress directly, and the average upcrossing frequency indirectly, because of its dependence on the mean square dynamic stress.

To place an upper bound on the significance of an error in the prediction of modal damping an analysis similar to the previous section may be performed. If only the dynamic component of a single mode is presumed to contribute to the total mean square stress, then proceeding as before leads immediately to the following conclusion:

$$\frac{F^*}{F} = \left\{\left(\frac{R_r(\omega_1)}{R_T(\omega_1)}\right)^* \Big/ \left(\frac{R_r(\omega_1)}{R_T(\omega_1)}\right)\right\}^{b/2} \tag{22}$$

All terms involving frequency directly cancel out because the natural frequency does not change in the example.

The method of computing mean square dynamic stress used in this analysis is somewhat unconventional and not widely used in the industry. Therefore, to reflect conventional practice the same upper bound on the sensitivity of fatigue damage calculations to variations in estimated total damping may be expressed as follows:

$$\frac{F^*}{F} = \left(\frac{\xi_T}{\xi_T^*}\right)^{b/2} \tag{23}$$

when ξ_T and ξ_T^* are the estimated and actual total modal damping ratios, which are commonly estimated in the range from 1% to 5%.

It is the position of the author that the uncertainty in estimating the ratio of the radiation to total damping is much less than the uncertainty in estimating the total modal damping itself. Furthermore, the use of Equation (12) leads to estimates of mean square dynamic stress which are bounded because the ratio of radiation to total damping is at most 1.0. No such upper bound exists when conventional methods of computing dynamic response are used.

Furthermore, conventional methods of estimating response require independent estimates of the modal wave force spectrum and the total modal damping. This ignores the fact that the modal radiation damping and the linear modal wave force spectrum are proportional to one another. Thus two sources of uncertainty enter the calculations where only one exists.

For the sake of example, suppose in either formulation the damping is underestimated by a factor of 2.0. This will lead to an overestimate of the fatigue life by a factor of

$$(2)^{b/2} = 4.14 \text{ for } b = 4.1 \tag{24}$$

for the extreme case of no static contribution to the stress.

THE EFFECT OF WAVE SPREADING ON FATIGUE

For a given sea state the stress time history at any particular point on the structure will depend on the directional distribution of wave energy. When the stress is linearly dependent on the wave amplitudes, the stress spectrum at a point designated by the character β may be expressed in terms of a transfer function.

$$S_s(\beta,\omega,\theta) = |H_{\eta s}(\beta,\omega,\theta)|^2 \, S_\eta(\omega,\theta) \tag{25}$$

where

$H_{\eta s}(\beta,\omega,\theta)$ - wave amplitude to stress transfer function

$S_{\eta s}(\omega,\theta)$ - directional wave amplitude spectrum

θ - angle of incidence of various wave components

Spreading Functions

The directional wave amplitude spectrum has the property that integration over all possible angles of incidence must yield the point wave amplitude spectrum.

$$S_\eta(\omega) = \int_0^{2\pi} S_\eta(\omega,\theta)d\theta \tag{26}$$

In general, the amount of spreading for a given sea state will depend on wave frequency. However, most commonly used models assume, for mathematical conveniences, that the wave spreading for each sea state is independent of frequency. The use of such simplified models is acceptable because at this time the ability to predict more complex descriptions of the sea is not available. In this paper spreading models will be of the frequency independent form as shown in the following equation.

$$S_\eta(\omega,\theta) = S_\eta(\omega)D(\theta) \tag{27}$$

There are two simple limiting forms of the spreading function, $D(\theta)$. The first is the uni-directional spectrum in which waves come from a single direction θ_o, and the second is the totally diffuse or omni-directional spectrum in which waves come from all directions with equal probability. These cases are given below.

Uni-directional

$$S_\eta(\omega,\theta) = S_\eta(\omega)\delta(\theta-\theta_o) \tag{28}$$

Omni-directional

$$S_\eta(\omega,\theta) = S_\eta(\omega)/2\pi \tag{29}$$

The most common non-trivial spreading function is known as the 'cosine squared'. It is given below.

$$S_\eta(\omega,\theta) = S_\eta(\omega)\frac{2}{\pi}\cos^2(\theta-\theta_o) \tag{30}$$

$$\text{for } \pi/2 \le \theta-\theta_o \le \pi/2$$

$$= 0 \text{ otherwise}$$

The cosine squared model is awkward to use in a sensitivity analysis because the extent of the spreading cannot be continuously varied from uni-directional to omni-directional by simple variations of a single parameter. An equally valid and much more flexible spreading model is introduced in the next section.

The Elliptical Spreading Model

The elliptical spreading function was initially suggested by Dunwoody and is described here for the first time. The function is given below (Dunwoody, 1979).

$$D(\theta-\theta_o) = \frac{\sqrt{1-e^2}}{2\pi(1-e\cos(\theta-\theta_o))} \tag{31}$$

In polar coordinates, $D(\theta-\theta_o)$ describes a family of ellipses based on the eccentricity parameter e. One of the focii of the ellipse lies on the origin of the coordinate system and the other focus lies along the direction θ_o. The eccentricity parameter can take on any value between zero and one. Zero corresponds to a completely diffuse sea with equal amplitudes of waves propagating in all directions. The spreading function, $D(\theta-\theta_o)$, is suitably normalized so that the

point wave amplitude spectrum, computed by integrating the directional spectrum over all angles, equals the original point spectrum. This angular spreading function has been chosen over other possibilities because the amount of spreading is a smooth function of a single parameter. The parameter, e, can be used as the measure of spreading in the computation of fatigue resistance. The parameter e may also be easily fitted to experimental wave spreading data.

Relative Rates of Fatigue Damage

Variation in the extent of wave spreading may change the rate of fatigue damage, F, as expressed in Equation 7, because of resulting changes in the mean square stress, the zero upcrossing frequency or the Wirsching correction factor. Two different spreading models may be compared by taking the ratio of the appropriate expressions for the rates of fatigue damage. The result will in general have the form of Equation 8. No simple generalizations can be made as to the effect of spreading on fatigue, with the exception that fatigue damage rates based on a worst case direction in a uni-directional sea will be reduced by spreading. Not much more can be concluded without evaluating a particular structure. To add some insight to this discussion, the particular example of a single vertical cylinder is presented in detail.

A simple caisson structure is shown in Figure 2. The structural properties are assumed to

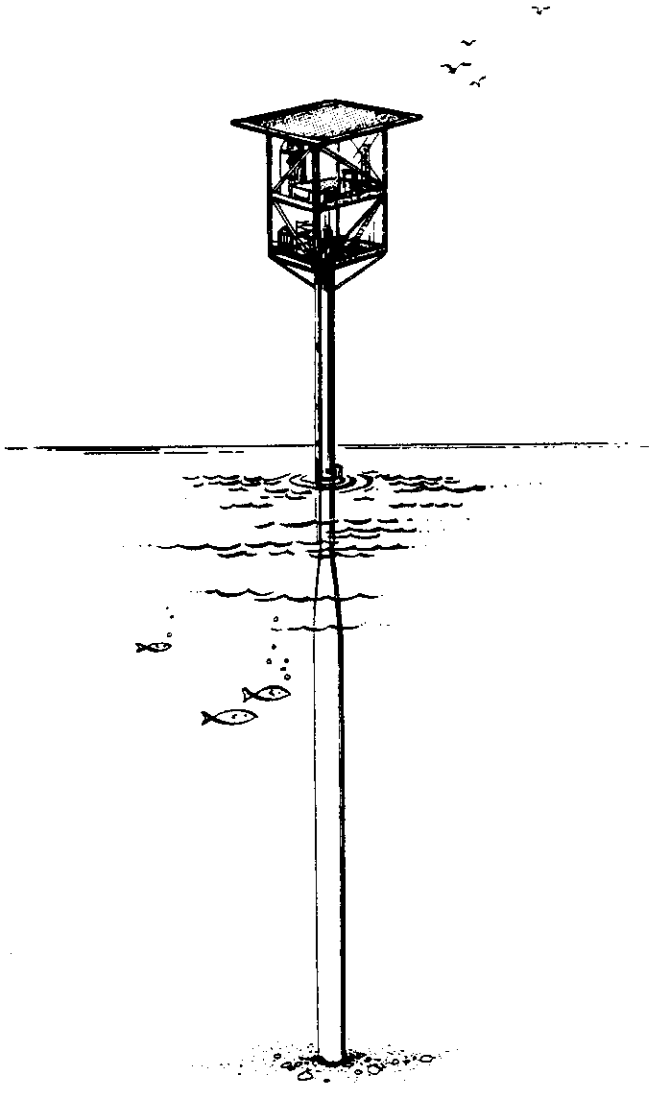

Figure 2 Caisson Production Platform

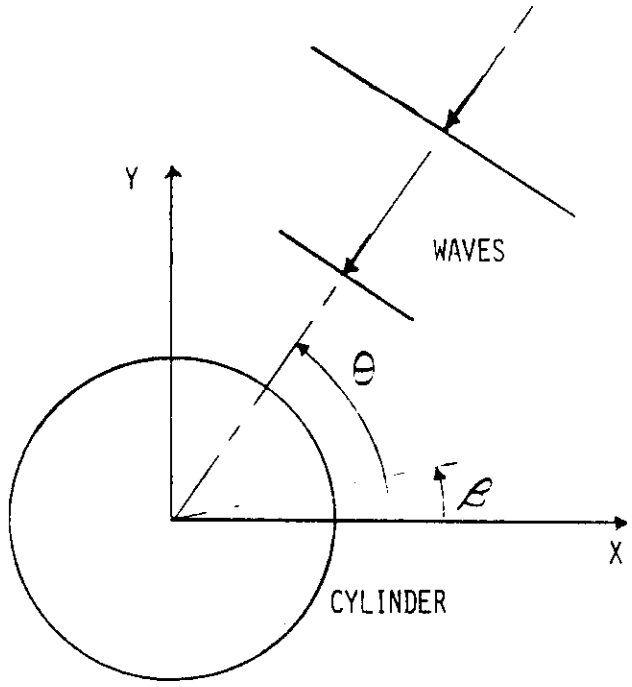

Figure 3 Coordinate System Definition

be symmetric with respect to the longitudinal axis. At any particular level on the structure, such as the mud line, the stress transfer function at a point on the perimeter defined by the angle β as defined in Figure 3, is given by the following equation.

$$H_{\eta s}(\beta,\omega,\theta) = H_{\eta s}(\omega)\cos(\theta-\beta) \tag{32}$$

where θ is the incidence angle of a regular wave component at the frequency ω.

To demonstrate the influence of spreading in this example the rate of fatigue damage F, corresponding to a spreading function $D(\theta)$ will be compared to the fatigue damage rate F_o, corresponding to a uni-directional spectrum incident on the structure from the angle θ_o. $D(\theta)$ is assumed to be a frequency independent spreading function which is symmetric about the mean incidence angle, θ_o.

For these conditions, each point on the caisson will have stress spectra whose frequency dependence will be independent of the amount of spreading. Put another way, if only the spreading function is varied, all the resulting stress spectra at a point will be proportional to one another. As a consequence the mean zero upcrossing frequency and the Wirsching correction factor will not change with spreading. The ratio of the fatigue damage rate, F, with spreading to the uni-directional case, F_o, will simplify to

$$\frac{F}{F_o} = \left(\frac{\sigma_s^2}{\sigma_{so}^2}\right)^{b/2} \tag{33}$$

The two relevant expressions for mean square stress are given below. Due to the axial symmetry of the caisson the mean incidence angle, θ_o, can be set to zero with no loss of generality. This has been done in all subsequent calculations.

$$\sigma_s^2 = \int_o^\infty |H_{\eta s}(\omega)|^2 S_\eta(\omega)\,d\omega \int_o^{2\pi} \cos^2(\theta-\beta) D(\theta)\,d\theta \tag{34}$$

$$\sigma_{so}^2 = \int_o^\infty |H_{\eta s}(\omega)|^2 S_\eta(\omega)\,d\omega \int_o^{2\pi} \cos^2(\theta-\beta)\,\delta(\theta)\,d\theta \tag{35}$$

Substitution into Equation 33 leads to

$$\frac{F}{F_o} = \frac{\int_o^{2\pi} \cos^2(\theta-\beta)\ D(\theta)\,d\theta}{\cos^2(\beta)} \tag{36}$$

The above ratio can be evaluated for various spreading functions $D(\theta)$. This is shown below for the cosine squared and elliptical spreading functions.

Cosine squared:

$$\frac{F}{F_o} = \left[\frac{3}{4} + \frac{1}{4}\tan^2\beta\right]^{b/2} \tag{37}$$

Hence, for the worst case direction $\beta = \theta_o = 0$, the fatigue damage rate is reduced to

$$\frac{F}{F_o} = \left[\frac{3}{4}\right]^{b/2} \tag{37a}$$

For $b/2 = 2.05$ (37b)

$$\frac{F}{F_o} = .554 \tag{37c}$$

and the fatigue life

$$\frac{1}{F} = 1.8 \times \frac{1}{F_o} \tag{37d}$$

The fatigue life is increased by a factor of 1.8.

Elliptical spreading:

$$\frac{F}{F_o} = [G + \tan^2\beta(1-G)]^{b/2} \tag{38}$$

where $$G = \int_o^{2\pi} \frac{\cos^2\theta \sqrt{1-e^2}}{2\pi(1-e\cos\theta)} d\theta \tag{39}$$

Again for the case $\beta = \theta_o = 0$ a simplified expression is obtained.

$$\frac{F}{F_o} = G^{b/2} \tag{40}$$

The ratio of the corresponding fatigue lives is simply

$$\frac{L}{L_o} = G^{-b/2} \tag{41}$$

These results are shown in the following table for various values of the spreading parameter e, and b/2 = 2.05.

TABLE 1

Spreading parameter e versus G, F/F_o and L/L_o for b/2 = 2.05

e	G	$\frac{F}{F_o}$	$\frac{L}{L_o}$	Description of Wave Spreading
0	0.5	.24	4.2	omni-directional
.5	0.53	.27	3.7	
.7	0.58	.33	3.0	
.8	0.62	.38	2.6	
.85	0.65	.41	2.4	
.9	0.69	.47	2.1	
.95	0.76	.57	1.8	approximate cosine squared
.99	0.87	.75	1.3	
1.0	1.0	1.0	1.0	uni-directional

These results show that cosine squared spreading extends the fatigue life by a factor of 1.8 while omni-directional spreading would increase the life to 4.2 times the uni-directional result. The possibility that omni-directional spreading might happen in nature may seem remote. However for any linear stress transfer function for a structure of arbitrary shape

$$|H_{\eta s}(\beta,\omega,\theta)| = |H_{\eta s}(\beta,\omega,\theta+\pi)| \tag{42}$$

It is therefore only necessary that the waves be uniformly distributed over π radians to achieve the maximum extension of fatigue life over the uni-directional spectrum coming from the worst case direction. Structural symmetry may also reduce the total angle over which the waves must be evenly spread to achieve the maximum benefits. In some cases, a realistic amount of spreading, such as cosine squared is sufficient to derive the maximum benefit. An example is the fatigue caused by the heave response of a square planform tension leg platform as discussed in Vandiver, 1980.

CONCLUSIONS

By means of general formulations and a specific example, the dependence of fatigue on the uncertainties related to natural frequencies and damping ratios have been demonstrated.

Uncertainties related to the prediction of structural natural frequencies are primarily related to the structural idealizations or models used in the design process. The greatest weakness is probably in the area of foundation modelling. The behavior of soil under cyclic loading conditions remains a rather uncertain field. Assumptions regarding soils stiffness have dramatic impact on the estimation of structural natural frequencies.

The uncertainties related to damping estimates have several sources. One of the greatest is a general lack of accurate estimates of damping on existing structures. This issue and a method for obtaining improved measurements of damping on existing sturctures are addressed by Campbell, 1980. The second reason for uncertainty is that direct estimation of individual components of damping are rarely made, and the knowledge required for making such estimates is not widely available in the industry. To understand the complete damping problem one must understand the fluid mechanics, the soil mechanics, the structural mechanics, and their interaction. A final source of misuse of damping is that the relationships between exciting forces and damping mechanisms are too frequently ignored. A versatile single parameter wave spreading function has been introduced and used to demonstrate for a particular example, the importance of wave spreading in fatigue calculations.

The purpose in this study was to highlight the significance that estimation of natural frequencies, damping ratios, and wave spreading has in the calculation of the fatigue life of a structure. The results are in a subjective sense quite general, even though a specific fatigue damage accumulation rule was assumed. Of the various high cycle damage accumulation rules proposed to date, none are so different that the qualitative insights contained in this paper would be invalidated. These insights should be of help to the designer in judging the relative importance of the various factors which must be considered in the performance of a fatigue life calculation.

These results might be extended by means of a sensitivity analysis on an actual numerical model of an offshore platform intended for use in, for example, the North Sea or the Gulf of Mexico. In a very recent paper (Vugts, 1981), the sensitivity of fatigue damage rate to variations in water depth, damping ratios and several other structural parameters has been investigated and is recommended to the reader.

REFERENCES

CAMPBELL, R.B., and Vandiver, J.K., 1980: The Estimation of Natural Frequencies and Damping Ratios of Offshore Structures", Proceedings of the 1980 Offshore Technology Conference, Paper No. OTC 3861, pp. 53-61, Houston.

CRANDALL, S.H., and Mark, W.D., 1973: Random Vibration in Mechanical Systems, Academic Press.

DUNWOODY, A.B., and Vandiver, J.K., August 1981: "The Influence of Separated Flow Drag on the Dynamic Response of Offshore Structures to Random Waves", Presented at the International Symposium on Hydrodynamics in Ocean Engineering, Trondheim, Norway.

DUNWOODY, A.B., 1979: Personal communication with the author, MIT.

KROGSTAD, H.E., et al., 1979: "Analysis of Wave Spectra from the Norwegian Continental Shelf", Proceedings of the POAC, Trondheim, Norway.

VANDIVER, J.K., February 1980: "Prediction of the Damping Controlled Response of Offshore Structures to Random Wave Excitation", Society of Petroleum Engineers Journal.

VUGTS, J.H., November 1981: "Dynamic Response and Fatigue Damage with Increasing Water Depths", Presented at the conference on "Safety of Deepwater Oil and Gas Production", Det Norske Veritas.

WIRSCHING, P.H. and Light, M.C., November 1979: "Probability-Based Fatigue Design Criteria for Offshore Structures", Report to the American Petroleum Institute, API-PRAC Project H15.

OTC 4285

Measured and Predicted Dynamic Response of a Single Pile Platform to Random Wave Excitation

by Michael F. Cook and J. Kim Vandiver, *Massachusetts Institute of Technology*

This paper was presented at the 14th Annual OTC in Houston, Texas, May 3-6, 1982. The material is subject to correction by the author. Permission to copy is restricted to an abstract of not more than 300 words.

ABSTRACT

The dynamic response characteristics of an operational single pile platform are investigated in detail. Wind, wave, and response time histories recorded on the platform in March 1980, form the basis for comparison of predicted and measured dynamic response. In the predictive analysis, the components of the total modal damping are separately computed. These damping components include the steel hysteretic, the wave radiation, the viscous hydrodynamic, and the soils damping. Response in the two fundamental bending modes of the structure are predicted using a technique based on the principle of reciprocity for ocean waves. Good agreement between predicted and measured response levels is attained. Combination of the results of the response prediction method with the results of a dynamic finite element model of the platform leads to a versatile expression for the mean rate of accumulation of fatigue damage. This expression, wave spreading factors, and climatological data are used to estimate a fatigue life for the structure.

INTRODUCTION

The understanding of the dynamic response of deepwater structures is a key element in the prediction of fatigue life. This is particularly true of structures with lightly damped natural vibration modes whose natural periods exceed three seconds. There are very few structures that respond linearly in most sea conditions and have sufficiently simple configurations to allow accurate theoretical predictions of dynamic response in directionally spread random seas. The vertical cylindrical caisson satisfies these conditions.

A complete dynamic analysis of a single caisson structure is described in this paper. The modal damping ratio is predicted by analytic means. A finite element model is used to predict the natural mode shapes and soil behavior. The mean square response of the structure is predicted and compared to field measurements with very good agreement. A fatigue life computation is presented which accounts for variation in directional spreading of the seas.

The caisson has many similarities to other more complex fixed deepwater structures. It has similar mode shapes, natural periods, and damping ratios. The caisson has the same range of Reynolds numbers and Keulegan-Carpenter numbers as large tubular members on jacket structures. It has similar soil behavior. As a consequence the insights gained from an in-depth analysis of this simple structure provide a better understanding of the behavior of much larger and complex but dynamically similar deepwater platforms.

PLATFORM DESCRIPTION

The single pile platform which is the focus of this report is a triple-decked single well gas production platform located in South Marsh Island Block 33 in the Gulf of Mexico. A three dimensional drawing of the platform, which is operated by AMOCO Oil Company, is shown in Figure 1. The caisson stands in 89 feet of water and the pile diameter is four feet at the water line and seven at the mudline. The annulus between the main pile and the drive pile is grouted. The natural periods of the two orthogonal fundamental flexural modes of the structure are almost identical, each with a value of approximately 3.1 seconds. With these natural periods, the platform exhibits significant first mode dynamic response.

In March, 1980, the authors recorded wind, wave and response time histories on the structure for later analysis and comparison with predicted response values. A complete description of the data analysis is contained in Ref. [1]. A total of six reels of data were recorded on three separate days. A summary of the pertinent information derived from the five reels which contained horizontal biaxial accelerometer data is shown in Table 1. The other reel of data, reel 2, had time histories from four accelerometers distributed vertically over the structure but pointing in the same direction. This data was used to estimate mode shapes and is reported in OTC Paper No. 4286 [2]. One of the five remaining data sets, reel 5, included tests of a dynamic absorber. These results are described in OTC Paper No. 4283 [3].

SINGLE-DEGREE-OF-FREEDOM EQUIVALENT MODEL

This single pile platform responds significantly in only its fundamental bending modes. To predict the response in these natural modes, an equivalent, linear, single degree of freedom (SDOF) system was defined for both modes. This technique is applicable for structures which behave linearly and have small damping. The total response is obtained by superposition of the modal responses.

The equation of motion that represents first mode response of the caisson when excited by ocean waves contains terms which depend on the relative acceleration and velocity between the water particles and the generalized coordinates which represent platform motions. For this structure in commonly occurring low to moderate sea states non-linear drag force or velocity dependent excitation is negligible and can be dropped. However, this does not necessarily imply that viscous damping losses can be ignored. These must be evaluated separately.

When the total damping is small, damping can be modelled using an equivalent linear dashpot which equates platform energy losses with the SDOF model energy losses. The SDOF equivalent equation for a mode is of the form

$$M\ddot{q} + (R_{ST} + R_{RAD} + R_{VH} + R_{SOIL})\dot{q} + Kq = F(t) \quad (1)$$

where M = modal virtual mass of the structure (includes added mass)

R_{ST} = modal steel hysteretic damping

R_{RAD} = modal radiation or wave making damping

R_{VH} = modal viscous hydrodynamic damping

R_{SOIL} = modal soils damping

K = modal stiffness of the structure

q = generalized coordinate obtained from modal analysis for the particular mode

$F(t)$ = total linear modal force

The undamped modal natural frequency, ω_n, and damping ratio, ξ_T, are

$$\omega_n = \sqrt{K/M} \quad (2)$$

$$\xi_T = \frac{R_T}{2\omega_n M} = \frac{R_{ST}+R_{RAD}+R_{VH}+R_{SOIL}}{2\omega_n M}$$

$$= \xi_{ST} + \xi_{RAD} + \xi_{VH} + \xi_{SOIL} \quad (3)$$

Using these, the SDOF equivalent system reduces to

$$\ddot{q} + 2\omega_n \xi_T \dot{q} + \omega_n^2 q = F(t)/M \quad (4)$$

To use this equation to accurately predict response requires knowledge of the total modal damping present within the vibrating system. As suggested in Equation 3, the total modal damping is a combination of four major damping sources. In the next four sections, each source will be identified and an equivalent modal damping ratio will be estimated from theoretical considerations.

DAMPING RATIO PREDICTION

Steel Hysteretic Damping

Steel hysteretic damping refers to the energy lost due to internal dissipation within a steel member under cyclic loading. As discussed in Ref. [1], the fraction of the total strain energy dissipated per cycle due to steel hysteretic damping within the outer pile of the caisson may be approximated by the following:

$$\frac{\Delta V_{ST}}{V_{ST}} = 2JE = 2\pi(.0047) \quad (5)$$

where ΔV_{ST} = strain energy dissipated in the outer pile per cycle

V_{ST} = peak strain energy stored in the outer pile

J = constant = 500×10^{-12}/psi for SAE 1020 steel

E = Youngs modulus = 29.5×10^6 psi for SAE 1020 steel.

The energy loss per cycle can be simply expressed in terms of a linear equivalent damping ratio for a single degree of freedom system. The correct relationship is given by

$$4\pi\xi_{ST} = \frac{\Delta V_{ST}}{V_{ST}} \quad (6)$$

Therefore,

$$\xi_{ST} = \frac{.0047}{2} = 0.24\% \quad (7)$$

This damping ratio is assumed to apply to the other materials in the structure as well; particularly the grout. The grout would probably have somewhat higher losses than this and therefore the value of 0.24% as an overall material hysteretic damping is likely a lower bound. In the remainder of the report this damping will continue to be referred to as ξ_{ST}, in reference to the losses in the steel. However, it is applied to the entire mechanical energy of the structure.

Radiation (Wave Making) Damping

A platform oscillating in the ocean creates waves which radiate outward, dissipating energy away from the structure. For a vertical cylinder of uniform diameter, the modal radiation damping can be estimated using linear potential flow theory. A derivation is contained in a 1976 report by Petrauskas [4].

Based on these results, an approximate expression for the modal radiation damping coefficient for a non-uniform vertical cylinder which creates deepwater radiated waves is

$$R_{RAD}(\omega) = \frac{\pi \rho_w \omega}{e^{2kh} + 4kh} \left[\int_{-h}^{0} d(z) p_1(\frac{kd}{2}) \psi(z) e^{k(z+h)} dz \int_{-h}^{0} \psi(z) e^{k(z+h)} dz \right] \quad . . . . . (8)$$

where z = vertical coordinate, positive upwards from the water line

ρ_w = density of water

ω = frequency of radiated waves

k = wave number

$d(z)$ = cylinder diameter

h = water depth

$\psi(z)$ = mode shape (estimated from finite element model)

$p_1(kd/2) = \frac{\pi}{2} (\frac{kd}{2})^3$ for $\frac{kd}{2} < \frac{1}{2}$

Equation 8 was evaluated numerically using the parameters associated with the operational single pile platform in first mode response. The modal radiation damping ratio was found to be

$$\xi_{RAD} = 0.11\% \quad . . . . . (9)$$

This result is approximate in the sense that the Petrauskas result is strictly applicable to a cylinder with a uniform diameter. Equation 8 relaxes this constraint to allow for a diameter which changes slowly and then only at a substantial distance below the waterline. As a check on this result, the radiation damping was computed for a cylinder with a constant diameter of four feet. For it $\xi_{RAD} = 0.10\%$.

Viscous Hydrodynamic Damping

Viscous hydrodynamic damping is related to the separated flow drag force term in Morison's equation. An expression for the modal viscous hydrodynamic damping coefficient applicable for first mode response of a vertical cylinder as shown by Dunwoody [5] is

$$R_{VH} = \int_{-h}^{0} \frac{1}{2} \rho_w d C_D \sqrt{\frac{8}{\pi}} \sigma_r^*(z) \psi^2(z) dz \quad . . . . (10)$$

where C_D = drag coefficient

σ_r^* = r.m.s. relative velocity.

As defined here, R_{VH} is proportional to the relative velocity, which increases with sea state, and can only be obtained by iteration. However, if water particle velocities are assumed to be much larger than structural velocities, σ_r^* can be approximated by the r.m.s. water particle velocity, σ_u, which can be estimated from Equation 11.

$$\sigma_u^2(z) = \int_0^{\infty} 4\pi^2 f^2 G_\eta(f) e^{2kz} df \quad . . . . . (11)$$

where f = cyclic frequency (Hz)

$G_\eta(f)$ = wave amplitude spectrum

Equation 11 is valid for deep water waves which decay exponentially. Using a Bretschneider (ITTC)[6] two parameter wave spectrum,

$$G_\eta(f) = \frac{1.25}{4} H_s^2 \frac{fp^4}{f^5} e^{-1.25(f_p/f)^4} \quad . . . . . (12)$$

where H_s = significant wave height

f_p = peak wave frequency (Hz).

estimates of the modal viscous hydrodynamic damping were obtained for the sea states corresponding to experimentally derived values of H_s and f_p. Typical values of ξ_{VH} in the experiments were in the vicinity of 0.15%. The detailed results will be summarized later. As computed above, the modal viscous hydrodynamic damping is probably an upper bound since a unidirectional wave spectrum has been used to compute σ_u. Spreading would decrease the effective σ_u.

Soils Damping

Compared with the other components of the total damping, the characterization and modelling of soils damping is more complex and less well established. Two types of soil damping exist; material (internal) soil damping, which is a hysteretic form of damping, and geometric (radiation) damping, which is analogous to wave making damping. Material damping is usually specified as the fraction of soil strain energy dissipated per cycle and is expressed as 4π times a constant soils damping ratio, ξ_{smd}, which is believed to have a value between 3 and 10%. ξ_{smd} is also known as the specific damping ratio. Geometric damping is present only if the frequency of oscillation exceeds a threshold value which depends on the soil stratum. In general, geometric damping is not significant for small structures at the frequencies associated with wave loading, in Gulf of Mexico sediments.

As developed in detail in Ref. [1], an equivalent modal soils damping ratio ξ_{SOIL} can be estimated from the soil material damping ratio ξ_{smd} by computing the ratio of the energy loss per cycle in the soil to the total caisson energy. The method utilizes the lumped soil spring foundation of the finite element idealization of the caisson to compute the soil strain energy. The final expression for ξ_{SOIL} is

$$\xi_{SOIL} = \frac{\Delta V_{SOIL}}{4\pi V_T} = \frac{\xi_{smd}}{M\omega_n^2} \sum_{i=1}^{n} K_s(z_i) \psi^2(z_i) \quad . . . . (13)$$

where $\Delta V_{SOIL} = 4\pi \xi_{smd} V_{SOIL}$

$= 4\pi \xi_{smd} (\frac{1}{2} \Sigma K_s(z_i) \psi^2(z_i) a_o^2)$

$V_T = \frac{1}{2} K a_o^2 = \frac{1}{2} M \omega_n^2 a_o^2$ = total caisson energy

$K_s(z_i)$ = lumped soil spring stiffness at $z = z_i$

$\psi^2(z_i)$ = value of the mode shape at $z = z_i$

n = number of lumped soil springs used in this finite element model.

Equation 13 was evaluated using the four soil springs of the finite element model of the caisson and the results are shown in Table 2. This technique is approximate and research leading to the development of new techniques is warranted.

TOTAL DAMPING RATIO MEASUREMENTS

The total modal damping was estimated for each of the two fundamental bending modes from biaxial accelerometer data recorded in March 1980. To isolate the fundamental modal directions, a correlation function rotation scheme based on a Mohr's circle algorithm was used. In this analysis, the modal orientation is defined as that orientation for which the time histories from a biaxial pair of accelerometers would have a minimum coherence at the natural frequencies of the two fundamental bending modes. This procedure is described in Ref. [1]. Once the modal orientation is determined, single-channel MEM (Maximum Entropy Method) spectral analysis is used to estimate natural frequencies and damping ratios. The damping ratio estimate is based on the half-power bandwidth method [7].

The results of the damping estimation are shown in Table 2 for three different days of testing. In this table, items 2, 3, 4,6, and 7 were theoretically obtained, as previously described; item 1 is an experimental value. The error bounds on the measured total damping ratio are 95% confidence bounds. The viscous hydrodynamic damping was estimated, assuming a drag coefficient of 1.0 and applying values of H_s and ω_p derived from the measured wave spectra. Row 5 is the soils damping required to make the total experimental damping value equal the total theoretical. The values shown suggest an average value of $\xi_{SOIL} = 0.6\%$, which falls in the expected range of the analytically estimated values.

RESPONSE PREDICTION

After the modal equivalent damping components have been estimated, the next step is to predict modal response. The reciprocity method of response prediction, proposed by Vandiver [8], will be used for this purpose. This approach utilizes the principle of reciprocity for ocean waves which relates the radiation damping of a structure oscillating in a calm sea to the linear wave force exerted on the structure if it were held fixed in incident waves. This technique yields a simple result for the mean squre modal response and its use is valid only for lightly damped modes excited by linear wave forces. This method directly incorporates wave spreading effects.

The caisson is an ideal structure to test this modal response prediction technique because the structure is axi-symmetric and the two fundamental bending natural frequencies are almost identical.

To demonstrate the performance of this response prediction method, the coordinate system shown in Figure 2 was used. In this figure, the x and y axes define the orientation of the two fundamental bending modes of the caisson. The angle θ_o defines the angle between the x-modal direction and the mean wave direction in a directionally spread sea. The terms σ_x^2 and σ_y^2 represent the mean square modal displacement response on the helideck along the x and y modal axes, respectively.

The prediction of the mean square modal response of the x-mode within two half power bandwidths of the resonant frequency f_x is shown in Equation 14.

$$\sigma_x^2 = \frac{C_x \rho_w g^3}{80\pi^5 M_x f_x^5} G_\eta(f_x) \frac{\xi_{RAD}(f_x)}{\xi_T(f_x)} \quad \ldots\ldots\ldots (14)$$

The expression for the y-mode is identical with the x subscripts replaced by y subscripts. The term C_x depends on both structural geometry and the directional wave amplitude spectrum. In this paper, the directional wave amplitude spectrum is modelled using frequency independent spreading functions as defined in the following equation.

$$G_\eta(f,\theta) = G_\eta(f)\, D(\theta) \quad \ldots\ldots\ldots\ldots (15)$$

where $G_\eta(f,\theta)$ = directional wave amplitude spectrum

$D(\theta)$ = spreading function

θ = angle of incidence of various wave components

When integrated over all possible wave incidence angles, the directional wave amplitude spectrum satisfies

$$G_\eta(f) = \int_0^{2\pi} G_\eta(f,\theta)\, d\theta \quad \ldots\ldots\ldots\ldots (16)$$

For a single pile platform, the expressions from Ref. [8] for C_x and C_y simplify to

$$C_x = 2\int_0^{2\pi} D(\theta)\cos^2\theta d\theta \quad \ldots\ldots\ldots\ldots (17)$$

and

$$C_y = 2\int_0^{2\pi} D(\theta)\sin^2\theta d\theta \quad \ldots\ldots\ldots\ldots (18)$$

The sum of Equations 17 and 18 is trivial to evaluate, because $\sin^2\theta$ plus $\cos^2\theta$ yields 1.0 and the integral

$$\int_0^{2\pi} D(\theta)d\theta = 1.0 \quad \ldots\ldots\ldots\ldots (19)$$

and therefore

$$C_x + C_y = 2.0 \quad \ldots\ldots\ldots\ldots (20)$$

Therefore, even though the actual spreading function is unknown, the total mean square response may be predicted by summing the individual mean square responses σ_x^2 and σ_y^2.

$$\sigma_x^2 + \sigma_y^2 = \frac{\rho_w g^3}{40\pi^5 M_x f_x^5} G_\eta(f_x) \frac{\xi_{RAD}(f_x)}{\xi_T(f_x)} \quad \ldots (21)$$

where it has been assumed that the natural frequencies, modal masses and damping ratios of both modes are approximately equal. The x subscript has been retained

in Equation 21 to reflect the properties of both modes. It has also been assumed that the responses of the two modes x and y at their common natural frequency are uncorrelated. This has been confirmed in the field experiments. The coherence between the two modal responses is less than 0.05.

The measured data is in terms of acceleration. For purposes of comparing predicted and measured data it is convenient to express Equation 21 in terms of mean square acceleration. The mean square response within a half power bandwidth of the natural frequency is a narrow band random process and the following simple relation may be used for either the x or y directed modes.

$$\sigma_{\ddot{x}}^2 = 16\pi^4 f_x^4 \sigma_x^2 \quad \ldots\ldots\ldots\ldots\ldots\ldots \quad (22)$$

Therefore, the total mean square acceleration may be expressed as,

$$\sigma_a^2 = \sigma_{\ddot{x}}^2 + \sigma_{\ddot{y}}^2 = \frac{2\rho_w g^3}{5\pi M_x f_x} G_\eta(f_x) \frac{\xi_{RAD}(f_x)}{\xi_T(f_x)} \quad \ldots\ldots \quad (23)$$

The natural frequency f_x of this platform was measured as well as the total modal damping ξ_T. The modal mass was determined from the finite element model and the radiation damping was computed theoretically. Therefore using measured values of the wave amplitude spectrum evaluated at the natural frequency it is possible to predict the total mean square acceleration response of the structure and compare it to that observed.

The results are summarized in Table 3 for data taken on two separate days. The predicted and measured values are in very close agreement. The actual error in the predictions is substantially less than might have been expected considering the uncertainty in the estimates of the total damping ratio. This is the first known experimental confirmation of the response prediction technique embodied in Equation 14.

DESCRIPTION OF THE FINITE ELEMENT MODEL

In order to estimate both the fundamental flexural mode shape and the relationship between platform dynamics and stresses within the pile, a 21-node two-dimensional dynamic finite element (F.E.) model of the single pile platform was developed. In this model, the platform was represented using 14 beam elements and the soil was replaced by four linear soil springs. A schematic of the F.E. model is shown in Figure 3 and a detailed description of its formulation is contained in Ref. [1]. To achieve model natural periods which closely matched the measured values required iteration of the soil spring stiffnesses.

Both the fundamental flexural mode shape and the soil spring stiffnesses required in the damping estimation were obtained from the optimized F.E. model. In addition, the maximum stress in the pile, when subjected to sinusoidal wave excitation, at the natural frequency was found to be at a level approximately 26 feet below the mudline. For vibration in the fundamental mode, the helicopter deck displacement to maximum stress transfer function was determined to be 4.95 KSI/foot. This value is required later in the prediction of fatigue life.

DYNAMIC RESPONSE FATIGUE LIFE ESTIMATION

For offshore structures experiencing significant dynamic response in low and moderate sea states, the governing design criteria is often the prevention of failure caused by low stress, high cycle fatigue. To estimate the dynamic response fatigue life of the operational single pile platform, the reciprocity method of response prediction and the dynamic finite element model were combined with a fatigue accumulation model which assumes the stress process is a narrow band Gaussian process with Rayleigh distributed peaks. The result is a versatile expression for the mean rate of accumulation of fatigue damage. The details of this procecure are outlined below.

The expression for the mean rate of accumulation of fatigue damage, based on a stress range S-N curve, is from Ref. [9]

$$F_i = \frac{\nu_o^+}{c} (2^3 \sigma_s^2)^{b/2} \Gamma(1+b/2) \quad \ldots\ldots\ldots \quad (24)$$

where F_i = mean rate of accumulation of fatigue damage at a location in the structure which experiences a mean square stress σ_s^2

ν_o^+ = average zero upcrossing rate of the stress process

$\Gamma(\ )$ = Gamma function

b, c = constants of the stress range S-N curve.

The dynamic finite element model was used to determine the relationship between the maximum stress in the pile and helideck displacements in mode x. Mathematically, this relationship can be expressed as

$$\sigma_s^2 = B^2 \sigma_x^2 \quad \ldots\ldots\ldots\ldots\ldots\ldots \quad (25)$$

where B = maximum stress/helideck displacement transfer function

B = 4.95 KSI/ft.

A value of σ_x^2 was estimated using the reciprocity method, as defined in Equation 14, in conjunction with the Bretschneider (ITTC) wave spectrum of Equation 12. This technique requires that the wave environment at the location be modelled with a set of significant wave height (H_s) and peak wave period (T_p) pairs, each with an assigned annual probability of occurrence (P_i). The resulting expression for the mean rate of accumulation of dynamic response fatigue damage in mode x due to sea state i is shown in Equation 26.

$$F_i = \frac{f_x}{c} \left[\frac{B^2 \rho_w g^3}{32\pi^5} \frac{C_x H_s^2}{M_x} \frac{f_p^4}{f_x^{10}} \frac{\xi_{RAD}}{\xi_T} e^{-1.25\left(\frac{f_p}{f_x}\right)^4} \right]^{b/2} \cdot \Gamma(1+b/2) \quad \ldots\ldots\ldots\ldots \quad (26)$$

where $\nu_o^+ = f_x$

$f_p = 1/T_p$

In this equation, all the parameters which affect the dynamic response fatigue life of a structure are included in a readily usable form. Finally, a fatigue

life estimate (FLE) can be obtained using

$$FLE = 1 \Big/ \sum_{i=1}^{j} F_i P_i \quad \ldots\ldots\ldots\ldots\ldots\ldots (27)$$

where j = total number of sea states.

Fatigue Life Calculation

The fatigue life of the operational single pile platform was estimated using the twelve Gulf of Mexico sea states given in Ref. [10]. For each sea state, Equation 26 was used to compute the rate of accumulation of fatigue damage associated with first mode response of the caisson. The AWS-X modified stress range S-N curve was used to determine values for b and c ($b = 4.38$, $c = 2.64 \times 10^{11}$). In addition, it was assumed that the modal frequency and modal mass remain constant over the lifetime of the structure. For the initial estimate, the ratio ξ_{RAD}/ξ_T was fixed for all sea states at 0.2. The selection of a representative value of C_x is not straightforward. However, two useful limiting cases may be easily evaluated.

The worst case scenario is one in which over the lifetime of the structure the seas are unidirectional and only excite the x directed mode. In other words, all waves are incident at $\theta=0$. For this case, the response in the y direction must be zero and therefore, from Equation 20, $C_x = 2.0$.

The least damaging case is one in which the directional spreading is uniform over all angles. The result of this is that both modes must respond equally and therefore, $C_x=C_y=1.0$.

These two limiting cases will yield upper and lower bound fatigue life estimates for this caisson when substituted into Equations 26 and 27. The result for the uniform spreading case is a fatigue life of 161 years. Unidirectional spreading reduces this estimate to a worst case fatigue life of 35 years. These calculations were computed using a conservative estimate of $\xi_{RAD}/\xi_T = 0.2$. In fact, the field measurements indicate it is approximately half that value. Accounting for this increases the estimated fatigue life by a factor of approximately four. These results indicate that the fatigue life of this structure is between 140 and 644 years. These predictions do not account for fatigue damage caused by quasi-static response of the structure to large low frequency waves. Though many fewer in number, these waves will reduce the fatigue life somewhat. Non-linear drag exciting forces at the natural frequency of the structure have also been neglected.

Many factors influence fatigue life predictions. Natural frequencies, damping ratios, and wave spreading are particularly important. For a more complete discussion of the sensitivity of fatigue life predictions to these factors the reader is directed to Ref. [11].

CONCLUSIONS

In this paper a complete dynamic analysis of a single caisson platform has been presented. A finite element model provided mode shapes, stress transfer functions and some insight into the behavior of the soil. Predictions of all components of damping were made. Field measurements were used to obtain estimates of natural frequencies, damping ratios and mode shapes (see OTC 4286). The measured mean square response was compared to predictions based on the reciprocity method and found to be quite accurate. Finally, an analysis of the fatigue life of the structure was performed, in such a way that the sensitivity of fatigue calculations to directional spreading of the waves was clearly indicated.

NOMENCLATURE

a_o	modal amplitude
b, c	constants of the stress range S-N curve
B	maximum stress in the pile per foot of helideck displacement
C_D	drag coefficient
C_x, C_y	constants dependent on directional spreading
d	pile diameter
$D(\theta)$	wave spreading function
E	Young's modulus of elasticity
f	cyclic frequency (Hz)
f_p	peak wave frequency
FLE	fatigue life estimate
F(t)	modal wave force on fixed structure
$G_\eta(f)$	wave amplitude spectrum
$G_\eta(f,\theta)$	directional wave amplitude spectrum
h	water depth
H_s	significant wave height
J	constant in steel hysteretic damping expression
k	wave number
K	total modal stiffness
$K_s(z_i)$	soil spring stiffness at $z=z_i$
M	total modal virtual mass
P_i	annual probability of occurrence for sea state i
$P_1(kd/2)$	function defined in [4]
q	modal displacement coordinate
R_{RAD}	modal radiation damping coefficient
R_{ST}	modal steel hysteretic damping coefficient
R_T	total modal damping coefficient

R_{VH}	modal viscous hydrodynamic damping coefficient
T_p	peak wave period
V_{SOIL}	peak strain energy stored in the soil during a cycle
ΔV_{SOIL}	strain energy dissipated in the soil per cycle
V_{ST}	peak strain energy stored in the steel members during a cycle
ΔV_{ST}	strain energy dissipated in the steel members per cycle
V_T	maximum energy stored in the total structure during a cycle
$\Gamma( )$	Gamma function
θ	wave incidence angle
θ_c	mean wave direction of directionally spread sea
ν_0^+	zero upcrossing frequency of stress process (Hz)
ξ_{RAD}	modal radiation damping ratio
ξ_{smd}	specific damping ratio of soils
ξ_{SOIL}	modal soils damping ratio
ξ_{ST}	modal steel hysteretic damping ratio
ξ_T	total modal damping ratio
ξ_{VH}	modal viscous hydrodynamic damping ratio
ρ_w	density of water
$\psi(z)$	mode shape ordinate at elevation z
ω_n	undamped modal natural frequency
σ_a^2	total mean square helideck acceleration due to x and y first mode responses
$\sigma_{\dot{r}}$	root mean square relative velocity
σ_x^2, σ_y^2	mean square helideck displacement in x and y modes
$\sigma_{\ddot{x}}^2$, $\sigma_{\ddot{y}}^2$	mean square helideck accelerations in x and y modes

ACKNOWLEDGEMENTS

This research was sponsored by the Branch of Marine Oil and Gas Operations of the U.S. Geological Survey and by the Massachusetts Institute of Technology/Woods Hole Oceanographic Institution Joint Program in Ocean Engineering. The authors would like to thank Amoco for providing access to the caisson and logistics support in conducting the experiments. Amoco engineer Don Green was especially helpful in conducting the field experiments.

REFERENCES

1. Cook, M.F., "Damping Estimation, Response Prediction and Fatigue Calculation of an Operational Single Pile Platform," Engineer Thesis, Massachusetts Institute of Technology and Woods Hole Oceanographic Institution, January, 1982.

2. Briggs, M.J. and Vandiver, J.K., "Multichannel Maximum Entropy Method of Spectral Analysis Applied to Offshore Platforms," Proceedings of the 1982 Offshore Technology Conference, Paper No.4286, Houston, Texas, May 1982.

3. Lu, X. and Vandiver, J.K., "Damping and Natural Frequency Estimation Using the Least Pth Optimization Technique," Proceedings of the 1982 Offshore Technology Conference, Paper No. 4283, Houston, Texas, May, 1982.

4. Petrauskas, C., "Hydrodynamic Damping and 'Added Mass' for Flexible Offshore Platforms," U.S. Army Coastal Engineering Research Center, Report CERC-TP-76-18, October, 1976.

5. Dunwoody, A.B. and Vandiver, J.K., "The Influence of Separated Flow on the Dynamic Response of Offshore Structures to Random Waves," Proceedings of the Hydrodynamics In Ocean Engineering Conference, Trondheim, Norway, August 1981.

6. Connor, J.J. and Sunder, S.S., "Wave Theories, Wave Statistics and Hydrodynamic Loads," Department of Civil Engineering, Massachusetts Institute of Technology, January, 1980.

7. Campbell, R.B., and Vandiver, J.K., "The Estimation of Natural Frequencies and Damping Ratios of Offshore Structures", Proceedings of the 1980 Offshore Technology Conference, Paper No. 3861, Houston, Texas, May 1980.

8. Vandiver, J.K., "Prediction of the Damping Controlled Response of Offshore Structures to Random Excitation," Society of Petroleum Engineers Journal February 1980.

9. Crandall, S.H., Mark, W.D., Random Vibration in Mechanical Systems, Academic Press, New York, 1963.

10. Kinra, R.K., Marshall, P.W., "Fatigue Analysis of tne Cognac Platform", Proceedings of the 1979 Offshore Technology Conference, Paper No. 3378, Houston, Texas, May, 1979.

11. Vandiver, J.K., "The Sensitivity of Fatigue Life Estimates to Variations in Structural Natural Periods, Modal Damping Ratios, and Directional Spreading of the Seas," Proceedings of the Third International Conference on the Behavior of Offshore Structures, M.I.T., 1982.

TABLE 1

SUMMARY OF WAVE, WIND AND RESPONSE DATA

	REEL #1	REEL #3	REEL #4	*REEL #5	REEL #6
Date	3/24/80	3/25/80	3/28/80	3/28/80	3/28/80
Time	1510 - 1630	1215 - 1335	1050 - 1210	1510 - 1615	1630 - 1715
Observed Wave Height (ft)	NW 1-3	ENE 5-8	ENE 2-4	ESE 3-5	ESE 3-5
Observed Wind Speed (knots)	NW @ 20	ENE @ 30	ENE @ 10	ESE @ 20	ESE @ 20
Peak Wave Period (sec)	-	7.28	6.79	7.10	7.10
Significant Wave Height (ft)	-	4.12	3.32	3.59	3.80
Orientation of Mode x	25°S of E	13°N of E	35°N of E	7°S of E	15°S of E
Mode x Natural Frequency Est. (Hz)	.325	.323	.323	.323	.324
x Mode Total Damping Ratio Est.	1.1+/-.3	1.0+/-.4	.9+/-.2	1.9+/-.6	.9+/-.4
Orientation of Mode y	20°N of E	32°S of E	10°S of E	38°N of E	30°N of E
Mode y Natural Frequency Est. (Hz)	.327	.328	.327	.327	.323
y Mode Total Damping Ratio Est.	1.3+/-.3	1.4+/-.4	1.1+/-.3	1.9+/-.7	1.5+/-.5

*Dynamic Absorber was operating during this reel. See OTC 4283

TABLE 2

DAMPING SUMMARY

MODAL DAMPING RATIO ESTIMATES (%)	Reel 1, 3/24/80		Reel 3, 3/25/80		Reel 4, 3/28/80	
	Mode x	Mode y	Mode x	Mode y	Mode x	Mode y
1. ξ_T - Total Measured	1.1+/-.3	1.3+/-.3	1.0+/-.4	1.4+/-.4	.9+/-.2	1.1+/-.3
2. ξ_{ST} - Steel Hysteretic	0.24	0.24	0.24	0.24	0.24	0.24
3. ξ_{RAD} - Radiation	0.11	0.11	0.11	0.11	0.11	0.11
4. ξ_{VH} - Viscous Hydrodynamic	0.11	0.11	0.17	0.17	0.14	0.14
5. $\xi_T - (\xi_{RAD} + \xi_{VH} + \xi_{ST})$	.64	.84	.48	.88	.41	.61
6. ξ_{SOIL} for $\xi_{smd} = 0.03$	0.53	0.53	0.53	0.53	0.53	0.53
7. ξ_{SOIL} for $\xi_{smd} = 0.05$	0.88	0.88	0.88	0.88	0.88	0.88

TABLE 3

COMPARISON OF PREDICTED AND MEASURED HELIDECK ACCELERATION RESPONSES

	REEL 3	REEL 4
Date Recorded	3/25/80	3/28/80
Natural frequency f_x (Hz)	.323	.323
$G_\eta(f_x)$ (ft^2/Hz)	1.2	.7
$\xi_{RAD}(f_x)$ (%)	.11	.11
$\xi_T(f_x)$ (%)	1.0+/-.4	.9+/-.2
ξ_{RAD}/ξ_T	.110	.122
σ_{ap}^2 (ft^2/sec^4)	1.09	.71
(95% confidence bounds)	(.78 to 1.82)	(.58 to .91)
σ_{am}^2 (ft^2/sec^4)	.91	.72

M = 3162 lb-sec^2/ft, (slugs), modal mass

ρ_w = 1.988 lb-sec^2/ft^4 (slugs/ft^3)

g = 32.11 ft/sec^2

σ_{ap}^2 = total predicted mean square helideck displacement

σ_{am}^2 = total measured mean square helideck displacement

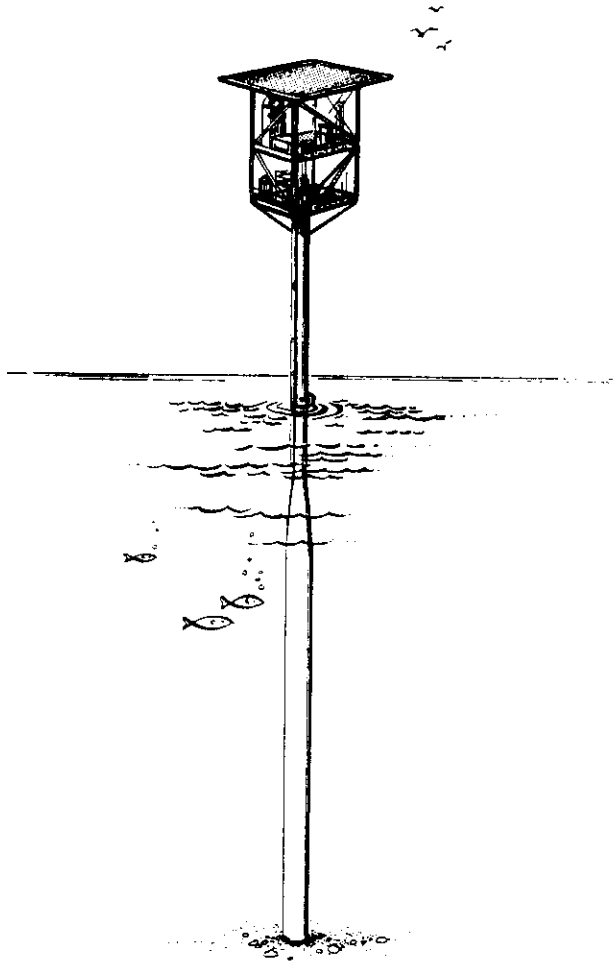

Fig. 1 — Caisson production platform

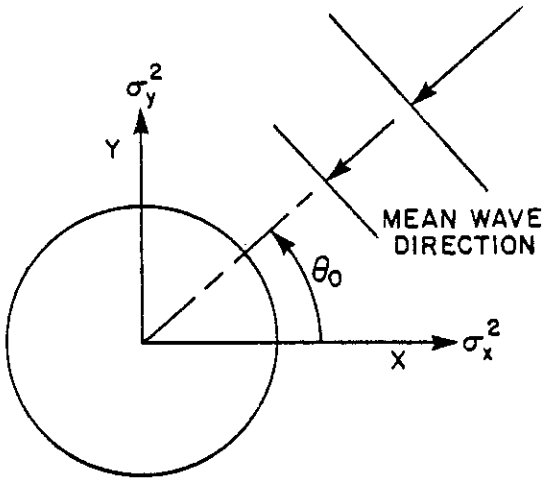

Fig. 2 — Coordinate system definition

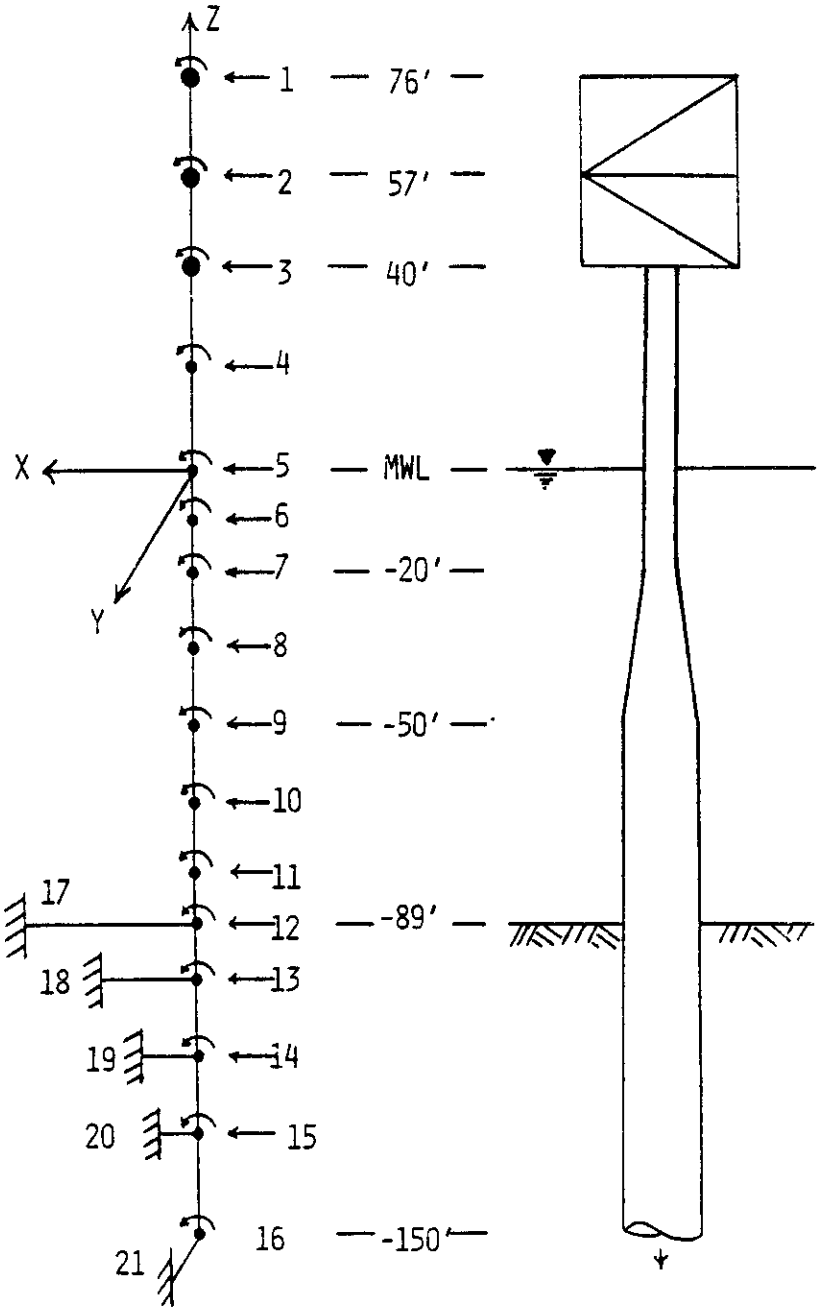

Fig. 3 — Finite element model

DIRECT WAVE FORCE MEASUREMENTS ON A MODEL TENSION LEG PLATFORM

by

Professor J. Kim Vandiver
Massachusetts Institute of Technology

Abstract

A 1:50 scale model of a tension leg platform without tethers was rigidly attached to a five degree of freedom load cell frame. Regular waves with prototype periods of 4.7 to 14.1 seconds were passed through the model. For each wave frequency wave amplitude to wave force transfer functions were measured as a function of incidence angle. Wave incidence angles were varied in five degree increments. Force transfer functions for the five rigid body degrees of freedom in heave, pitch, roll, surge, and sway were measured and compared with numerical predictions.

By applying the principle of reciprocity for linear wave forces, these results may be used to calculate the radiation (wave making) damping for motion of the TLP in these five rigid body modes. Furthermore the results may be used to directly estimate the dynamic response at a natural period of the tethered structure in heave, pitch, or roll, including the effects of directional wave spreading. Sample calculations of radiation damping and dynamic response prediction are included.

INTRODUCTION

For large floating structures such as TLP's there are two common approaches for the prediction of dynamic response to wave exciting forces: model testing and numerical prediction. Both approaches have weaknesses. Dynamically scaled models have scale ratios of 50 to 1 or greater, because accurate modelling requires that water depth be scaled linearly with the structure. As a consequence, Reynolds number similitude is never achieved. This causes concern, because, for example, the modal damping ratios in heave, pitch, and roll are likely not modelled correctly and are very difficult to compensate for when one attempts to scale up to the prototype size.

Numerical models are not entirely trustworthy either, because among other factors, no data from an actual structure is available to benchmark the code. Furthermore, for structures of complicated shape, the solutions

for exciting forces and damping require many approximations.

A third method is available - the direct measurement of exciting forces on scale models, held fixed in place by load cells. This method has the advantage that it is much less sensitive to lack of Reynolds scaling than a dynamically responding model. This is true, because, near the natural frequencies of a dynamically responding model, small inaccuracies in damping lead to large inaccuracies in observed response. A fixed model does not exhibit resonant behavior and therefore small variations in viscous forces cause negligible errors in determining exciting forces. The disadvantage of the fixed model approach is that it can only be applied easily in wave conditions that result in linear wave force relations and linear structural response. Fortunately, due to their very large size, TLP's respond linearly at normal wave frequencies in all but the most severe sea states.

Directly measured exciting forces can be used to predict dynamic response including the effects of directional spreading of the seas. Directly measured forces can be used to calculate the radiation damping of individual structural response modes such as heave, pitch, and roll. This paper recounts the historical, theoretical, and experimental framework which substantiates this approach and presents the results of such a model test conducted on a model of a TLP in 1979.

Historical Perspective

The fundamental principles relating linear wave exciting forces to radiation damping for structures in water were published in Russian by Haskins, in 1957 [1].

Newman put these relationships into a form readily useable by free surface hydrodynamicists in 1962 [2]. His work showed the reciprocal relationship between the six generalized exciting forces on a fixed structure and the six radiation damping coefficients for rigid body motions in heave, pitch, roll, surge, sway, and yaw.

In the early 1960's, similar work was being pursued in the field of acoustics. Working at first independently and later together, Smith and Lyon made important discoveries regarding the response of resonators to

acoustic excitation [3,4]. Of relevance here, it was shown that a single degree of freedom resonator (such as a piston in a wall) excited by a broad band sound field would respond in proportion to the ratio of the sound radiation damping to the total damping of the resonator. This appears on the surface to contradict conventional wisdom regarding the vibration of mechanical systems. One expects that as damping is increased response must decrease. This is generally true except in the case that one chooses to increase radiation damping. An increase in radiation damping increases the ratio of radiation to total mechanical damping and results in increased dynamic response. This is easily explained by the principle of reciprocity. An increase in radiation damping can only be accomplished if the exciting forces due to incoming waves also increase. It is this increase in exciting force that accounts for the increase in response. However, the response has an upper bound corresponding to the ratio of radiation to total damping being 1.0. This early work of Smith and Lyon opened a new field in sound and vibration known as Statistical Energy Analysis (SEA) [5].

Developments in hydrodynamics proceeded quite separately from acoustics. In 1968, Vugts performed a series of model tests, designed to test, in addition to other objectives, the relations of Haskinds as elucidated by Newman. In a towing tank, wave forces on two-dimensional ship sections held fixed in place were measured. The same sections were then oscillated in calm water and the radiated waves were measured. The theoretical relationship between radiation damping coefficients and rigid body exciting forces were confirmed [6].

Natural modes of many ocean structures are very lightly damped. The bending modes of fixed jackets and the heave, pitch, and roll modes of TLP's are good examples. The significant dynamic response of these natural modes is often confined to very narrow bands near their natural frequencies. These bands are narrow by comparison to common ocean wave spectra. The resonant response of an individual structure mode to the relatively broadband exciting forces of wind driven ocean waves is analogous to the response of a resonator excited by a broad band sound field. Might the results of Smith and Lyon have analogies in the response of structures to ocean waves?

With Lyon's guidance, in 1975, Vandiver showed, by an analogy to acoustics, that the resonant response of a structure excited by ocean waves should also be in proportion to the ratio of radiation to total damping for that mode [7]. Simple experiments conducted on a nearby, 4-legged offshore platform with a bending natural period of 1.0 second suggested that the ratio was approximately 0.1. Schott deduced from measurements conducted by Ruhl on Shell's South Pass 62C structure (π=1.6s) that the ratio of radiation to total damping was approximately 0.08 [8].

The response prediction problem at that time was not yet completely formulated, because unlike the omnidirectional nature of a broadband sound pressure field in a room, ocean waves tend to be highly directional in response to local weather conditions. In 1980, a response prediction technique which included the influence of the directional wave spectrum was presented [9]. In this paper, the Newman relationship between exciting forces and radiation damping for rigid body motions was extended to include the motions of structures exhibiting elastic deformations. A model testing procedure was proposed, in which the measured exciting forces on a model held fixed in place would be used to predict response in a directionally spread sea. Furthermore, by applying the principle of reciprocity, model test measurements of exciting forces could be used to estimate modal radiation damping coefficients.

In 1979, such a model test was conducted on a TLP. This test was intended to be a demonstration of the feasibility of obtaining useful data from a model held fixed in place by load cells. This paper focuses on the relevant theory and results of that test.

A final note of historical significance: in 1980, field tests were conducted on a Gulf of Mexico structure to establish the validity of the response prediction technique described in reference [9]. The positive results of this experiment were published in 1982 [10].

Theoretical Considerations

The dynamic response of a lightly damped structural vibration mode to broad band stationary random excitation is usually dominated by the response in a narrow band near the natural frequency. In fact, approximately 80% of the total energy of response is confined to a range of frequency, two half power bandwidths wide centered on the natural frequency.

From random vibration considerations the average energy of response included in this narrow band of frequencies is given by:

$$\langle E \rangle = \frac{2\pi}{5} \frac{S_F(\omega_o)}{R_T} \tag{1}$$

where ω_o = natural frequency

$S_F(\omega_o)$ = exciting force spectrum at the natural frequency

R_T = total modal damping coefficient

A remarkable feature of this result is that the response energy is not dependent on either the mass or stiffness of the system: only the force spectrum and damping at the natural frequency really matter. The linear wave force spectrum for a structural mode can be expressed as a product of the magnitude squared of the wave amplitude to wave force transfer function and the directional wave spectrum:

$$S_F(\omega,\theta) = S_\eta(\omega,\theta) \left|\Gamma(\omega,\theta)\right|^2 \tag{2}$$

where $S_\eta(\omega,\theta)$ = directional wave spectrum

$\Gamma(\omega,\theta)$ = wave amplitude to modal wave force transfer function for a structure held fixed in place

$\left| \quad \right|$ = denotes magnitude of

As a consequence of reciprocity as expressed by Newman [2], the modal radiation damping coefficient can be expressed as

$$R_{RAD}(\omega) = \frac{\omega^3}{2\rho g^3} \left\langle \left|\Gamma(\omega,\theta)\right|^2 \right\rangle_\theta \tag{3}$$

where ρ = density of water

g = acceleration of gravity

$\left\langle \left|\Gamma(\omega,\theta)\right|^2 \right\rangle_\theta$ = mean square value of $\Gamma(\omega,\theta)$ computed with respect to θ, for θ=0 to 2π

As shown in reference [9], Equations 1, 2, and 3 can be combined to produce the following expresssion for the damping controlled mean square response energy of the mode.

$$\langle E \rangle = \frac{4\pi}{5} C_1 \frac{\rho g^3}{\omega_o^3} S_\eta(\omega_o) \frac{R_{RAD}(\omega_o)}{R_T(\omega_o)} \tag{4}$$

As expected, the response energy is proportional to the ratio of the radiation to total damping for the mode. It is also linearly proportional to the point wave amplitude spectrum evaluated at the natural frequency of the mode. This is a direct consequence of the fact that this equation results from a linear theory.

A significant property of this equation is that even if the exact ratio of radiation to total damping is not known, the upper bound value is 1.0, thus providing an upper bound estimate on response energy, even if the actual damping is unknown.

One item in the equation is not generally known. It is the quantity noted as C_1. This factor includes the effects of the structural geometry and the directional nature of the seas on the wave force spectrum. It is only necessary to evaluate it at the natural frequency, ω_o. It is given by

$$C_1 = \frac{\int_o^{2\pi} S_\eta(\omega_o,\theta) |\Gamma(\omega_o,\theta)|^2 d\theta}{S_\eta(\omega_o) < |\Gamma(\omega_o,\theta)|^2 >_\theta} \tag{5}$$

The directional wave force spectrum is assumed to be expressible as the product of the point spectrum and a spreading function valid in the relevant narrow band of frequencies near the natural frequency of the mode. In a design calculation the directional wave spectrum is assumed to be prescribed. It remains to estimate the directionally dependent wave amplitude to wave force transfer function $|\Gamma(\omega,\theta)|$. This transfer function can be measured in a test on a model held fixed in place. Such a test was conducted at MIT in 1979 on a model of a TLP.

Model Description

The model is shown in Figure 1. It consisted of four large cylindrical columns connected together by the deck and by small tubular braces. A typical column is shown in Figure 2. The model was ballasted to float at its design water line as if the tension elements were in place. The dis-

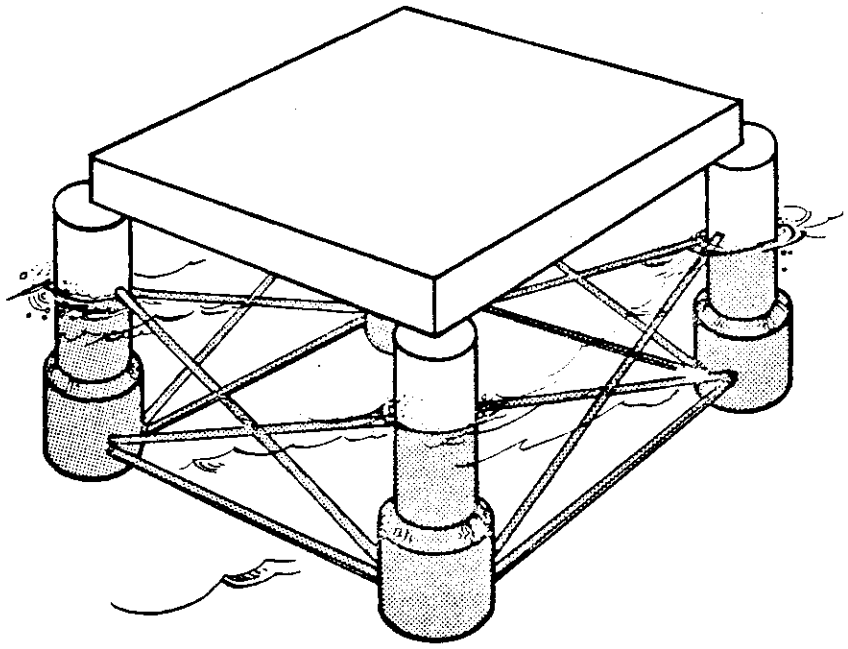

FIGURE 1. TLP MODEL

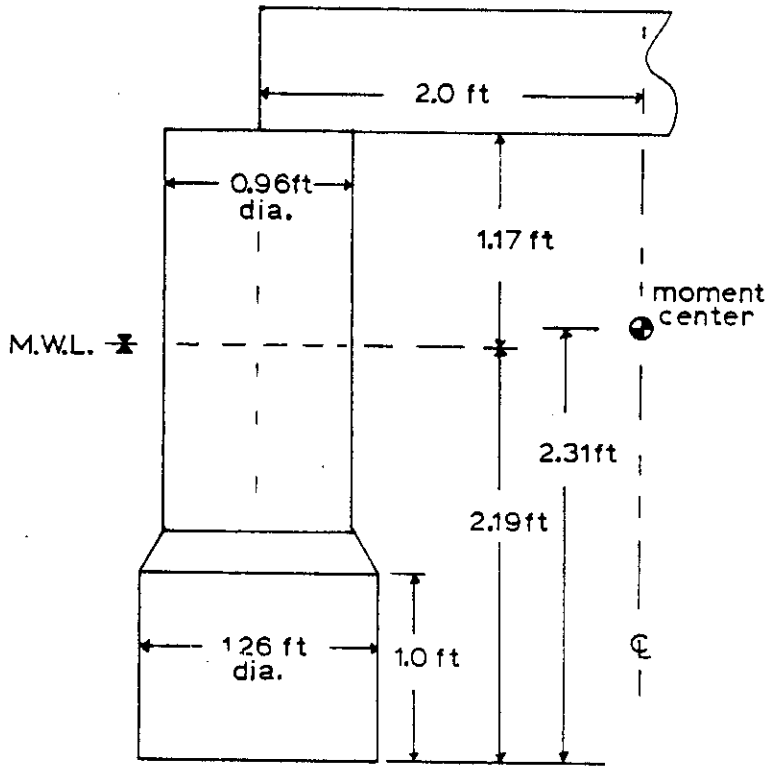

FIGURE 2. DIMENSIONS of a TYPICAL COLUMN

placement of the model was 560 pounds (254 kg). The distance between leg centers was 4.0 feet (1.22 m).

The model was rigidly attached via five load cells to a rigid steel bridge spanning the towing tank. Three load cells (V1, V2, V3 in Figure 3) oriented vertically were attached to the deck of the model at the vertices of an equilateral triangle. The connection points to the model could be varied in 5° increments up to 45°. The points were at a constant radius from the center of the deck. Two horizontal cells, orthogonal to one another were attached to the center of the deck of the model. These horizontal cells could rotate with the model. Through various trigonometric relations, these five load cell outputs could be combined to yield the total rigid body exciting forces in heave, pitch, roll, surge, and sway. Yaw moment was not measured.

The load cell outputs and the output of the wave staff were sampled at 50 Hz per channel using a Digital Equipment Corporation MINC 11/03 laboratory computer.

The model was constructed so that the angle of incidence of the waves could be varied by rotating the model under the bridge in five degree increments from 0 to 45° incidence. The computer software was written so as to be able to resolve the rigid body exciting forces at all possible incidence angles. Because of the square shape and twofold symmetry of the model, it was not necessary to rotate the model more than 45°. For example, the pitch moment transfer function for angles of incidence greater than 45° can be obtained from the roll moment transfer function for incidence angles of less than 45° from the following relationship

$$|\text{Pitch moment } (\theta)| = |\text{Roll moment } (90°-\theta)| \qquad (6)$$

Model Test Procedures

Exciting forces were measured at ten incidence angles and seven regular wave frequencies. The model had a nominal scale ratio of 50:1, so the model wave frequencies were higher by the factor of $\sqrt{50}$ than prototype wave frequencies and wave heights were 1/50 prototype wave heights.

For each combination of wave frequency and incidence angle three wave amplitudes were used to confirm linearity of the wave force transfer

function. In prototype scale the wave heights varied from 3 to 12 feet (.9 to 3.7 m).

Table 1 shows the model and corresponding prototype wave periods, frequencies, and wave lengths.

TABLE 1

MODEL FREQUENCIES AND CORRESPONDING PROTOTYPE FREQUENCIES, WAVELENGTHS, AND PERIODS

f_{model} (Hz)	f_{pro} (Hz)	ω_{pro} (rad/sec)	τ_{pro} (sec)	λ_{pro} (feet)
1.5	.212	1.33	4.71	114
1.131	.160	1.005	6.25	200
1.013	.143	.900	6.98	250
0.90	.127	.800	7.86	316
0.788	.111	.700	8.97	412
0.675	.0955	.600	10.48	562
0.50	.0707	.444	14.14	1024

In the planning of this experiment, it was recognized that this particular model was too large for the MIT tank. The tank is 8 feet 4 inches wide (2.54 m), and the maximum diagonal measurement of the model is in excess of six feet (2m). At a 45° wave incidence angle there was less than 12 inches (.3m) of wall clearance on each side. It was expected, and later confirmed, that for short wave periods cross tank waves generated around the model might create considerable difficulty. However, since the objective of the experiment was to prove feasibility, it was felt that objectives could be met.

Another problem to be expected with a model which is large compared to the width of the tank is the reflection of waves back toward the wave maker. This model was approximately 30 feet (9.1m) from the wave maker. The wave staff was placed halfway in between. After turning on the wave maker, data acquisition could commence only after steady state regular waves were passing the model. Reliable data acquisition terminated once substantial standing waves developed between the model and the wave maker. Useable data windows ten to twenty seconds in length were achieved.

The most serious mechanical difficulty encountered in the experiment resulted from the requirement that the model mounted on load cells must have natural frequencies considerably higher than the highest wave frequencies to be tested. The design of the support system for this experiment emphasized maximum stiffness. As a result, the lowest natural frequency of the frame, with the 560 pound model attached, in water was approximately 4Hz. The highest wave frequency used in the test was 1.5Hz. Dynamic response of the model was not a problem.

Numerical Predictions

Wave amplitude to wave force transfer functions were measured for heave, pitch, roll, surge, and sway at seven wave frequencies and ten angles of incidence. The measured transfer functions were compared to numerical predictions provided by Ron Nordgren of Shell Development Corp. The numerical predictions were generated by a computer code known as MOSAS. MOSAS is a wave force and motion simulation program originally developed for the prediction of seakeeping behavior of semi-submersibles. It has been thoroughly described in reference [11], and therefore shall not be described in detail here.

Comparison of Experimental Results and Numerical Predictions

A typical data set is presented as the magnitude of a transfer function, plotted in polar coordinates as a function of wave incidence angle. Each plot represents one rigid body degree of freedom transfer function at one wave frequency. Five types of transfer functions were determined at seven wave frequencies. Of the thirty-five possible combinations, four are given as examples in Figures 4 to 6.

The examples shown are the surge force transfer function at prototype wave periods of 10.5 and 6.25 seconds and the pitch moment transfer function at the same wave periods. A prototype period of 6.25 seconds corresponds to a wave length exactly equal to the major leg spacing of 200 feet (60.96m). The plots are shown for angles of incidence of 0 to 90° only. Due to the symmetry of the TLP the transfer functions have mirror images about the 0° and 90° axis.

Both the surge and pitch transfer functions at the longer wave period (10.5 seconds) show quite good agreement between prediction and measurement (Figure 4). This might have been anticipated. The computer prediction is

more accurate for long period waves because diffraction effects are less important. The model test results are more reliable, because the wall effect is less troublesome.

On the other hand, the results for the 6.25 second waves show very poor agreement for angles of incidence greater than 45°. For these tests, cross tank waves were a significant problem. Also, only an approximate correction for diffraction was made in the numerical predictions. The pitch moment transfer functions were computed about a point which is at the center of the platform in the horizontal plane and 2.31 feet (.704m) above the bottom of the columns (Figure 2).

Radiation Damping

The radiation damping coefficients for rigid body motions may be computed using the data shown in the transfer functions. The surge resonance of a TLP has such a long period (order of 2 minutes in 2000 feet (610m)) that the linear radiation damping is insignificant. This is confirmed by the fact that second order forces account for the long period drift motions of the TLP. However, pitch resonances, for example, occur at much shorter periods and the ratio of radiation to total damping may be very important.

The radiation damping for pitch motions about the moment center shown in Figure 2 may be computed from experimental data using a discrete form of Equation 3 as shown below.

$$R_{rad}(\omega_o) = \frac{\omega_o^3}{2\rho g^3} \left(\frac{1}{n+1}\right) \sum_{i=0}^{n} \left|\Gamma_p(\omega_o, i\Delta\theta)\right|^2 \qquad (7)$$

For our experiments $\Delta\theta=5°$ and n=35. For values of n>17 the symmetry properties of $\Gamma_p(\omega,\theta)$ are invoked. As an example, the pitch radiation damping coefficient at an oscillation period of 6.25 seconds was computed using the data from Figure 5. Because the wall disturbance was so great, the computer predicted values were used in place of the measured ones. The result was

$$R_{rad,\ pitch}^{(T=6.25S)} = 2.36 \times 10^9 \quad (n\text{-}m\text{-}s) \qquad (8)$$

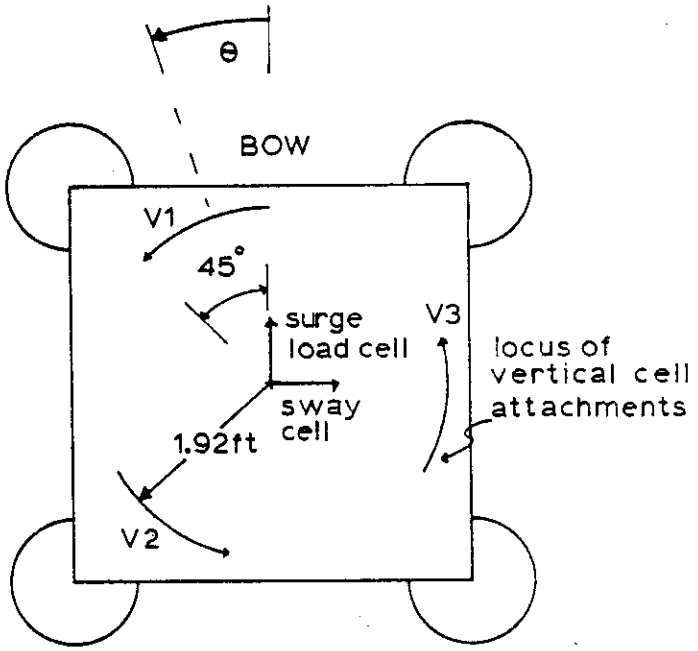

FIGURE 3. DECK ATTACHMENT POINTS FOR LOAD CELLS

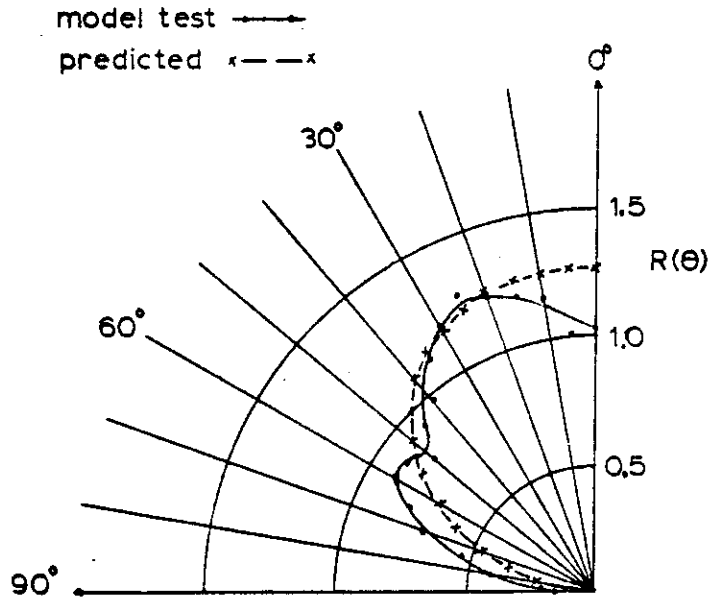

$H_p(\theta) = R(\theta) \times 83.54 \times 10^6$ n-m/m

$H_s(\theta) = R(\theta) \times 4.27 \times 10^6$ n/m

T = 10.5 s

FIGURE 4. SURGE FORCE & PITCH MOMENT PER METER WAVE AMPLITUDE

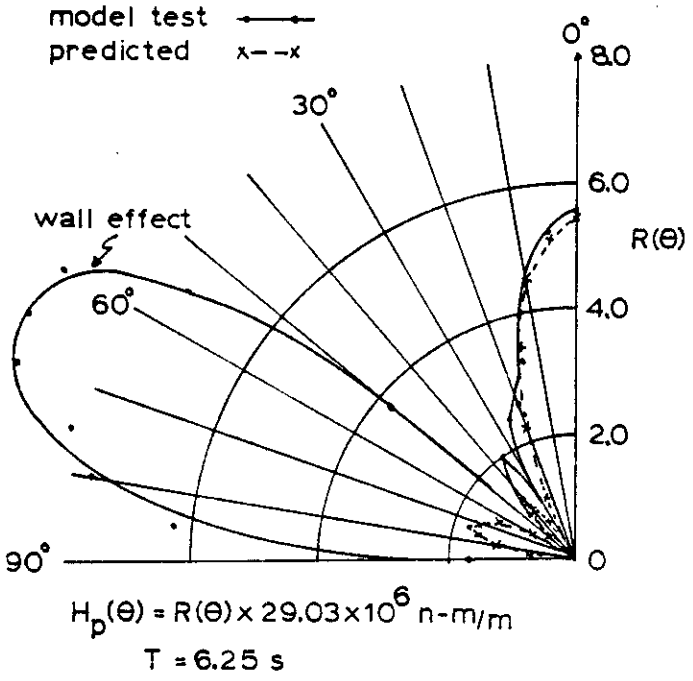

FIGURE 5. PITCH MOMENT PER METER WAVE AMPLITUDE at T = 6.25 s

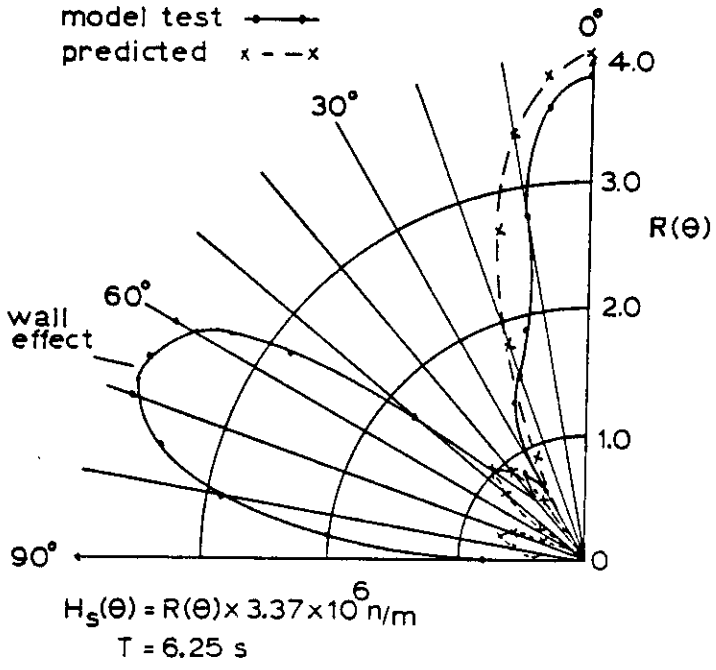

FIGURE 6. SURGE FORCE PER METER WAVE AMPLITUDE at T = 6.25 s

To obtain the ratio of radiation to total damping, the other sources of damping, coming from the material, viscous hydrodynamic, and foundation losses must also be estimated. An example of such an estimate is given in reference [10]. This estimated radiation damping would vary somewhat depending on the actual mode shape of the pitching motions, which would depend upon water depth as well as mass distribution on the structure.

RESPONSE PREDICTION

With estimates of the transfer functions available it is a relatively simple matter to estimate the damping controlled resonant response of one of the structural modes. The computation of the constant C_1 with Equation 5 is the key.

As an example, the computation of the pitch response at a natural period of 6.25 seconds is presented here for a fully developed Pierson-Moskowitz sea state.

The worst case would be for unidirectional waves incident on the bow at $\theta=0^o$. For this case, the computation of C_1 is quite simplified.

$$C_1 = \frac{\int_o^{2\pi} S_\eta(\omega_o)\,\delta(\theta=0)\,|\Gamma_p(\omega_o,\theta)|^2\,d\theta}{S_\eta(\omega_o)\,\langle|\Gamma_p(\omega_o,\theta)|^2\rangle_\theta} = \frac{|\Gamma p(\omega_o,\theta=0)|^2}{\langle|\Gamma_p(\omega_o,\theta)|^2\rangle_\theta}$$

$$= \frac{|\Gamma_p(\omega_o,0)|^2}{\frac{2\rho g^3}{\omega_o^3}\,R_{rad}} \qquad (9)$$

where $\delta(\theta=0)$ is the delta function at $\theta=0$. The value for $|\Gamma_p(\omega_o,0)|$ can be obtained from Figure 6, and R_{rad} has been previously computed.

$$|\Gamma_p(\omega=1.005\ \text{rad/S},\ \theta=0)|^2 = 2.48 \times 10^{16}\, n^2$$

Substitution of the appropriate values yields $C_1 = 5.7$.

For a Pierson-Moskowitz sea corresponding to a wind speed of 40 knots(20 m/s), $S_\eta(\omega_o) = .73\ m^2\text{-S}$.

Substitution of values for C_1, ω_o, and $S_\eta(\omega_o)$ into Equation (4)

yields an estimate of the response energy in pitch motion in the damping controlled region about ω_o.

$$\langle E \rangle = 9.7 \times 10^6 \frac{R_{rad}}{R_T} \text{ n-m} = 7.1 \times 10^6 \frac{R_{rad}}{R_T} \text{ ft -lbs} \qquad (10)$$

This is the average energy of response of the pitch mode at all frequencies included in the two half power bandwidth region centered on ω_o. This average energy can be interpreted as the average maximum strain energy or kinetic energy, and can therefore be used to compute directly mean square values of the deflections of the tension elements or rotational velocities of the structure. Furthermore, if the wave forces are represented by a stationary Gaussian random process, then the response is also stationary and Gaussian and knowledge of the mean square response is all that is required to compute the statistics of response peaks according to the Rayleigh probability distribution.

This example is overly conservative due to the unidirectional nature of the waves. If a cosine squared spreading function was introduced in Equation 5 and the result was numerically evaluated, C_1 would reduce to 3.47. This results in a 39% reduction in predicted response energy. With additional wave spreading C_1 tends to 1.0.

Until one has accurate information on the ratio R_{rad}/R_T a conservative upper bound value of 1.0 may be used.

This example described simple pitch rotations about a fixed point. For an actual TLP the pitch mode will be more complex and refinements in the measurements and predictions would be necessary. The theory as presented is appropriate.

Conclusions

The direct measurement of linear wave forces on a model held fixed in place may be used to predict the dynamic response of a natural mode of a TLP. The effects of directional wave spreading may be easily taken into account. The relation between radiation damping and exciting forces has been shown to be a key link in the understanding of the response prediction problem.

Acknowledgements

This work was sponsored by the Branch of Marine Oil and Gas Operations of the U.S. Geological Survey and by Shell Oil Company. The model was provided by Shell. Special thanks is extended to Ron Nordgren of Shell for his preparation of the numerical predictions. Mike Cook and Bruce Dunwoody, recent students, made invaluable contributions in model preparation, data acquisition, and data reduction.

REFERENCES

1. Haskind, M.D.: "The Exciting Forces and Wetting of Ships in Waves, Isvestia Akademii Nauk S.S.S.R., Otdelenie Tekhnicheskikh Nauk (1957) No. 7, 65-79 (English translation available as David Taylor Model Basin Translation No. 307, March 1962).

2. Newman, J.N.: "The Exciting Forces on Fixed Bodies in Waves," J. of Ship Research, SNAME (Dec. 1962) 6, No. 3.

3. Smith, P.W. Jr., "Estimating structural response to noise," J. Acoust. Soc. Am. 32, 929(A)(1960).

4. Lyon, R.H. and G. Maidanik, "Power flow between linearly coupled oscillators," J. Acoust. Soc. Am. 34, 623-639(1962).

5. Lyon, R.H.: Statistical Energy Analysis of Dynamical Systems: Theory and Applications, MIT Press, Cambridge, MA(1975).

6. Vugts, J.H.: "The Hydrodynamic Coefficients for Swaying, Heaving and Rolling Cylinders in a Free Surface," International Shipbuilding Progress(1968)15.

7. Vandiver, J.K.: "Structural Evaluation of Fixed Offshore Platforms," Doctoral Dissertation, MIT, January 1975.

8. Schott, W.E. III: "Response and Radiation of Structures in an Irregular Seaway," MS Thesis, MIT, Dept. of Ocean Engineering, Cambridge, MA(June 1977).

9. Vandiver, J.K.: "Prediction of the Damping-Controlled Response of Structures to Random Wave Excitation," Society of Petroleum Engineers Journal, Feb. 1980.

10. Cook, M.F., Vandiver, J.K.: "Measured and Predicted Dynamic Response of a Single Pile Platform to Random Wave Excitation," Proc. 1982 Offshore Technology Conference, Paper No. 4285.

11. van Opstal, G.H. et al.: "MOSAS: A Motion and Strength Analysis System for Semisubmersible Units and Floating Structures," Proc. 1974 Offshore Technology Conference, Paper No. 2105.

MEASUREMENTS OF THE VORTEX EXCITED STRUMMING VIBRATIONS OF MARINE CABLES

J. K. Vandiver, Massachusetts Institute of Technology, Cambridge, MA 02139

O. M. Griffin, Naval Research Laboratory, Washington, DC 20375

ABSTRACT

Field experiments were conducted during the summer of 1981 to study the strumming vibrations of marine cables. One of the objectives of the experiments was to validate and, if necessary, to provide a data base for modifying the computer code NATFREQ. This code was developed at the California Institute of Technology for the Naval Civil Engineering Laboratory (NCEL) to calculate the natural frequencies and mode shapes of taut cables with large numbers of attached discrete masses. Time histories of the measured hydrodynamic drag coefficients, current speeds, and cable strumming responses are presented here for selected test runs with a bare cable and for a cable with attached masses. Also, a comparison is made between NATFREQ- predicted and measured natural frequencies and mode shapes for the test cable.

INTRODUCTION

The vortex-excited oscillations of marine cables, commonly termed strumming, result in early fatigue, larger hydrodynamic forces and amplified flow noise, and sometimes lead to structural damage and eventually to costly failures. Flow-excited oscillations very often are a critical factor in the design of underwater cable arrays, mooring systems, drilling risers, and offshore platforms, since the components of these complex structures usually have bluff cylindrical shapes which are conducive to vortex shedding when flowing water is incident upon them. An understanding of the basic nature of vortex-excited oscillations is an important consideration in the reliable and economical design and operation of offshore structures and cable systems. The resonant strumming response of bare cables is discussed in detail in a recent NCEL/NRL report (1). The suppression of strumming vibrations is dealt with in a separate NCEL-sponsored report (2).

As part of the overall NCEL cable dynamics research program, a series of laboratory and field experiments have been conducted to investigate the effects of attached masses and sensor housings (discrete or lumped masses) on the overall cable system response. Towing channel experiments were conducted with a "strumming rig" developed for the NCEL cable dynamics program and the test findings recently were reported (3). A test program was conducted during

the summer of 1981 to investigate further the strumming vibrations of marine cables in a controlled field environment. The experiments were funded by NCEL, the USGS and industry sponsors, planned by NRL and MIT, and conducted at the field site by MIT. A primary objective of the test program was to acquire data to validate and, if necessary, to provide a basis for modifying the NCEL-sponsored computer code NATFREQ (4). This code was developed in order to calculate the natural frequencies and mode shapes of taut marine cables with large numbers of attached masses.

The purpose of this paper is to describe the field test program and to present some initial results from it. Also, calculations using the NATFREQ code have been made at NRL for all of the field test runs and a comparison is made with selected test data that have been analyzed in sufficient detail. Time histories of the measured hydrodynamic drag coefficients, current speeds, and cable strumming responses are presented and discussed. Predictions are made of the hydrodynamic drag on a bare cable and these predictions are compared with the field test data for selected conditions when the cable was observed to be resonantly strumming.

THE TEST SITE AND INSTRUMENTATION

The Test Site

The site chosen for the experiment was a sandbar located at the mouth of Holbrook Cove near Castine, Maine. This was the same site used for previous experiments during the mid-1970's by Vandiver and Mazel (5,6). At low tide the sandbar was exposed allowing easy access to the test equipment, while at high tide it was covered by about ten feet of water. The test section was oriented normal to the direction of the current which varied from 0 to 2.4 ft/s over the tidal cycle with only small spatial variation over the test section length at any given moment.

The data acquisition station for the experiment was the *R/V Edgerton* which was chartered from the MIT Sea Grant Program. The *Edgerton* was moored for the duration of the experiment approximately 300 feet from the sandbar and connected to the instruments on the sandbar by umbilicals.

Prior to the data acquisition phase of the experiment, several days were needed to prepare the site. A foundation for the experiment was needed to anchor the supports which were to hold the ends of the test cylinders. To accomplish this, six 4.5 inch diameter steel pipes were water jetted into the sandbar utilizing the fire pump aboard the *Edgerton*. These six pipes were made of two five foot sections joined by couplings so that the overall length of each was ten feet. In addition, one two-inch diameter by six foot long steel pipe was jetted into the sandbar

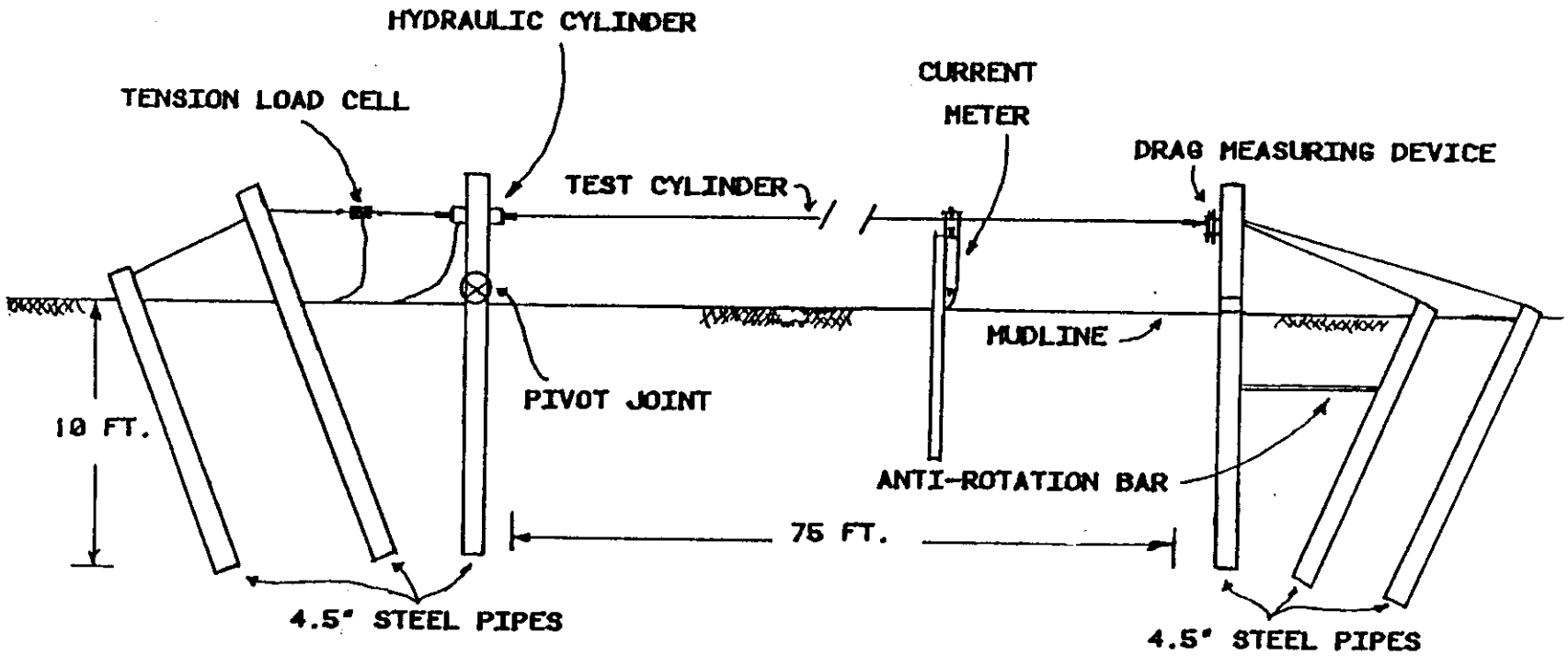

FIGURE 1. SCHEMATIC DIAGRAM OF THE EXPERIMENT TEST SECTION

to be used as a current meter mount. Finally, a section of angle iron was clamped to the pipe used to support the drag measuring mechanism and attached to another support pipe to prevent any rotation of the drag mechanism mount. Figure 1 shows a schematic diagram of the set-up of the experiment.

Test Instrumentation

Drag measurement system. The drag measurement system was located at the west end of the cable system as shown in Figure 1. The device was welded onto a support pipe 2.5 feet above the mud line. The mean drag force at the termination of the cable was used to generate a moment about a freely rotating vertical shaft located a few inches beyond the termination point. The bearings supporting the shaft carried the entire tension load without preventing rotation. The moment was balanced by a load cell which restrained a lever arm connected to the shaft (see Figure 2). From the known level-arm lengths and the load cell measurements the mean drag force on one half of the cable could be determined. The load cell signal was carried by wires in the cable and umbilical to the *Edgerton* where it was conditioned and recorded.

Current measurement system. The current was measured by a Neil Brown Instrument Systems DRCM-2 Acoustic Current Meter located 12.5 ft from the west end of the test cable and 2 ft upstream. It was set so that it determined both normal and tangential components of the current at the level of the test cable. Signals from the current meter traveled through umbilicals to the *Edgerton* where they were monitored and recorded. In addition, a current meter traverse was made using an Endeco current meter to determine any spatial variations in current along the test section. The current was found to be spatially uniform to within 3.0 percent from end to end for all but the lowest current speeds ($V < 0.5$ ft/s).

Tension measurement system. The tension measuring and adjusting system was located at the east end of the experimental test set up (see Figure 1). Extensions were made to the two inner water jetted posts at this end. As shown in the diagram, a five foot extension was made to the center post and a three foot extension was made to the innermost post. This three foot extension was different from the rest in that its attachment to the jetted pipe at the mudline was a pin connection as compared to the standard pipe couplings used on the other extensions. Onto this pivoting post, a hydraulic cylinder was mounted 2.5 feet above the mudline. The test cable in the experiments was connected at one end to this hydraulic cylinder and at the other end to the drag measuring device. To the back of the hydraulic cylinder one end of a Sensotec Model RM In-Line load cell was connected. The other end of the cell was attached via a cable

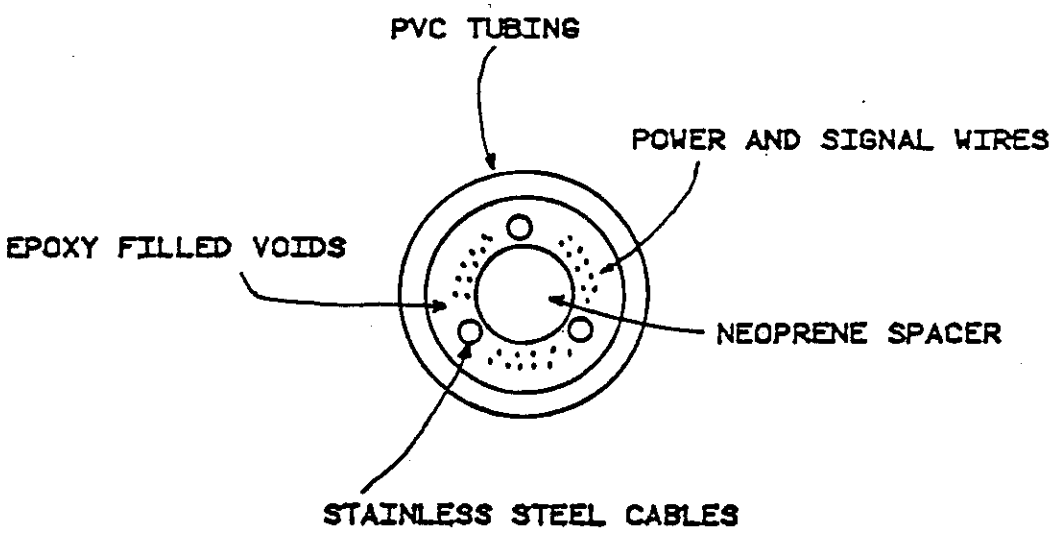

FIGURE 2. SECTION OF TEST CABLE

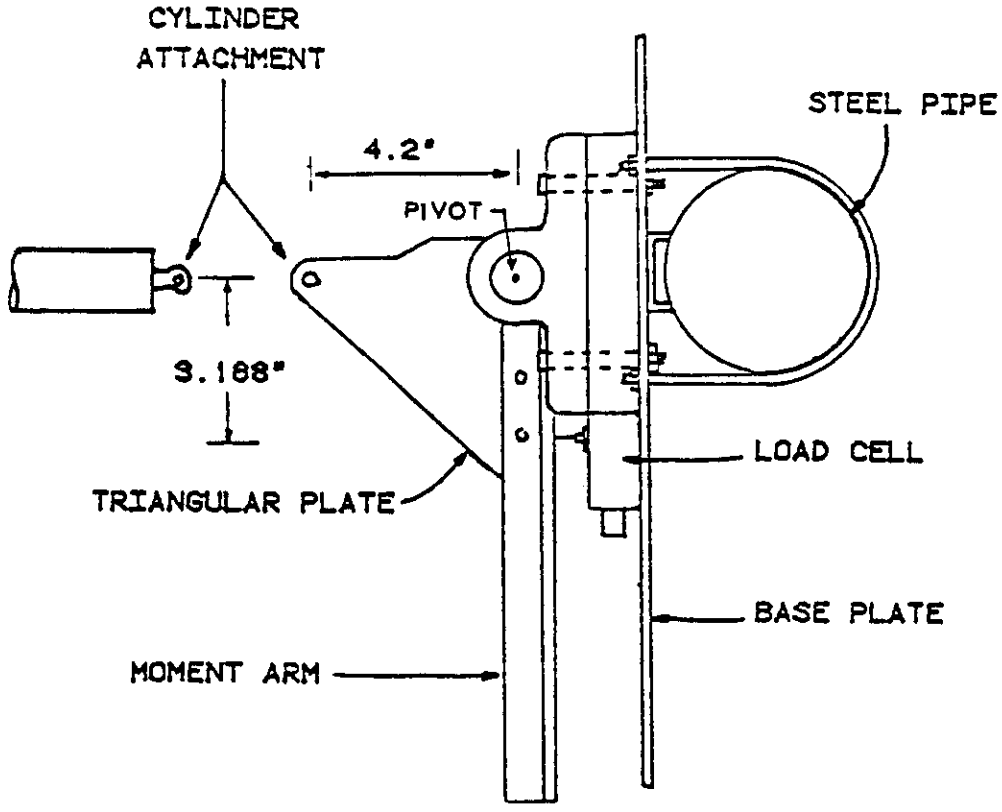

FIGURE 3. DIAGRAM OF THE DRAG MEASURING DEVICE - TOP VIEW

to the center post. The output from the tension load cell was transmitted through the umbilicals to the *Edgerton* where it was monitored. Hydraulic hose ran from a pump on the *Edgerton* to the hydraulic cylinder so that the tension could be changed as desired. Additional details concerning the test instrumentation are given by McGlothlin (7).

Data Acquisition Systems

During the experiment, data taken from the instruments on the sandbar were recorded in two ways. First, analog signals from the fourteen accelerometers in the cable as well as current and drag were digitized, at 30.0 Hz per channel, onto floppy disks using a Digital Equipment MINC-23 Computer. Second, analog signals from the drag cell, current meter, and six accelerometers were recorded by a Hewlett-Packard 3968A Recorder onto eight-track tape. The disks were limited to record lengths of eight and one half minutes and were used to take data several times during each two and one half hour data acquisition period. A Hewlett-Packard 3582A Spectrum Analyzer was set up to monitor the real time outputs of the accelerometers. The eight-track tape was used to provide a continuous record of the complete two and one half hour data cycle.

THE TEST CABLE SYSTEM

The Cable

A 75 foot long composite cable was developed specifically for the experiments that were conducted in the summer of 1981. Figure 3 shows a cross-section of the test cable. The outer sheath for this cable was a 75 foot long piece of clear flexible PVC tubing, which was 1.25 in. O.D. by 1.0 in. I.D. Three 0.125 in. stainless steel cables ran through the tubing and served as the tension carrying members. A cylindrical piece of 0.5 in. O.D. neoprene rubber was used to keep the stainless steel cables spaced 120 degrees apart. The neoprene rubber spacer was continuous along the length except at seven positions where biaxial pairs of accelerometers were placed. Starting at the east end, these positions were at L/8, L/6, L/4, 2L/5, L/2, 5L/8, and 3L/4. These accelerometers were used to measure the response of the cable as it was excited by the vortex shedding. The accelerometers were Sundstrand Mini-Pal Model 2180 Servo Accelerometers which were sensitive to the direction of gravity. The biaxial pairing of these accelerometers made it possible to determine their orientation and to extract real vertical and horizontal accelerations of the cable at the seven locations.

Three bundles of ten wires each ran along the sides of the neoprene spacer to provide power and signal connections to the accelerometers and also to provide power and signal con-

nections to the drag measuring system. Finally, an Emerson and Cuming flexible epoxy was used to fill the voids in the cable and make it watertight. The weight per unit length of this composite cable was 0.77 lb/ft in air.

The Attached Masses

In some experiments, lumped masses were fastened to the bare cable to simulate the effects of sensor housings and other attached bodies. The lumped masses were made of cylindrical PVC stock and each was 12.0 in. long and of 3.5 in. diameter. A 1.25 in. hole was drilled through the center of each lumped mass so that the cable could pass through. In addition, four 0.625 in. holes were drilled symmetrically around this 1.25 in. center hole so that copper tubes filled with lead could be inserted to change the mass of the lumps. In the field, it was difficult to force the cable through the holes drilled in the PVC so the masses were split in half along the length of their axes. The masses were then placed on the cable in halves and held together by hose clamps. Different tests were run by varying the number and location of lumped masses and by changing the mass of the attachments.

MEASUREMENTS OF CABLE STRUMMING

Bare Cable

Several test runs were conducted with the bare cable during the experiments to provide a basis for comparison to the cable with attached masses. A 300 second time history for one bare cable test run is shown in Figure 4. The cable was resonantly strumming at 1.9 Hz in the third mode normal to the current and non-resonantly vibrating in the fifth mode in line with the flow at 3.8 Hz. The vertical and horizontal RMS displacement amplitudes were derived from the time records of the accelerometer pair at a location L/6 along the cable. For the third mode this location corresponds to an antinode of the cable vibration. The fifth mode amplitudes at this location are one-half the antinode maximum. The vertical displacement amplitude is approximately ± 0.6 to 0.7 diameters (RMS) over the length of the record. The tension in this test was 360 pounds. The damping ratio measured in air for the third mode was 0.15 percent. The reduced damping (1) for this cable was $\zeta_s/\mu = 2\pi St^2 k_s = 0.06$.

The average drag force coefficient on the cable is approximately $C \cong 3.2$; this is considerably greater than the drag coefficient $C_{DO} = 1.2$ that would be expected if the cable were restrained from oscillating under these flow conditions. The drag coefficient on the strumming cable was predicted with the equation

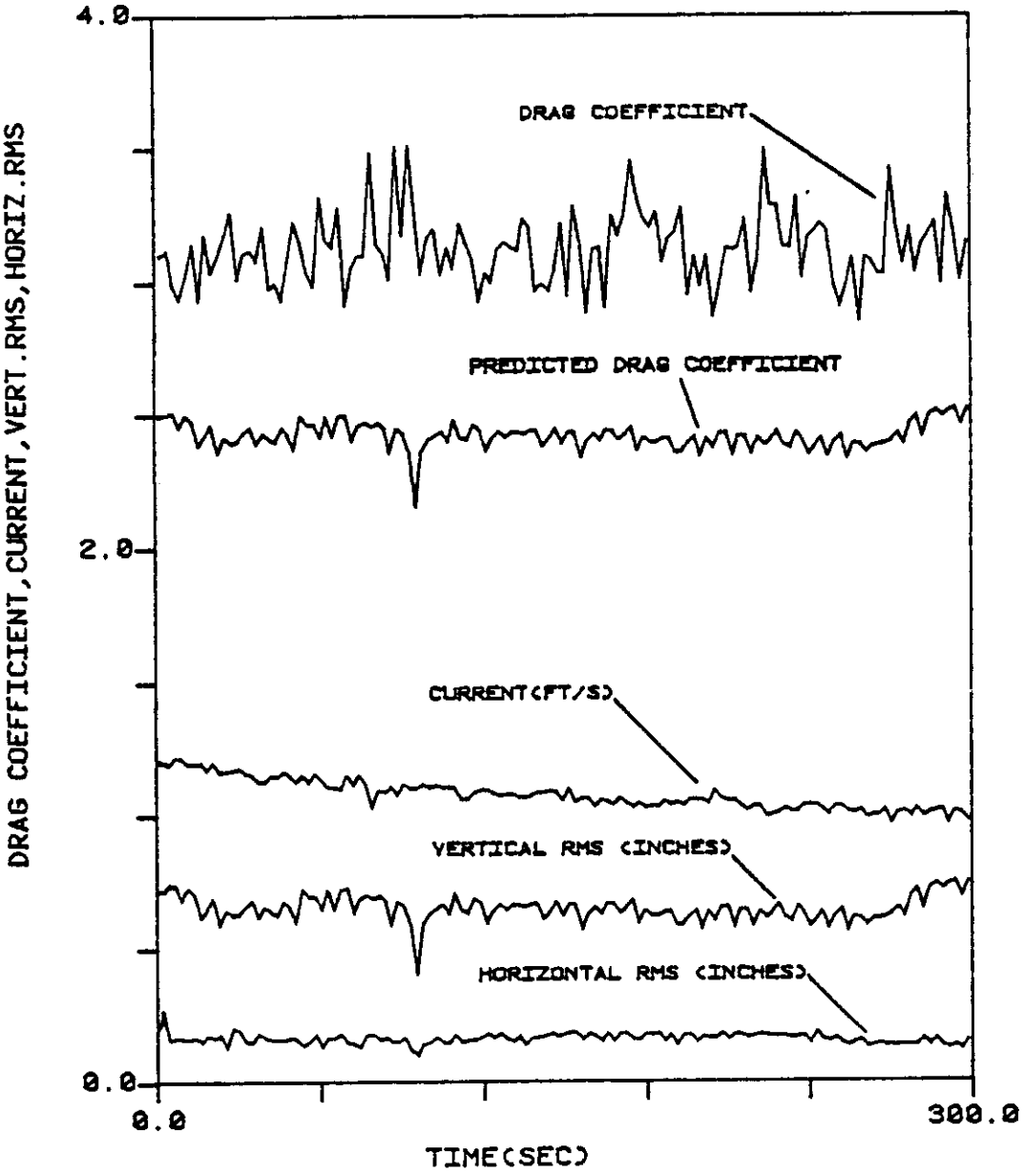

FIGURE 4. PREDICTED DRAG COEFF. FOR BARE CABLE DURING THIRD MODE VERTICAL AND FIFTH MODE HORIZONTAL RESPONSE. VERTICAL RMS AT L/6.

$$C_{D,AVG} = C_{DO}\,[1 + 1.043\,(2\bar{Y}_{RMS}/D)^{0.65}],$$

which is derived from the original equation proposed by Skop, Griffin and Ramberg (8,9). Here C_{DO} is the stationary cable drag coefficient. This equation takes into account the modal distribution in displacement amplitude along the cable. $\bar{Y}_{RMS}/D$ is the root-mean-square antinode displacement in diameters. The strumming drag coefficient predicted using this equation is in the range C_D = 2.4 to 2.6 as shown in Figure 4; this is approximately 15 percent below the drag force coefficient measured at the field site. The results of these field test runs clearly verify the large amplification in hydrodynamic drag due to strumming that has been measured previously in laboratory-scale experiments (1,8,9).

Cable with Attached Masses

Ten test runs were conducted at the field site with different combinations of locations, numbers, and masses of the attached cylindrical lumps. Tests were run in air and in water for each of the ten combinations. The in-air tests provided measures of the structural damping from vibration decay tests and of the natural frequencies and mode shapes. An example taken from one of the more complex test runs is shown in Figure 5. Six masses were attached to the cable: two light cylinders (m = 4.4 lb_m or 2 kg) at x = L/8 and L/2; and four heavy cylinders (m = 10.0 lb_m or 4.5 kg) at x = L/3, 5L/8, 3L/4 and 7L/8. The RMS strumming response data shown for a two and one half hour time period in Figure 5 were recorded at x = 3L/4, where both one of the attached masses and an accelerometer pair were located.

Several important results of the experiments can be observed from Figure 5. The vibration level over the time of the test run was approximately 0.3 diameters (RMS), indicating that the attached mass did not act as a node of the cable system vibration pattern. The drag coefficient of the system was C_D = 2.4 to 3.2 which again represented a substantial amplification from the stationary cable value of $C_{DO} \cong 1.2$. The relative contributions have not yet been determined. Several segments of the time history in Figure 5 exhibit nearly constant drag and vertical RMS response levels; this is indicative of resonant lock-on between the cable vibrations and the current-induced vortex shedding. A more detailed assessment of the cable system strumming data is underway to provide further understanding of the strumming phenomenon and additional guidance for marine cable system designers.

NATFREQ PREDICTIONS

The natural frequencies and mode shapes for the field test runs were calculated at NRL with the NCEL-developed computer code NATFREQ (4). This code was developed to calcu-

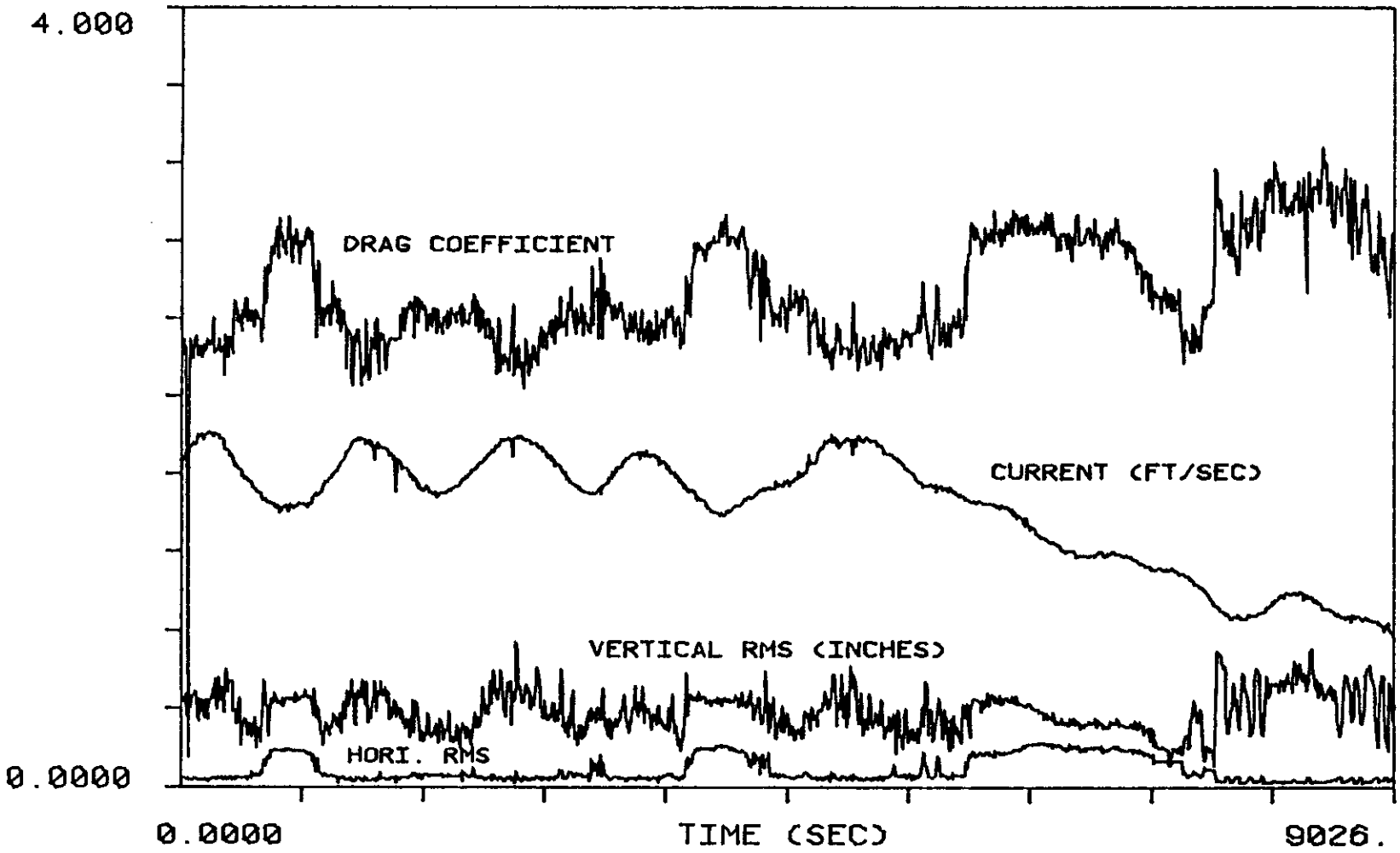

FIG 5. CABLE WITH LUMPED MASSES 10-AUG-81

RMS DATA AT X=3/4 L

late the properties of taut cables with large numbers of attached discrete masses. The equations of motion are solved by an iterative technique which allows the accurate calculation of extremely high mode numbers. It is possible with NATFREQ also to calculate the strumming drag on the cable according to the method of Skop, Griffin and Ramberg (8.9), exclusive of the drag due to any of the attached masses.

Computations were made for all of the MIT test runs, both in air and in water. The first twelve natural frequencies and mode shapes were computed, though typically only the first six cable strumming modes were excited by the currents at the test site. An example of the mode shapes is given in Figure 6. For this case the cable was fitted with seven attached 4.4 lb_m lumps. The lumps were equally spaced at intervals of the cable length divided by eight. That is, at distances from one end specified by NL/8, for N = 1 to 7.

A partial tabulation of calculated and measured natural frequencies for the same distribution of attached masses is given in Table 1. The measurements were obtained from vibration decay tests conducted in air. Typical damping ratios were 0.2 to 0.5 percent of the critical damping. Excellent agreement was obtained between the measured and computed frequencies for several of the natural cable modes. These results give a first indication of the applicability of NATFREQ to the calculation of the flow-induced vibrations of full-scale marine cable systems. Additional comparisons between the field measurements and the code predictions are underway.

SUMMARY AND CONCLUDING REMARKS

A test program has been conducted to investigate the effects of attached masses and sensor housings on the strumming response of marine cable systems. The tests were conducted during the summer of 1981 to investigate the strumming response of marine cables in a well-controlled field environment. This paper describes the test set-up, the instrumentation used, and some of the results obtained at the site.

Both an instrumented bare cable and the same cable with varying numbers and types of attached masses were employed in the experiments. The hydrodynamic drag coefficient for the bare cable was measured over extended time periods of up to two and one half hours. The measured average drag force coefficient was as large as $C_D = 3.2$, as compared to $C_{DO} \cong 1.2$ for a non-strumming bare cable under the same flow conditions. Vibrations were excited in the first six strumming modes of the cable at levels up to ± 0.6 to 0.7 diameters (RMS).

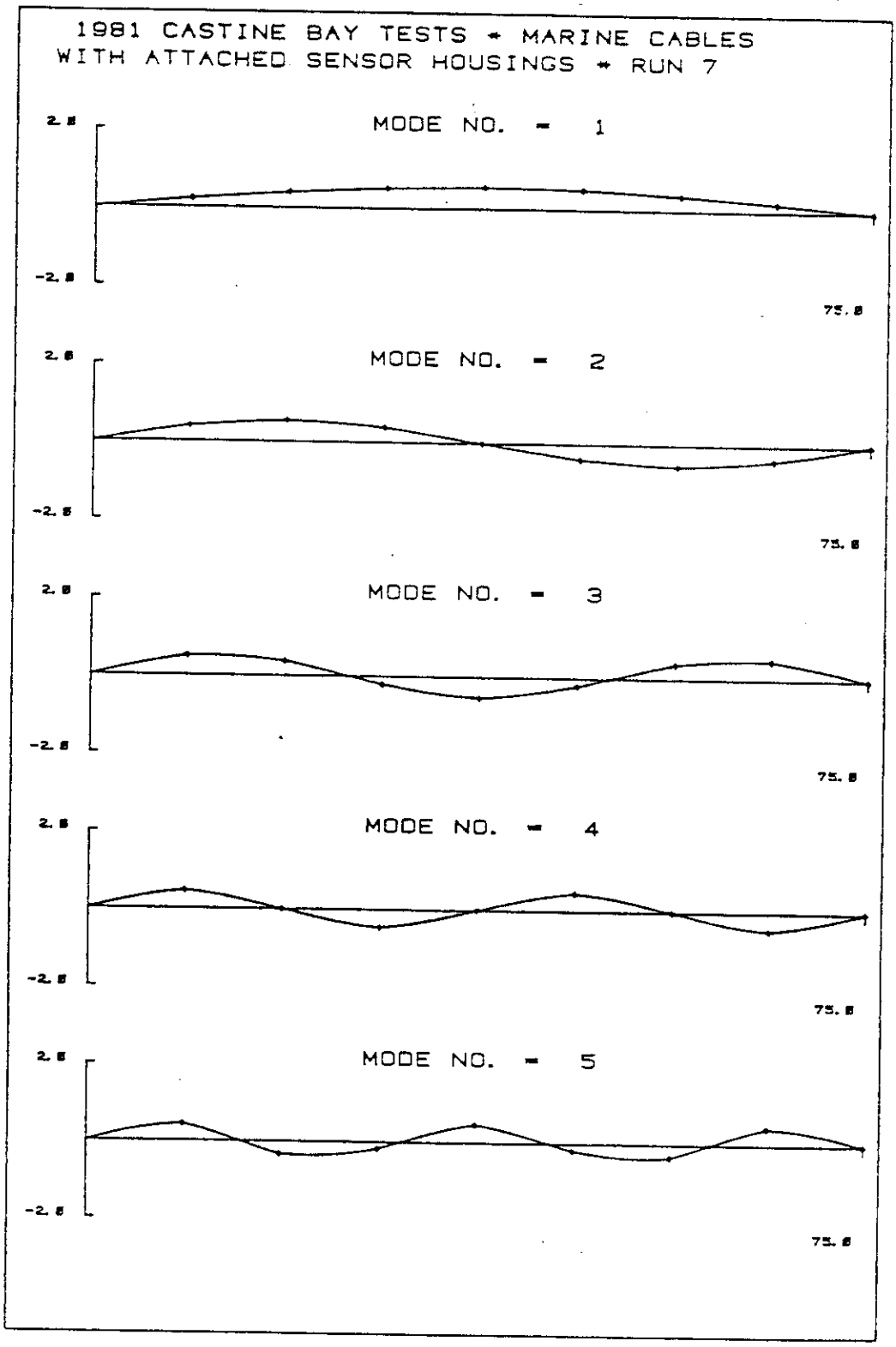

Fig. 6 — Modal vibration patterns computed with NATFREQ. Attached masses at NL/8, N = 1 to 7.

Table 1 — Measured and NATFREQ-Predicted Natural Frequencies (In Air)

Seven 4.4 lb_m Attached Discrete Masses at:

NL/8, for N = 1 to 7.

Natural Frequency, f_n/Hz		
Mode Number	Predicted	Measured
1	0.759	— — —
2	1.513	1.540
3	2.257	— — —
4	2.983	3.066
5	3.675	— — —
6	4.301	— — —
7	4.787	5.040
8	7.710	— — —

Cable specifications:

Length, L = 75 ft; Diameter, D = 1.25in.;
Specific Gravity, SG = 1.41;
Tension = 500 lb.

The cable with attached masses also underwent large-amplitude strumming vibrations. In one test described in detail vibration levels of up to ±0.3 diameters (RMS) were recorded at the location of one of six attached masses over a two and one half hour time period. The measured drag force coefficient on the cable with the six masses was in the range C_D = 2.4 to 3.2 over the same time period.

One objective of the field test program was to acquire data to validate and, if necessary, to provide a basis for modifying the NCEL-developed computer code NATFREQ (4). An initial comparison has been made of the NATFREQ-predicted and the measured natural frequencies of the cable with attached masses. Excellent agreement has been obtained and further comparisons are underway.

ACKNOWLEDGEMENTS

The experiments described in this paper were funded as part of the marine cable dynamics exploratory development program of the Naval Civil Engineering Laboratory, by the U.S. Geo-

logical Survey, and by a consortium of companies active in offshore engineering: The American Bureau of Shipping, Brown, and Root, Inc., Chevron Oil Field Research, Conoco, Inc., Exxon Production Research, Shell Development Company, and Union Oil Company. The experiments described here were part of a larger program which included tests of a steel pipe at the Castine site. These tests will be described in future publications.

REFERENCES

1. O. M. Griffin, S. E. Ramberg, R. A. Skop, D. J. Meggitt and S. S. Sergev, "The Strumming of Marine Cables: State-of-the-Art," NCEL Technical Note No. N-1608 (May 1981).

2. J. E. Kline, A. Brisbane and E. M. Fitzgerald, "Cable Strumming Suppression," MAR Incorporated Technical Report 249 (July 1980).

3. J. E. Kline, E. Fitzgerald, C. Tyler and T. Brzeska, "The Dynamic Response of a Moored Hydrophone Housing Assembly Subjected to a Steady Uniform Flow," MAR Incorporated Technical Report No. 237 on NCEL Contract No. N68305-78-C-0049 (February 1980).

4. S. S. Sergev and W. D. Iwan, "The Natural Frequencies and Mode Shapes of Cables with Attached Masses," NCEL Technical Note No. N-1583 (August 1980).

5. J. K. Vandiver and T. W. Pham, "Performance Evaluation of Various Strumming Suppression Devices," MIT Ocean Engineering Department Report 77-2 (March 1977).

6. J. K. Vandiver and C. H. Mazel, "A Field Study of Vortex-Excited Excited Vibrations of Marine Cables," Offshore Technology Conference Paper OTC 2491 (May 1976).

7. J. C. McGlothlin, "Drag Coefficients of Long Flexible Cylinders Subject to Vortex Induced Vibrations," M.S. Thesis, MIT Ocean Engineering Department (January 1982).

8. R. A. Skop, O. M. Griffin, and S. E. Ramberg, "Strumming Predictions for the SEACON II Experimental Mooring," Offshore Technology Conference Preprint OTC 2491 (May 1977).

9. O. M. Griffin, "Steady Hydrodynamic Loads Due to Vortex Shedding from the OTEC Cold Water Pipe," NRL Memorandum Report 4698 (January 1982).

OTC 4286

Multichannel Maximum Entropy Method of Spectral Analysis Applied to Offshore Platforms

by Michael J. Briggs, *Union Oil Co. of California,* and J. Kim Vandiver, *Massachusetts Institute of Technology*

ABSTRACT

The Maximum Entropy Method (MEM) is a nonlinear data adaptive method of spectral analysis which is capable of generating a higher resolution spectral estimate from shorter data records than conventional Fast Fourier Transform (FFT) methods. The MEM method has proved to be useful in the calculation of natural frequency and damping ratio estimates and their variances from ambient platform acceleration measurements. This paper presents the results of an extension of the single channel MEM to multichannel applications. A transfer function estimate using the multichannel MEM method of spectral analysis was used in mode shape identification for an Amoco offshore caisson platform located in 89 feet of water in the Gulf of Mexico. Transfer function estimates obtained from multichannel spectral analysis are superior to those obtained using autospectral methods in terms of their relative insensitivity to input and output noise. Comparison of these relative acceleration magnitudes with the relative displacement amplitudes obtained from a finite element model of the caisson platform gave reasonable agreement. Thus, this technique can be a useful tool (in conjunction with the cross-spectral estimates of magnitude, phase, and coherence) in mode shape identification for offshore platforms.

INTRODUCTION

As the petroleum industry moves into deeper waters to tap new reserves of oil and gas, the cost and size of the offshore platforms increases considerably. Substantial interest has been generated in methods of detecting structural damage by measuring shifts in natural frequencies from undamaged conditions [1,2,3]. Lack of reproducibility in determination of the natural frequencies of modes higher than the fundamentals has led researchers to conclude that detection of damage by above-waterline measurement of acceleration response to environmental loads is not feasible. One of the fundamental problems is that non-failure related sources of change are so large as to obscure changes in natural frequency which are caused by significant levels of damage.

These problems have led researchers to consider alternate measurement techniques, including (1) below-waterline measurement of global and local modes and (2) forced excitation with shakers and impulse hammers [4]. Rather than simple measurement of changes in natural frequencies; determination of mode shapes and transfer functions are being attempted [5,6]. The success of these various techniques will depend in part upon the development of powerful digital signal processing tools.

Design verification is another aspect of structural dynamics that can benefit from advances in signal processing. For the design of safe fatigue-resistant structures in ever more hostile environments, it is necessary to verify by accurate measurement the adequacy of present design methods and assumptions. Predicted and measured values of natural frequencies, damping ratios, and mode shapes are but a few of the values which should be compared. Where discrepancies occur, improvements can be made for future designs.

The first spectral estimator to be used was the periodogram. The periodogram and its variations are methods which operate directly on the data by Fourier transforming to obtain the spectral estimates. In 1958 Blackman and Tukey [7] introduced their autocorrelative method which involves the Fourier transform of the windowed autocorrelation function estimate. It is a moving average (MA) or all zero method which suffers from a severe "bias vs. variance" tradeoff. Resolution is lost due to (1) the finite record length of the autocorrelation function estimate (assumed zero beyond known lag products) and (2) the windowing operation itself. In 1965 Cooley and Tukey sparked a revival of the Fast Fourier Transform (FFT) which had been known for years but was not practical until the advent of the high speed digital computer. The direct method of calculating spectral estimates involving magnitude squaring of the transform of windowed data records became popular. Unfortunately, this method unreasonably assumes that

the data is zero outside the selected number of lags and repeats itself periodically.

In 1967 Burg [8] introduced the concept of the Maximum Entropy Method (MEM) of auto-spectral analysis. Entropy is a measure of the average information content contained in a signal. Maximizing entropy therefore maximizes the information transmitted in a signal. MEM is one of the family of nonlinear, data-adaptive methods of spectral analysis which are capable of generating a higher resolution spectral estimate from shorter data records than conventional Fast Fourier Transform (FFT) methods. This ability to use shorter data records can be an important consideration where (1) stationarity, (2) logistics of data collection, and/or (3) computer processing time and cost are a problem. Because MEM is data-adaptive, it does not suffer from the severe "bias vs. variance" tradeoff due to finite record length requirements of conventional methods. When calculating spectral estimates at one frequency, it is able to adjust itself to be least disturbed by power at neighboring frequencies.

Researchers have successfully applied the MEM method to such diverse fields as geophysics, neurophysics, and radar imagery. Campbell [9] applied the single channel version of MEM to the dual problem of natural frequency and damping ratio estimation of offshore platforms. He was able to more accurately evaluate these two parameters as well as place 95% confidence limits on these estimates. The multichannel MEM method of spectral analysis is applied in this paper to the problem of mode shape and transfer function estimation in the hope that both structural monitoring and design verification technologies may benefit.

MULTICHANNEL MAXIMUM ENTROPY METHOD OF SPECTRAL ANALYSIS

In order to assist understanding of the multichannel MEM algorithm, a brief review of the single channel MEM model as a prediction error (PE) filter will be presented. An error series, e(n), is defined as the difference between the desired or true signal, d(n), and the actual or predicted signal, y(n). The desired value is chosen as the input signal advanced one time unit ahead. The actual signal represents past values of the input signal. These past or previous values of the time series are used to predict the next value (hence the prediction error terminology). According to least squares theory, a mean square error or error power (ie. variance for zero mean process), P(L), is defined as the expected value of the square of the error signal. The energy contained in this error power must be minimized in such a way that the input signal is whitened (or the output becomes uncorrelated) as the filter order is increased [10]. The Normal or Wiener-Levinson equations are obtained as a result of this minimization and are given by

$$[R]\{A\} = \{P\} \quad \text{.....(1)}$$

where:

$[R]$ = (L+1)x(L+1) matrix of autocorrelation coefficients, 0 to 1 lags

$\{A\}$ = (L+1)x1 column vector of prediction error filter coefficients

$\{P\}$ = (L+1)x1 column vector of prediction errors

The L+1 Normal equations are then solved by the Levinson-Durbin recursion to obtain the PE filter coefficients, A. This algorithm takes advantage of the special Toeplitz symmetry of the Normal equations whereby all diagonal values in the correlation matrix are the same. The MEM spectral estimate, Sx, defined between the Nyquist frequency, fny, is then given by

$$Sx(f) = |A(f)|^2 \, Sw(f) \qquad -fny \le f \le fny \quad \text{...(2)}$$

$$= \frac{2\sigma^2(L)\,\Delta}{\left|1 - \sum_{m=1}^{L} A(m)\exp(-j2\pi fm\Delta)\right|^2}$$

where $\sigma^2(L)$ or $Sw(f)/2\Delta$ is the prediction error or white noise variance and the denominator is the magnitude squared of the Fourier transform of the PE filter coefficients. The Δ is the time increment in seconds between sampled data points. Note that the one in the denominator is actually the A(0) PE filter coefficient term.

Thus, the single channel MEM filter can be written in a form that structural dynamicists are familiar. That is, the MEM spectral estimate, Sx(f), (ie. output spectrum) is the product of the prediction error spectrum, Sw(f), (ie. input spectrum) and the magnitude of the transfer function of the PE filter squared, A(f). The MEM spectral estimate is obtained by (1) calculating the PE filter coefficients out to the desired filter order of length L, (2) calculating the PE due to a white noise signal at filter order L, (3) taking the magnitude squared of the Fourier transform of the PE coefficients, and (4) performing the operations indicated in Eq. 2.

For the multichannel MEM algorithm, the development is analogous to the single channel case. The expected mean-square values of forward and backward errors of length M ($M \le L$) are minimized for the optimum filter. As a result, the Normal equations for the pxp (p=2 for two-channel case) forward filter coefficients, CF, (analogous to the PE filter coefficients of the single channel case) are given by

$$[RF]\left\{CF(M,m)\right\} = \left\{V\right\} \quad \text{.....(3)}$$

where:

$[RF]$= forward R-matrix, Toeplitz, square block submatrices

$\{V\}^T$ = forward power matrix, [P(M) 0 0...0]

m = coefficient number

The R4 element or 2x2 submatrix of the RF matrix for a lag of 4 for the two-channel case is

$$\{R4\} = \begin{bmatrix} R11(4) & R12(4) \\ R21(4) & R22(4) \end{bmatrix} \quad \text{.....(4)}$$

where the diagonals are the autocorrelations and the off-diagonals are the cross-correlations between channels 1 and 2.

The single-sided multichannel MEM spectral estimate matrix is a function of the Fourier transform of the forward filter coefficient matrix and is given by

$$G(f) = 2\Delta[CF^{-1}(1/z)]^* \, P(M) \, [CF^{-1}(1/z)] \quad \text{..(5)}$$

where $z = \exp(-j2\pi f\Delta)$. Since the forward power, P, satisfies the condition that it is greater than zero, the filter coefficient matrices are nonsingular and invertible. Equation 5 reduces to Eq. 2 for the single channel case if matrices are replaced by vectors and vectors by scalars. The inverse matrix operations become divisions and the product of the filter coefficients with their complex conjugates gives the magnitude squared as before.

The forward filter coefficient matrix, CF, is calculated using a correlation extension method based on the Rissanen recursion. It involves the triangular decomposition of the R-matrix into a diagonal form from which psuedo-forward filter coefficients are calculated. A savings in computer storage is realized. The interested reader is referred to the papers by Strand [11] and Rissanen [12] for more details on this method.

MULTICHANNEL SPECTRAL ESTIMATION

The primary emphasis of this paper is in the application of multichannel spectral estimates to mode shape identification. In mode shape analysis, the resonant frequencies of the platform are first identified and then the order and shape of the normal modes can be determined. The more transducers (accelerometers) used, the easier the task of identifying the modes, especially the higher modes.

Normally, multichannel spectral analysis estimates include only autospectra and cross-spectral magnitude, phase, and coherence estimates. The transfer function estimate can be used to give relative displacements between accelerometer locations. Since, as we shall see, the cross-spectral transfer function estimate tends to be an unbiased estimate in comparison to autospectral estimates; it is a particularly useful quantity in mode shape identification.

The autospectral density and the cross-spectral magnitude estimates reveal peaks which may be due to either normal modes of the platform, machine noise, or excitation peaks. They are used to locate natural frequencies and half-power damping ratio estimates. The autospectra are real and non-negative. The one-sided cross-spectrum is given by

$$Gxy(f) = |Gxy(f)| \exp(-j\theta xy(f)) \qquad 0 \le f < \infty \quad \ldots\ldots(6)$$

where the magnitude and the phase are defined as

$$|Gxy(f)| = \text{SQRT}\,[Cxy^2(f) + Qxy^2(f)] \qquad 0 \le f < \infty \quad \ldots\ldots(7)$$

$$\theta xy(f) = \text{ARCTAN}\,[Qxy(f) / Cxy(f)] \qquad 0 \le f < \infty \quad \ldots\ldots(8)$$

The magnitude is real-valued and even and the phase is a real-valued and odd function of frequency f. Coupling between modes can cause the phase values to be other than zero or 180 degrees. The coincident or co-spectra density function, Cxy(f), is a real-valued even function of frequency f. The quadrature spectral density function, Qxy(f), is a real-valued odd function and is shifted 90 degrees from the co-spectra estimate.

The coherence squared (or coherence, if the square root is taken) is a normalized cross-spectrum defined by

$$\gamma^2 xy(f) = Gxy^2(f) / [Gxx(f) * Gyy(f)] \quad \ldots\ldots(9)$$

It is a measure of the fraction or portion of one signal which is due to the other. It satisfies the inequality $0 \le \gamma^2 xy(f) \le 1$. When it has a value of zero, the two channels are said to be incoherent or uncorrelated at the particular frequency. When the coherence is zero for all frequencies, the two channels are statistically independent. When the coherence equals unity at a particular frequency, the two channels are fully coherent, correlated, or dependent. Extraneous noise in the measurement will cause the coherence value to be less than unity. The predicted modal deflections will be underpredicted if the coherence is much less than unity.

For an ideal, causal, stable, linear physical system; the measured output or response, y(t), is related to the measured input or excitation, x(t), by the convolution or superposition integral.

$$y(t) = \int_0^t h(\tau)\, x(t - \tau)\, d\tau \quad \ldots\ldots\ldots\ldots(10)$$

where $h(\tau)$ is the unit impulse response. The corresponding frequency domain expression in terms of the transfer function or frequency response function, H(f), is

$$Y(f) = H(f)\, X(f) \quad \ldots\ldots\ldots\ldots\ldots\ldots(11)$$

The single-sided auto and cross-spectra in terms of the transfer function are

$$Gyy(f) = |H(f)|^2\, Gxx(f) \quad \ldots\ldots\ldots\ldots\ldots(12)$$

$$Gxy(f) = H(f)\, Gxx(f) \quad \ldots\ldots\ldots\ldots\ldots(13)$$

Consider a system with input, m(t), and output, n(t), noise terms related to the true input, u(t), and true output, v(t), signals by

$$x(t) = u(t) + m(t) \quad \ldots\ldots\ldots\ldots\ldots\ldots(14)$$

$$y(t) = v(t) + n(t) \quad \ldots\ldots\ldots\ldots\ldots\ldots(15)$$

Thus, x(t) and y(t) are the measured values of input and output respectively. The noise terms are assumed to be uncorrelated with the true signals and with each other if the cross-spectral terms are zero. After some manipulations, the transfer function estimates for the autospectral, Ha(f), and the cross-spectral, Hc(f), derivations are found to be

$$|Ha|^2 = |H|^2 \left[\frac{1 + Gnn/Gvv}{1 + Gmm/Guu}\right] \quad \ldots\ldots\ldots\ldots\ldots(16)$$

$$|Hc| = H \left[\frac{1}{1 + Gmm/Guu}\right] \quad \ldots\ldots\ldots\ldots\ldots(17)$$

where H is the true transfer function. Thus, regardless of the amount of input noise; if output noise is present, the autospectral derivation for the transfer function estimate will always give a biased estimate of the true transfer function. The cross-spectral derivation, however, will give an unbiased estimate of the true value when the input noise satisfies the inequality

$$G_{mm} << G_{uu} \quad \ldots\ldots\ldots\ldots\ldots\ldots\ldots\ldots\ldots\ldots (18)$$

regardless of the amount of output noise, Gnn. Therefore, the cross-spectral method of calculating the transfer function estimate is always superior to the estimate calculated using the autospectra whenever independent noise is present [13].

The transfer function estimate is defined as

$$\begin{aligned} H_{xy}(f) &= G_{xy}(f) \,/\, G_{xx}(f) \qquad 0 \le f < \infty \quad \ldots\ldots (19) \\ &= H_r(f) - j\, H_i(f) \end{aligned}$$

where Gxx(f) is considered to be the input signal whether or not it actually is an excitation. Analogous to the cross-spectral estimate, the transfer function is composed of (1) a component, Hr(f), which is a real-valued even function of frequency f; and (2) a component, Hi(f), which is a real-valued odd function. It can be defined in terms of a magnitude (ie. gain), Hxy(f) , and phase, ϕxy(f). These must satisfy

$$H_{xy}(f) = |H_{xy}(f)| \exp(-j\phi_{xy}(f)) \qquad 0 \le f < \infty \ldots (20)$$

where:

$$|H_{xy}(f)| = |G_{xy}(f)| \,/\, G_{xx}(f) \qquad 0 \le f < \infty \ldots\ldots (21)$$

$$\begin{aligned} \phi_{xy}(f) &= \text{ARCTAN}\,[H_i(f) \,/\, H_r(f)] \quad \ldots\ldots\ldots (22) \\ &= \theta_{xy}(f) \end{aligned}$$

Thus, the phase, ϕxy(f), of the transfer function estimate is identical to the phase of the cross-spectral estimate θxy(f).

PERFORMANCE OF MULTICHANNEL MEM MODE SHAPE ESTIMATOR ON OFFSHORE CAISSON PLATFORM

In order to ascertain the multichannel MEM algorithm's ability to generate realistic "mode shapes" of a structure, a comparison of relative acceleration magnitudes obtained using MEM transfer function estimates was made with relative displacement amplitudes obtained from a finite element model. An offshore caisson production platform located in 89 feet of water in the Gulf Of Mexico operated by Amoco was used for this comparison. It consists of a single, vertical cylindrical caisson which varies in diameter from 7 ft at the mudline to 4 ft at the MLW. Figure 1 is a three-dimensional view of the structure. It is 265 ft overall; extending 100 ft below the mudline, 89 ft through the water column, and 76 ft above the surface. It supports three decks and a boat landing. The helicopter deck is 76 ft above the water, the production deck is 57 ft and the wellhead deck is 40 ft. Additional details on this platform are contained in a companion paper by Cook [14]. This platform is an ideal structure for estimating cross-spectral estimates because of (1) its symmetry, (2) lack of interference from neighboring legs, and (3) absence of drilling activity and large unaccountable deck loads.

The instrumentation for this series of tests consisted of four accelerometers and a Tandberg 4-channel analog (FM) tape recorder. The accelerometers were Endevco QA 116-16 force balance type. They can measure up to ± 1 g, resolve down to 10^{-6} g's, and have a sensitivity of 1 volt per g. The Tandberg Model 100 tape recorder uses standard 1/4 inch tape and records simultaneously on four channels. The amplifier gain was selected to give an accelerometer output of 100 volts per g. Data was recorded at 1-7/8 ips.

In order to measure the flexural mode shapes of the platform, four accelerometers oriented in a northerly direction were placed in the same vertical plane running through the platform centerline. An anemometer was used to measure a wind speed and direction of 20 knots from ENE. Visual observation ascertained a sea state of 5 to 8 ft.

A sampling rate of 6.4 Hz (0.16 sec interval) was used in the data reduction. A total of 80 minutes (4800 sec, 30720 data points) of data was analysed. Of this amount, 29696 data points (58 segments of 512 points each) were used in calculating the correlation function estimates to lag lengths of 512 points or 80 seconds. A preview of the analog data indicated that no over-ranges occurred. The lag length of 512 lags was chosen as an appropriate tradeoff between resolution and variance. An "overlap and save" technique was used to calculate the correlation function estimates.

In order to compare the multichannel MEM method of spectral analysis to conventional correlative methods, a comparison with the Blackman-Tukey method (BTM) was made. A parameter study on the effects of different window shapes (ie. Boxcar, Bartlett, Hanning, and Parzen) and durations (ie. 128, 256, and 512 lags) on the BTM method indicated that only the Hanning window with a lag length of at least 256 lags is capable of giving satisfactory "bias vs. variance" tradeoff without severe sidelobe leakage. Akaike's Final Prediction Error (FPE) model order criterion [6,11] indicated an optimum value of 80 lags for the MEM method. Thus, a window duration (for the BTM) or a model order (for the MEM) of 80 was selected. Comparisons of the multichannel cross-spectral magnitude, phase, and coherence squared estimates were made. For the sake of brevity, only the cross-spectral magnitude estimates are presented here. Figures 2 and 3 are for the BTM and MEM methods respectively. The effect of sidelobe leakage on the BTM magnitude estimate is clearly seen in Figure 2.

The multichannel MEM method gives an improved estimate over the conventional Blackman-Tukey spectral analysis method. One of the reasons why the BTM method gave such good comparative results (especially at large lags) is due to the large amount of data processed. The real time and cost saving of the MEM method is in its ability to calculate spectral estimates using only small amounts of data with low model orders or filter lengths. From the parameter study, we know that the BTM method would have given better results for a window duration of 256 lags or greater; but this would have required correspondingly more computer time and cost. Also, the stationarity problem, due to varying environmental conditions, is particularly important here.

The helicopter and wellhead deck accelerometers are presented as an example of the mode shape identification process using the multichannel MEM transfer function estimates. Figures 3 - 5 show the cross-spectral estimates of magnitude, phase, and coherence squared respectively. To prevent rapid crossovers between ± 180 degrees, the absolute value of the phase estimate has been plotted. The

cross-spectral magnitude plot shows the relative energy content among the first three flexural modes. Only the fundamental flexural mode contains any significant amount of energy. The first three flexural modes have been estimated to be located at 0.32, 1.20, and 3.06 Hz respectively. Only the first two modes are positively identified, however, because of the low coherence estimates for the third mode.

The peaks or spikes on the cross-spectral estimate plots labeled TRN are due to tape recorder noise. Based on the phase and coherence estimates, these peaks do not represent true energy content of the response spectra. A test to verify this hypothesis was conducted whereby one channel of the tape recorder was grounded and an empty data record was recorded. This data was digitized and processed using the same cross-spectral analysis procedure. Based on the results of this test, the noise peaks located at 1.68 and 2.66 Hz are definitely attributable to tape recorder noise, probably caused by transport flutter. In addition, other noise peaks at 1.34, 2.01, and 2.20 Hz were also identified.

Transfer function estimates were calculated with the helicopter deck as a psuedo-input to give relative acceleration magnitudes (ie. relative accelerometer location displacements if doubly integrated) between the helicopter (H), production (P), wellhead (W), and boat landing (B) decks for mode shape identification. Figure 6 is a representative sample of the transfer function estimate between the helicopter deck and the wellhead deck. A summary of the cross-spectral estimates of the first three flexural modes for each of three combinations of accelerometer locations is given below.

Accelerometers	Phase (Deg)	Coherence Squared	Transfer Function
First Flexure = 0.32 Hz			
H and P	0	1.00	0.85
H and W	0	1.00	0.70
H and B	0	1.00	0.40
Second Flexure = 1.20 Hz			
H and P	0	1.00	0.57
H and W	12	0.70	0.07
H and B	180	0.95	0.65
Third Flexure = 3.06 Hz			
H and P	15	0.00	0.15
H and W	180	0.05	0.15
H and B	180	0.00	0.10

A two-dimensional model incorporating geometrical, mass, and stiffness properties of the caisson platform as well as soil conditions was used to perform a finite element analysis using the computer program ADINA. The model, consisting of two degree of freedom (DOF) beam and truss elements (translational and rotational), had enough DOF to get the first three mode shapes. Additional discussion of the modeling of the caisson and the soil properties is presented by Cook [14].

A comparison of the first three estimated flexural mode natural frequencies with those calculated using the finite element (FE) model is shown below.

Description	Mode 1, Hz	Mode 2, Hz	Mode 3, Hz
FE Model	0.33	1.06	3.12
MEM Method	0.32	1.20	3.06

Hong [15] calculated a value of 0.30 Hz for the fundamental flexural mode. A comparison of the first two relative mode shapes is given in Figure 7. Thus, the natural frequencies and mode shapes estimated using the MEM multichannel spectral analysis technique compares favorably with other reported values.

CONCLUSIONS

A multichannel MEM method of spectral analysis has been developed based on the triangular decomposition of the correlation matrix using an algorithm developed by Rissanen. It is far superior to cross-spectral estimates obtained using a Blackman-Tukey code with a Hanning window.

A transfer function estimate using the MEM multichannel method of spectral analysis was used in mode shape identification of an offshore caisson platform located in 89 ft of water. These transfer function estimates, using accelerometers as psuedo-inputs, give relative acceleration amplitudes (which if doubly integrated, would be relative displacement amplitudes) between two accelerometers. Comparison of these relative acceleration magnitudes with the relative displacement amplitudes obtained from a finite element model of the caisson platform gave reasonable agreement. The third flexural mode values were not positively identified, however, because of low coherence values. Thus, this technique can be a useful tool (in conjunction with the cross-spectral estimates of magnitude, phase, and coherence) in mode shape identification of offshore platforms.

NOMENCLATURE

A = prediction error filter coefficients
CF = forward filter coefficient
Cxy, Qxy = coincident and quadrature spectral density estimates
e(n) = error or residual between desired and actual signals d(n) and y(n)
f,fs,fny = cyclical, sampling, and Nyquist frequencies
G = multichannel MEM spectral estimate matrix
Gxx,Gyy = autospectral estimate for channel x and y
Guu,Gvv = autospectral estimate for true input and output u and v
Gmm,Gnn = autospectral estimate for input and output noise m and n
Gxy = cross-spectral magnitude or gain
H(f) = true frequency response
$h(\tau)$ = impulse response function
Ha,Hc = transfer function estimate using auto and cross-spectral derivations
Hxy = transfer function estimate from cross-spectral derivation
Hr,Hi = real and imaginary components of transfer function estimate

L,m	= desired number and current number of lags
p	= number of time series channels
P	= prediction error, error power, or forward power matrix
R, RF	= autocorrelation matrix, multichannel forward correlation matrix
Sx(f)	= two-sided MEM autospectral estimate
Sw(f)	= white noise variance or prediction error
V	= forward power matrix
X,Y	= Fourier transforms of input and output
γ^2xy(f)	= coherence squared for channels x and y
Δ	= sampling interval, seconds
σ^2(m)	= variance or prediction error of order m
θxy(f)	= cross-spectral phase estimate
ϕxy(f)	= cross-spectral transfer function phase est.
t, τ	= time variable and time delay

ACKNOWLEDGEMENTS

This research was sponsored by the Branch of Marine Oil and Gas Operations of the USGS and by the Massachusetts Institute of Technology/Woods Hole Oceanographic Institution Joint Program in Ocean Engineering. The authors would like to thank Amoco for providing access to the caisson and logistics support in conducting the experiments. Also, MIT graduate student Mike Cook for assisting in the data collection and preparing the finite element model. Acknowledgement is also given to Union Oil's Science and Technology Division for permission to publish this paper.

REFERENCES

1. Begg, R.D., et. al., "Structural Integrity Monitoring Using Digital Signal Processing of Vibration Signals," OTC 2549, Houston, 1976.
2. Vandiver, J.K., "Detection of Structural Failure on Fixed Platforms by Measurement of Dynamic Response," JPT, March, 1977, pp. 305-310.
3. Coppolino, R.N. and Rubin, S., "Detectability of Structural Failure in Offshore Platforms by Ambient Vibration Monitoring," OTC 3865, Houston, May, 1980.
4. Ruhl, J.A., "Forced Vibration Tests of a Deepwater Platform," OTC 3514, Houston, May, 1979.
5. Burke, B.G., et.al., "Characterization of Ambient Vibration Data by Response Shape Vectors," OTC 3862, Houston, May, 1980.
6. Briggs, M.J., "Multichannel Maximum Entropy Method of Spectral Analysis Applied to Offshore Structures," OE Thesis, Massachusetts Institute of Technology/Woods Hole Oceanographic Institution Joint Program in Ocean Engineering. 1981.
7. Blackman, R.B. and Tukey, J.W., The Measurement of Power Spectra, Dover, New York, 1958.
8. Burg, J.P., "Maximum Entropy Spectral Analysis," Ph.D. Thesis, Stanford University, 1975.
9. Campbell, R.B. and Vandiver, J.K., "The Estimation of Natural Frequencies and Damping Ratios of Offshore Structures," OTC 3861, Houston, May, 1980.
10. Baggeroer, A.B.,"Recent Signal Processing Advances in Spectral and Frequency Wavenumber Function Estimation and their Application to Offshore Structures," BOSS '79, London, 1979.
11. Strand, O.N., "Multichannel Complex Maximum Entropy (Autoregressive) Spectral Analysis," IEEE Trans. on Aut. Control, Vol. AC-22, No. 4, August, 1977, pp. 634-640.
12. Rissanen, J., "Algorithms for Triangular Decomposition of Block Hankel and Toeplitz Matrices with Application to Factoring Positive Matrix Polynomials," Math. of Computation, Vol. 27, No. 121, January, 1973 147-154.
13. Bendat, J.S. and Piersol, A.G., Engineering Applications of Correlation and Spectral Analysis, Wiley-Interscience, New York, 1980.
14. Cook, M.F. and Vandiver, J.K., "Measured and Predicted Dynamic Response of a Single-Pile Platform to Random Wave Excitation," OTC 4285, Houston, May, 1982.
15. Hong, F.T. and Brooks, J.C., "Dynamic Behavior and Design of Offshore Caissons," OTC 2555, Houston, May, 1976.

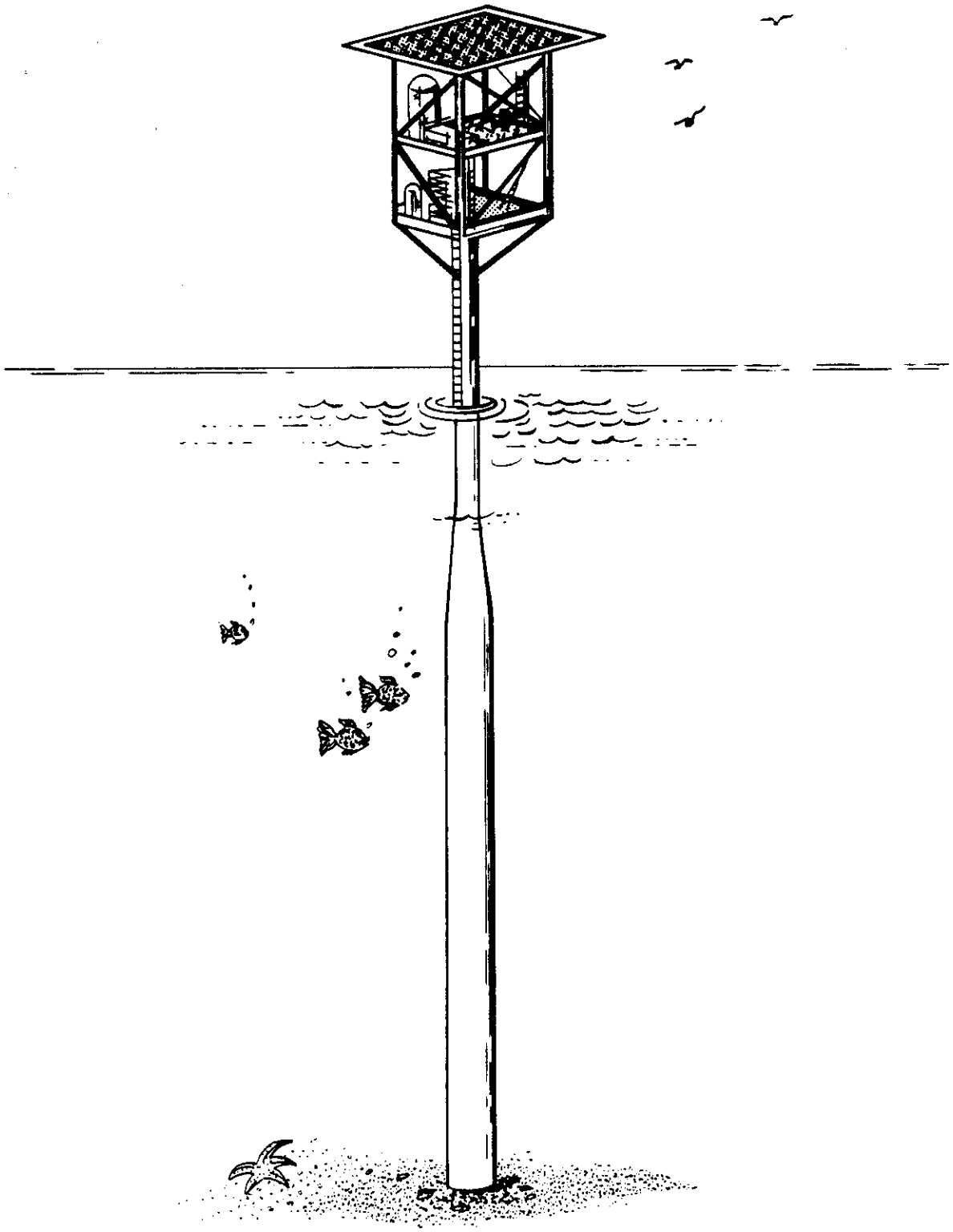

Fig. 1 — Offshore caisson platform

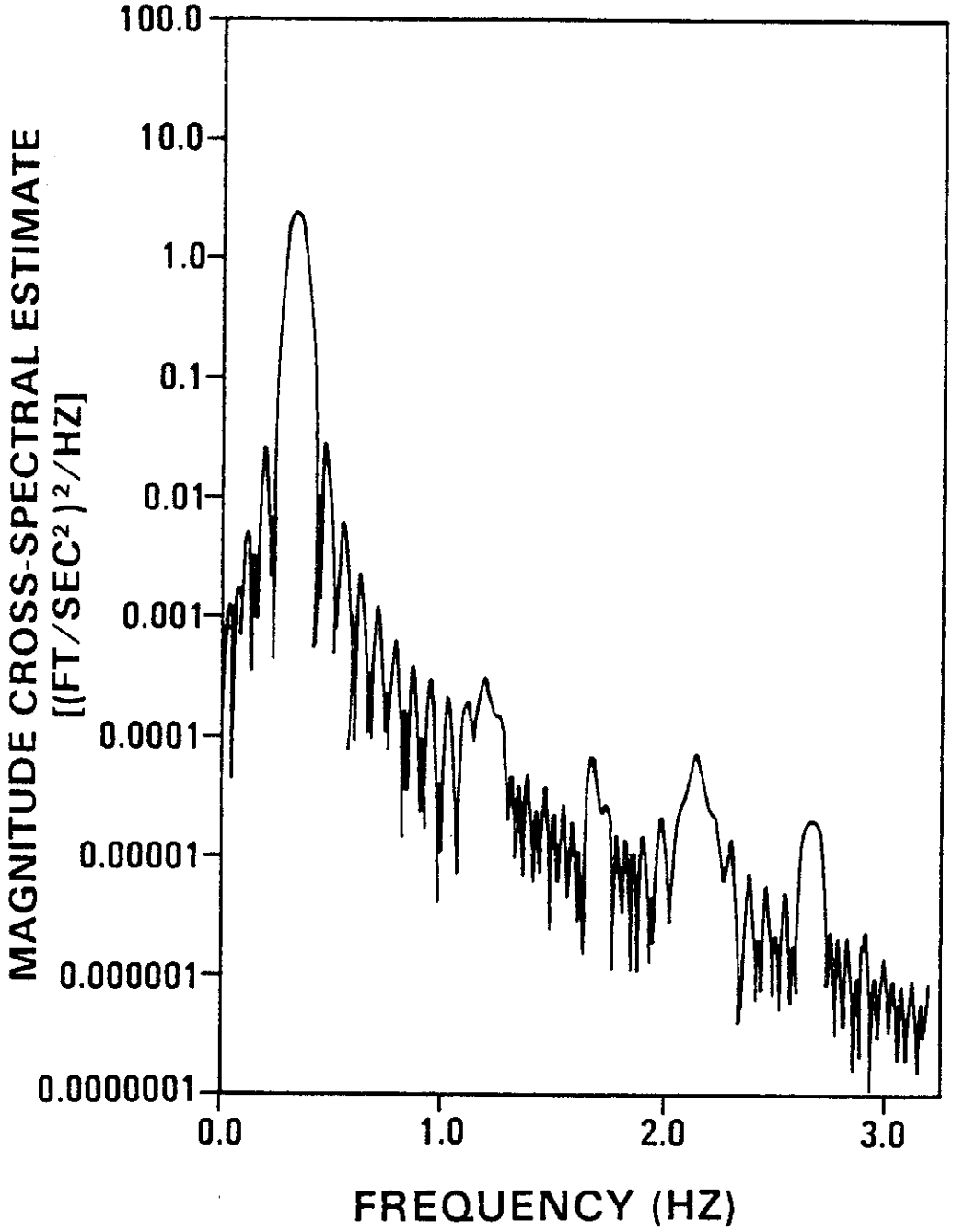

Fig. 2 — BTM magnitude cross-spectrum with Hanning Window

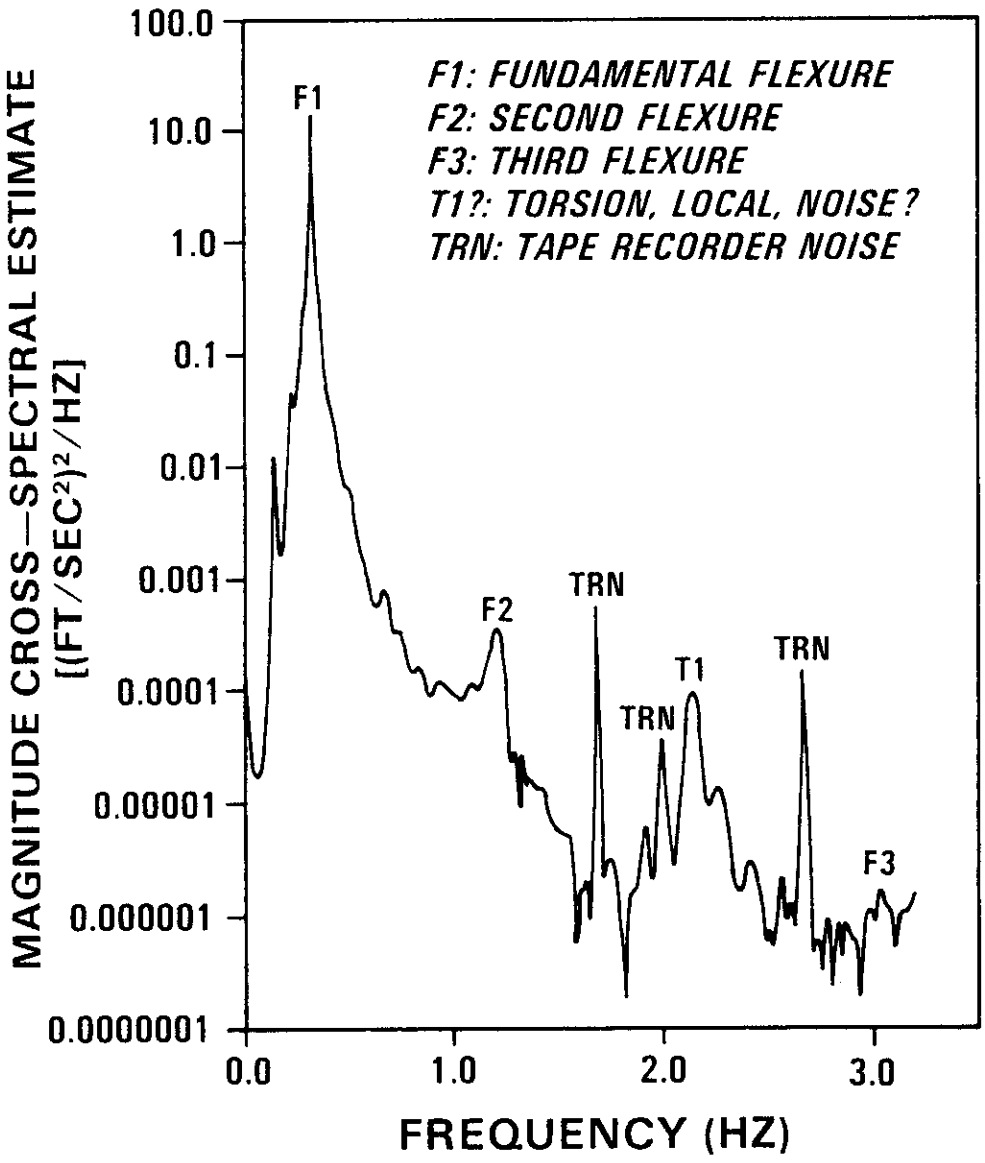

Fig. 3 — MEM magnitude cross-spectral estimates

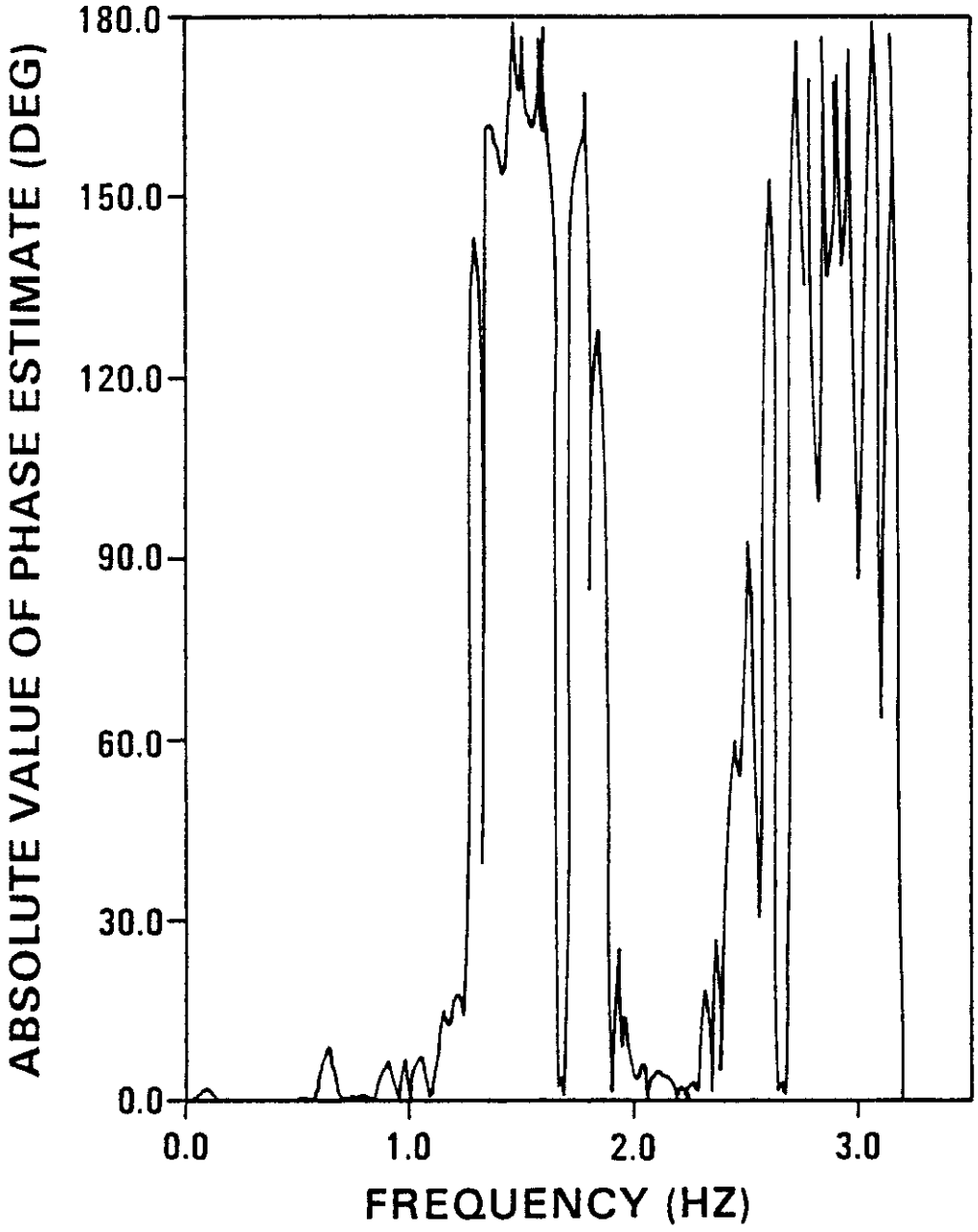

Fig. 4 — MEM phase estimates

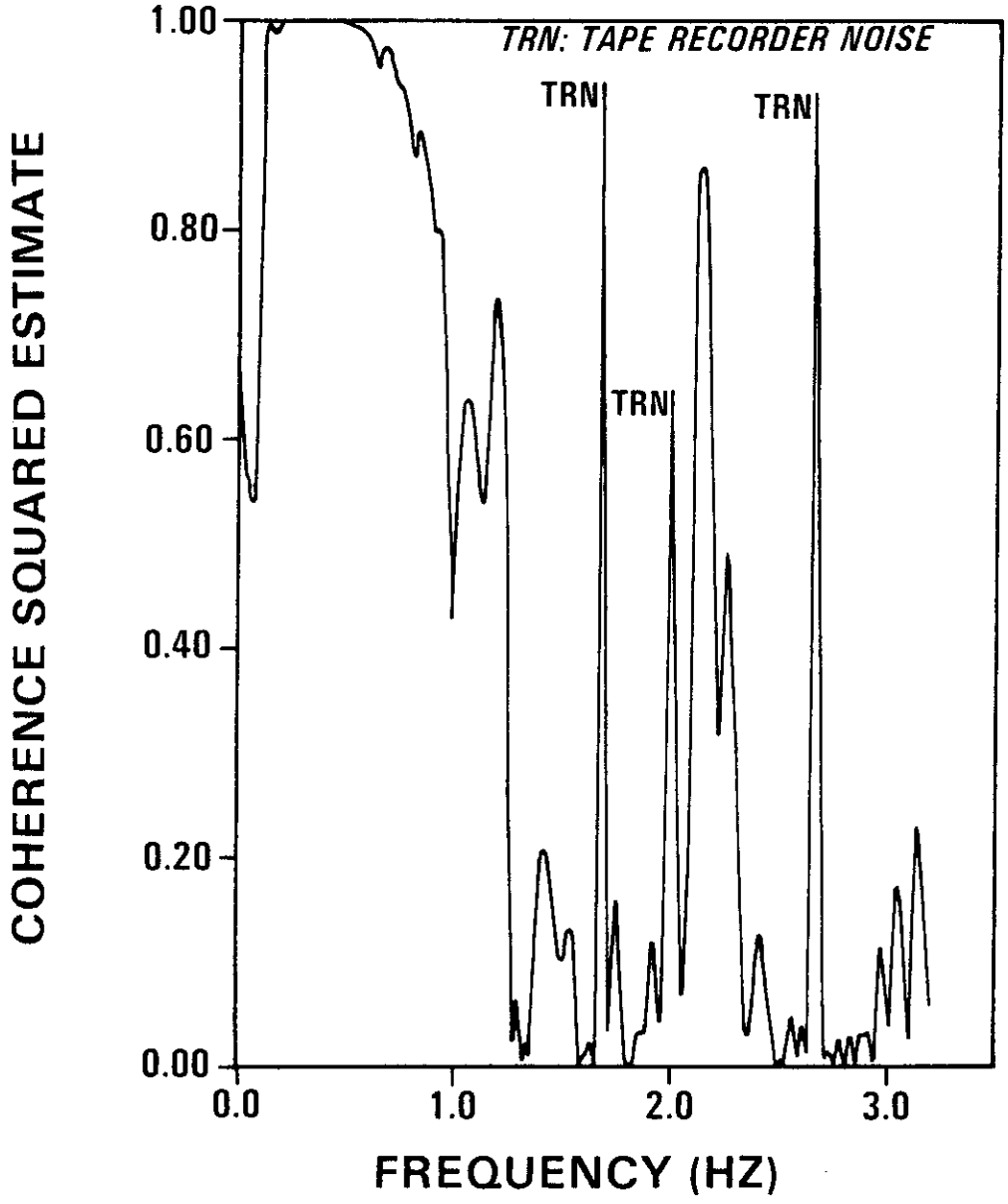

Fig. 5 — MEM coherence squared estimates

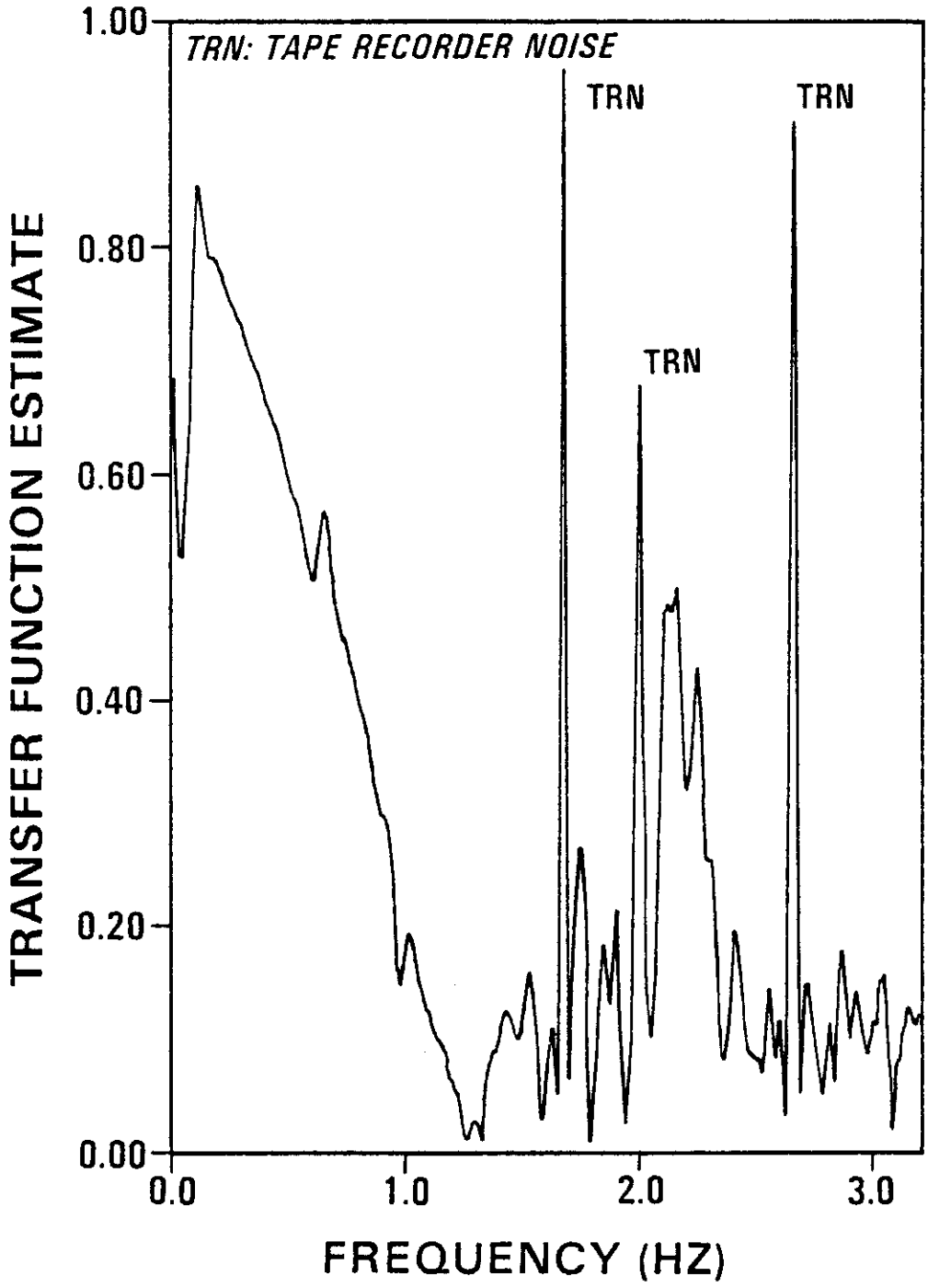

Fig. 6 — MEM transfer function estimates

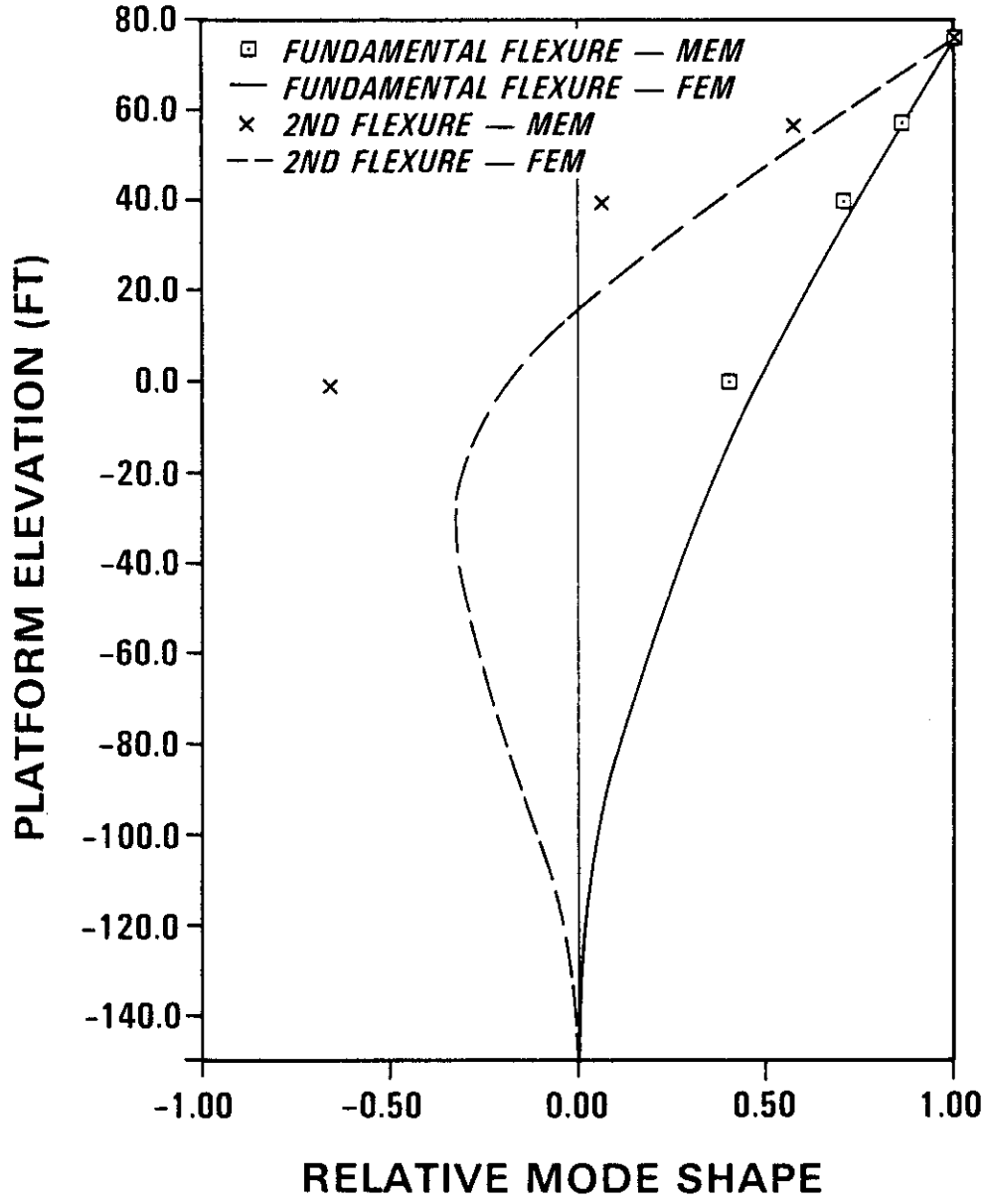

Fig. 7 — Comparison of mode shape estimates

81-DET-13

THE AMERICAN SOCIETY OF MECHANICAL ENGINEERS
345 E 47 St., New York, N.Y. 10017

J. K. Vandiver
Associate Professor,
Massachusetts Institute of Technology,
Cambridge, Mass.

A. B. Dunwoody
Research Engineer,
Dome Petroleum Co.,
Calgary, Alberta, Canada

R. B. Campbell
Research Engineer,
Exxon Production Research,
Houston, Texas

M. F. Cook
Research Assistant,
Massachusetts Institute of Technology,
Cambridge, Mass.

A Mathematical Basis for the Random Decrement Vibration Signature Analysis Technique

The mathematical basis for the Random Decrement Technique of vibration signature analysis is established. The general relationship between the auto-correlation function of a random process and the Randomdec signature is derived. For the particular case of a linear time invariant system excited by a zero-mean, stationary, Gaussian random process, a Randomdec signature of the output is shown to be proportional to the auto-correlation of the output. Example Randomdec signatures are computed from acceleration response time histories from an offshore platform.

Introduction

The Random Decrement Technique of vibration signature analysis was empirically developed in the late 1960's by Henry Cole [1-4]. Since that time, it has achieved rather widespread use, especially in the aerospace industry, for the analysis of experimentally generated vibration data [3-7]. The method is frequently used for the determination of modal damping ratios and the detection of mechanical failure. The method also forms the basis of another more general vibration analysis technique known as "Ibrahim Time Domain Modal Vibration Testing Technique" [8].

The Randomdec method has achieved rather widespread use because the instrumentation is rather simple, the data processing can be done in generally real time, and, most of all, because it appears to work. The missing element in the literature and in the day-to-day interpretation of the results of the technique is a sound mathematical formulation which shows exactly what a Randomdec signature is. Without such a theoretical basis, the accuracy of, for example, estimates of modal damping ratios of a multiple degree of freedom system cannot be determined.

This paper presents the mathematical basis for the Randomdec technique. The general relationship between the auto-correlation function of a random process and the Randomdec signature is derived. A completely general result is obtained. In the particular case of a linear, time invariant system excited by a zero mean, stationary, Gaussian random process, a Randomdec signature is shown to reduce to

$$D_{X_0}(\tau) = \frac{R_X(\tau)}{R_X(0)} X_0 \tag{1}$$

where $X(t)$ is the response of the linear system,
X_0 is the trigger level for the acquisition of sample time histories $X(t)$
$R_X(\tau)$ is the auto-correlation function of the random process $X(t)$,
$R_X(0) = R_X(\tau = 0)$.

This result reveals a small but important difference from the commonly believed interpretation of the Randomdec signature. It is usually accepted that if a linear system is excited by a stationary, Gaussian random process, then the Randomdec signature is the same as the free vibration response of that linear system to the set of specified initial conditions. The result of equation (1) shows that for the case of a specified initial amplitude, the signature is proportional to the auto-correlation function. The auto-correlation function is not, in general, proportional to the free vibration decay of the linear system. It happens that for the case of a single degree of freedom oscillator excited by a white noise, stationary, Gaussian process, the auto-correlation function is exactly proportional to the free vibration decay from a specified initial displacement. This special case is often used to argue on intuitive grounds that the Randomdec signatures resulting from nonwhite Gaussian stationary excitations also represent free decay curves. The error in previous analyses which leads to this conclusion is identified. Fortunately, most applications of the Randomdec method have been circumstances in which the excitation was sufficiently broadband that the free vibration decay interpretation did not lead to substantial errors.

Contributed by the Vibration and Sound Committee for presentation at the Design Engineering Technical Conference, Hartford, Conn., September 20-23, 1981, of THE AMERICAN SOCIETY OF MECHANICAL ENGINEERS. Manuscript received at ASME Headquarters June 3, 1981. Paper No. 81-DET-13.
Copies will be available until June 1982.

Discussion on this paper will be accepted at ASME Headquarters until November 30, 1981

The Definition and Intuitive Theory of the Randomdec Method

A Randomdec signature is simply the trace formed by a waveform averaging a number of specially selected segments from an observed time history. Each of the segments shares the common attribute of known initial conditions. Since one may specify an initial value and/or an initial slope for the selected segments, an infinite variety of possibilities exists for the resultant signature. The most popular choice is to only specify the initial amplitude for the segments. For a mechanical system, the physical interpretation of such initial conditions is a specification of the initial displacement, but not the velocity of the system at the time each segment is selected.

An equivalent definition of the Randomdec signature can be obtained using the concept of ensemble averages. In order to do this, one must first assume that the random process is ergodic. Accordingly, averages computed from a single time history are equivalent to averages computed across the ensemble of all potential time histories of the process. Under this assumption, the definition of the Randomdec signature is simply the conditional expected value of the random process. In conditioning the expected value, members of the ensemble are excluded from the computation unless they possess the specified values for the initial conditions. These concepts form the basis for the analytical treatment of the Randomdec signature throughout the remainder of the paper.

The intuitive theory of Randomdec is most easily demonstrated by the example of a single degree of freedom mechanical oscillator excited by a zero-mean, stationary, Gaussian random force. The equation of motion of this system is given by

$$M\ddot{X} + R\dot{X} + KX = F(t) \tag{2}$$

The response $X(t)$ is also a zero-mean, stationary, Gaussian process.

Consider a randomly selected segment of the response $X(t)$. At the beginning of the segment, for which t is arbitrarily set to zero, the segment has particular initial values for the amplitude and slope; $X(0) = a$ and $\dot{X}(0) = b$. If at the time $t = 0$ the excitation had been removed, then the response $X(t)$ would have been simply the transient decay from the initial conditions a and b.

If on the other hand the excitation had continued, the resulting response would have been the linear superposition of the transient decay due to initial conditions plus the convolution integral of the impulse response function for the system and the excitation as shown.

$$X(t) = ae^{-\xi\omega_0 t}\left[\cos\omega_1 t + \frac{\omega_0}{\omega_1}\sin\omega_1 t\right] + \frac{b}{\omega_1}e^{-\xi\omega_0 t}\sin\omega_1 t + \int_0^t h(t-\tau)F(\tau)d\tau \tag{3}$$

where $\omega_0 = \sqrt{K/M}, \omega_1 = \omega_0\sqrt{1-\xi^2}$.

As previously stated, the Randomdec signature is simply the average of a large number of segments of the response $X_i(t)$ given that each must start with the same initial conditions, a and b. Using an ensemble average, the Randomdec signature is the conditioned expected value of equation (3).

$$E[X(t)\,|a,b] = ae^{-\xi\omega_0 t}\left[\cos\omega_1 t + \frac{\omega_0\xi}{\omega_1}\sin\omega_1 t\right] + \frac{b}{\omega_1}e^{-\xi\omega_0 t}\sin\omega_1 t + \int_0^t h(t-\tau)E[F(\tau)\,|a,b]d\tau \tag{4}$$

where the expression $E[\ |a,b]$ should be interpreted as the expected value of the specified random variable, given that a and b are the initial conditions on the response $X_i(t)$.

The intuitive theory of Randomdec and also the solution proposed by Caughey [9] in a paper on earthquake response published in 1961 argue that because the input was specified as a zero mean, stationary, random process, then the expected value of the forcing function in the convolution integral of equation (4) must be zero, thereby proving that the expected value of $X(t)$, given the initial conditions a and b, is simply the transient decay of the system from those initial conditions. This is not true. The requirement of known values of the output at $t = 0$ has biased the expected value of the excitation in such a way that it is no longer necessarily zero, just because it is in general a zero mean input. This is demonstrated below for the general case of a linear, time invariant system excited by a random process, $F(t)$.

The cross correlation of the input at t_2 with an output at t_1 is given by

$$R_{XF}(t_1,t_2) = \int_{X_1}\int_{F_2} X_1F_2P(X_1,F_2)dX_1dF_2 \tag{5}$$

where X_1 and F_2 denote the processes of $X(t_1)$ and $F(t_2)$ and $P(X_1, F_2)$ is the joint probability density function of X_1 and F_2.

The joint pdf can be written in terms of a conditional pdf and a first order pdf as follows:

Nomenclature

Single Degree of Freedom Parameters

- $X, \dot{X}, \ddot{X}$ = displacement, velocity, and acceleration
- M, K, R = mass, spring, and damper constants
- $F(t)$ = force excitation
- ξ = damping ratio
- ω_0 = undamped natural frequency
- ω_1 = damped natural frequency
- a, b = initial displacement and velocity
- $h(t-\tau)$ = impulse response function

General Symbols

- $X(t)$ = time history of X
- X_0 = initial value of $X(t=0)$
- X_1, X_2 = random variables corresponding to possible values of $X(t)$ at two different times
- $E[\,]$ = expected value operator
- $R_X(\tau)$ = auto-correlation function for $X(t)$ at arbitrary lag τ
- $R_X(0)$ = auto-correlation at $\tau = 0$
- $\rho_X(\tau)$ = correlation function
- $R_{XF}(t_1,t_2)$ = cross correlation between $X(t_1)$ and $F(t_2)$
- $D_{X_0}(\tau)$ = Randomdec signature
- $\hat{D}_{X_0}(\tau)$ = estimated Randomdec signature
- $p(X_1)$ = probability density function (pdf) for the random variable X_1
- $p(X_1,F_2)$ = joint pdf for X_1, F_2
- $p(F_2\,|X_1)$ = conditioned pdf for F_2 given X_1
- m_1, m_2 = mean values of two different Gaussian random variables
- σ_1^2, σ_2^2 = mean squares of two Gaussian random variables
- $X_n(\tau)$ = n^{th} sample time history of $X(t)$
- N = total number of sample time histories

$$P(X_1,F_2)=P(X_1)P(F_2\,|X_1) \tag{6}$$

and equation (5) may be rewritten as

$$R_{XF}(t_1,t_2)=\int_{X_1} X_1P(X_1)\int_{F_2} F_2P(F_2\,|X_1)dF_2dX_1 \tag{7}$$

The integral over F_2 is the expected value of $F(t_2)$ given $X(t_1)$, where, to simplify the example, it was assumed that $dX(t_1)/dt$ was not specified. In most cases, the cross-correlation is not zero, which can only mean that the expected value of $F(t_2)$ given $X(t_1)$ cannot be, in general, zero.

The intention of this analysis was to establish that the intuitive arguments behind Randomdec and, for that matter, the earlier analysis of reference [9], are not generally correct. The derivation of the Randomdec signature is presented in the next section.

The General Relationship Between the Auto-Correlation Function and the Randomdec Signature

The Randomdec signature is computed by averaging an ensemble of time histories of a random process. The only common feature of the histories is that in each case the sample has started with the same initial conditions. To simplify the analysis, consider the case that only an initial amplitude, but not slope, is specified. In probabilistic terms, the task is to find the expected value of a random process $X(t)$, evaluated at $t=t_2$, given that at a previous time t_1, the random process had crossed the trigger level, X_0. A mathematical expression of this definition of the Randomdec expression is

$$D_{X_0}(t_1,t_2)\equiv E[X(t_2)\,|X(t_1)=X_0] \tag{8}$$

where the expression on the right is the expected value of $X(t_2)$ given $X(t_1)=X_0$, and the expression on the left is by definition the Randomdec signature.

The derivation to follow relates the Randomdec signature to the auto-correlation function of a random process. Since the derivation uses only the definitions of the auto-correlation function and the Randomdec signature, the result is entirely general.

The auto-correlation function of a random process $X(t)$ may be defined as follows, as shown in the text *Random Vibration* by Crandall and Mark [10]:

$$R_X(t_1,t_2)=E[X(t_1)X(t_2)]$$

$$=\int_{X_1}\int_{X_2} X_1X_2p(X_1,X_2)dX_1dX_2 \tag{9}$$

where the abbreviations X_1 and X_2 denote the random variables $X(t_1)$ and $X(t_2)$. $p(X_1,X_2)$ is the joint probability density function describing the distribution of X_1 and X_2. This joint probability density function may be expressed as the product of a conditional probability density function and a first order probability density function as shown as follows:

$$p(X_1,X_2)=p(X_2\,|X_1)p(X_1) \tag{10}$$

Substitution into equation (9) leads to

$$R_X(t_1,t_2)=\int_{X_1}\int_{X_2} X_1p(X_1)X_2p(X_2\,|X_1)dX_1dX_2 \tag{11}$$

These two integrals may be computed sequentially as follows.

$$R_X(t_1,t_2)=\int_{X_1} X_1p(X_1)\int_{X_2} X_2p(X_2\,|X_1)dX_2dX_1 \tag{12}$$

If X_1 is defined to be the trigger level X_0, then the integral over X_2 yields exactly the expected value of X_2 given $X(t_1)=X_1$ which is the definition of the Randomdec signature as given in equation (12). Therefore,

$$R_X(t_1,t_2)=\int_{X_1} X_1p(X_1)E[X_2\,|X(t_1)=X_1]dX_1 \tag{13}$$

$$R_X(t_1,t_2)=\int_{X_1} X_1p(X_1)D_{X_1}(t_1,t_2)dX_1 \tag{14}$$

An interpretation of equation (13) is that the auto-correlation function of the random process $X(t)$, computed between any two instants in time t_1 and t_2, is a weighted sum of all possible Randomdec signatures of $X(t)$. The weighting factor is the product of the trigger level X_1 and its probability of occurrence $p(X_1)$ at time t_1.

Results for Stationary Gaussian Random Processes

A specific case for which the mathematics are tractable is a linear, time-invariant system excited by a zero-mean, stationary, but not necessarily white, Gaussian random process. For this case, the system response will also be a zero-mean, stationary, Gaussian random process. The auto-correlation function contains a complete characterization of such a process. The following equations relating the probability distribution to the auto-correlation function can be found in Crandall and Mark:

$$p(X_1)=\frac{1}{\sqrt{2\pi\sigma_1^2}}\exp\left[\frac{-(X_1-m_1)^2}{2\sigma_1^2}\right] \tag{15}$$

$$p(X_1,X_2)=\frac{1}{2\pi\sigma_1\sigma_2\sqrt{1-\rho_{12}^2}}\exp\left\{\frac{-1}{2(1-\rho_{12}^2)}\left[\frac{(X_1-m_1)^2}{\sigma_1^2}-\frac{2\rho_{12}(X_1-m_1)(X_2-m_2)}{\sigma_1\sigma_2}+\frac{(X_2-m_2)^2}{\sigma_2^2}\right]\right\} \tag{16}$$

For stationary random processes, the auto-correlation function depends only on the time difference between t_1 and t_2 and not on t_1 and t_2 individually. Defining this time difference as

$$\tau=t_2-t_1, \tag{17}$$

setting $X(\tau=0)=X_0$, and noting that for the foregoing equations

$$m_1=m_2=0 \tag{18}$$

$$\sigma_1^2=\sigma_2^2=R_X(0) \tag{19}$$

$$\rho_{12}(\tau)=\frac{R_X(\tau)}{R_X(0)} \tag{20}$$

these expressions follow:

$$p(X_0)=\frac{1}{\sqrt{2\pi R_X(0)}}\exp\left[\frac{-X_0^2}{2R_X(0)}\right] \tag{21}$$

$$p(X_0,X_\tau)=\frac{1}{2\pi R_X(0)\sqrt{1-\frac{R_X^2(\tau)}{R_X^2(0)}}}\exp\left\{\frac{-1}{2\left(1-\frac{R_X^2(\tau)}{R_X^2(0)}\right)}\left[\frac{X_0^2}{R_X(0)}-\frac{2R_X(\tau)X_0X_\tau}{R_X^2(0)}+\frac{X_\tau^2}{R_X(0)}\right]\right\} \tag{22}$$

The conditional probability density function for $X(\tau)$ given X_0 also follows:

$$p(X_\tau\,|X_0)=p(X_0,X_\tau)/p(X_0) \tag{23}$$

$$p(X_\tau\,|X_0)=\frac{1}{\sqrt{2\pi R_X(0)\left(1-\frac{R_X^2(\tau)}{R_X^2(0)}\right)}}\exp\left\{\frac{-1}{2\left(1-\frac{R_X^2(\tau)}{R_X^2(0)}\right)}\right.$$

$$\left[\frac{X_0^2}{R_X(0)} - \frac{2R_X(\tau)X_0X_\tau}{R_X^2(0)} + \frac{X_\tau^2}{R_X(0)} - \frac{X_0^2}{R_X(0)}\left(1 - \frac{R_X^2(\tau)}{R_X^2(0)}\right)\right]\Bigg\} \tag{24}$$

$$p(X_\tau \mid X_0) = \frac{1}{\sqrt{2\pi\sigma_a^2}} \exp\left\{\frac{-1}{2\sigma_a^2}\left[X_\tau^2 - \frac{2R_X(\tau)}{R_X(0)}X_\tau X_0 + \frac{R_X^2(\tau)}{R_X^2(0)}X_0^2\right]\right\} \tag{25}$$

where

$$\sigma_a^2 = R_X(0)\left(1 - \frac{R_X^2(\tau)}{R_X^2(0)}\right)$$

$$p(X_\tau \mid X_0) = \frac{1}{\sqrt{2\pi\sigma_a^2}} \exp\left\{\frac{-1}{2\sigma_a^2}\left[X_\tau - \frac{R_X(\tau)}{R_X(0)}X_0\right]^2\right\} \tag{26}$$

From the definition of the Randomdec signature

$$D_{X_0}(\tau) = \int_{X_\tau} X_\tau p(X_\tau \mid X_0) dX_\tau \tag{27}$$

Therefore

$$D_{X_0}(\tau) = \int_{X_\tau} X_\tau \frac{1}{\sqrt{2\pi\sigma^2 a}} \exp\left\{\frac{-1}{2\sigma_a^2}\left[X_\tau - \frac{R_X(\tau)}{R_X(0)}X_0\right]^2\right\} dX_\tau \tag{28}$$

But this integral is simply the expected value of a simple Gaussian probability distribution. The result may be obtained by inspection.

$$D_{X_0}(\tau) = \frac{R_X(\tau)}{R_X(0)}X_0 \tag{29}$$

The Randomdec signature for a zero-mean, stationary, Gaussian random process is simply the product of the correlation function and the trigger level.

$$D_{X_0}(\tau) = \rho_X(\tau)X_0 = \frac{R_X(\tau)}{R_X(0)}X_0 \tag{30}$$

For this special case, the Randomdec signature is proportional to the auto-correlation function.

If $X(t)$ is the output of a linear time invariant system excited by a zero-mean, stationary, Gaussian random process, then $X(t)$ is also a zero-mean, stationary Gaussian random process. For such systems, it is commonly believed that the Randomdec signature represents the transient decay of that system, to the initial conditions specified by

$$X(0) = X_0$$
$$\frac{dX(0)}{dt} = 0 \tag{31}$$

Since it has been shown that the Randomdec signature must be proportional to the auto-correlation function, then it can only be the transient decay of the system from the specified set of initial conditions under the restriction that the product of the correlation coefficient and the trigger level also represent the transient decay. This is only exactly true when the input to the system is white noise. However, for sharply tuned systems, such as a lightly damped single degree of freedom oscillator, a band limited spectrum often yields results that are to sufficient accuracy equivalent to the response to white noise. This applies as well to bandpass filtered random processes. However, the filter's characteristics are then part of the linear system being evaluated.

The Variance of the Randomdec Signature

In the previous sections, the theoretical formulation of the Randomdec signature has been presented. As a practical matter, such a signature must be estimated from a limited number of finite length observations of an actual random process. The practical limitation on record length and number of records will introduce variance into the estimated signature. In this section, an estimate of the variance of the Randomdec signature is obtained for the case that the time history $X(t)$ is a zero mean, Gaussian, and stationary random process.

For a stationary random process, the theoretical Randomdec signature is a function of the delay τ and the trigger level $X(0) = X_0$, as stated in equation (32).

$$D_{X_0}(\tau) = E[X(\tau) \mid X(0) = X_0] \tag{32}$$

For a finite number of samples $X_n(\tau)$ of the random process, an estimate of $D_{X_0}(\tau)$ may be obtained by

$$\hat{D}_{X_0}(\tau) = \frac{1}{N}\sum_{n=1}^{N}(X_n(\tau) \mid X_n(0) = X_0) \tag{33}$$

If each time history is sampled at $m+1$ discrete delay intervals, then the delay τ may be replaced by m, the number of discrete lags. This yields a discrete formulation for the estimate of $D_{X_0}(\tau)$.

$$\hat{D}_{X_0}(m) = \frac{1}{N}\sum_{n=1}^{N}(X_n(m) \mid X_n(0) = -X_0) \tag{34}$$

The expected value of the estimate may be found as follows:

$$E[\hat{D}_{X_0}(m)] = \frac{1}{N}E\left[\sum_{n=1}^{N}(X_n(m) \mid X_n(0) = X_0)\right] \tag{35}$$

$$= \frac{1}{N}\sum_{n=1}^{N}E[X_n(m) \mid X_n(0) = X_0] \tag{36}$$

$$E[\hat{D}_{X_0}(m)] = \frac{1}{N}\sum_{n=1}^{N}\int X_{n,m}p(X_{n,m} \mid X_0)dX_{n,m} \tag{37}$$

$$= \frac{R_X(m)}{R_X(0)}X_0 \tag{38}$$

The last two equations follow directly from the analysis given in the previous section.

Therefore, it is concluded that

$$E[\hat{D}_{X_0}(m)] = \frac{R_X(m)}{R_X(0)}X_0 \tag{39}$$

Since this is the discrete equivalent to the continuous formulation of equation (30), the estimate of the Randomdec signature is unbiased.

To obtain the variance of the estimate requires first the estimate of the mean square of the Randomdec signature.

$$E[\hat{D}_{X_0}^2(m)] = \frac{1}{N^2}E\left[\left(\sum_{n=1}^{N}X_n(m) \mid X_n(0) = X_0\right)\left(\sum_{l=1}^{N}X_l(m) \mid X_l(0) = X_0\right)\right] \tag{40}$$

$$= \frac{1}{N^2}\sum_{n=1}^{N}\sum_{l=1}^{N}E[(X_n(m) \mid X_n(0) = X_0)(X_l(m) \mid X_l(0) = X_0)] \tag{41}$$

The expected value inside of the summation may also be expressed in probabilistic terms as follows:

$$E[X_n(m)\,|X_n(0)=X_0)(X_l(m)\,|X_l(0)=X_0)] =$$

$$= \int\int X_{n,m} X_{l,m} p(X_{n,m}\,|X_0, X_{l,m}\,|X_0) dX_{n,m} dX_{l,m} \tag{42}$$

These results then imply that

$$E[\hat{D}_{X_0}{}^2(m)] = \frac{1}{N^2}\left\{NR_X(0)\left[1-\frac{R_X{}^2(m)}{R_X{}^2(0)}\right)\right.$$

$$\left. + N\frac{R_X{}^2(m)X_0{}^2}{R_X{}^2(0)} + N(N-1)\frac{R_X{}^2(m)}{R_X{}^2(0)}X_0{}^2\right\} \tag{43}$$

The variance of the estimate is defined below in terms of the Randomdec signature.

$$\mathrm{Var}[\hat{D}_{X_0}{}^2(m)] = E[\hat{D}_{X_0}{}^2(m)] - E[\hat{D}_{X_0}(m)]^2 \tag{44}$$

Substitution of the previous results leads to

$$\mathrm{Var}[\hat{D}_{X_0}{}^2(m)] = \frac{1}{N^2}\left(NR_X(0)\left(1-\frac{R_X{}^2(m)}{R_X{}^2(0)}\right)\right.$$

$$\left. + N(N-1)\frac{R_X{}^2(m)}{R_X{}^2(0)}X_0{}^2\right)$$

$$- \frac{R_X{}^2(m)}{R_X{}^2(0)}X_0{}^2 + \left(N\frac{R_X{}^2(m)X_0{}^2}{R_X{}^2(0)}\right)\frac{1}{N^2} \tag{45}$$

$$= \frac{1}{N}R_X(0)\left(1-\frac{R_{X^2}(m)}{R_X{}^2(0)}\right) \tag{46}$$

$$= \frac{1}{N}R_X(0)\left(1-\frac{D_{X_0}{}^2(m)}{X_0{}^2}\right) \tag{47}$$

For a zero mean, Gaussian, and stationary random process, the variance of the Randomdec signature decreases with N, the number of averages used in computing the estimate. As expected, for zero lag ($m=0$), the variance is zero. This is because the signature is forced to be equal to the trigger level. For very large lag, the variance increases to $1/N$ times the mean square of $X(t)$, assuming $R_X(\tau)=0$ as $\tau\to\infty$. It is important to note that the variance is independent of trigger level. This is true because the variance was calculated assuming that there was no noise in the measurement. If substantial noise were present, then the choice of too low a trigger level would result in false triggers which would grossly increase the variance of the estimate. The result of equation (47) is valid for measurements with good signal-to-noise ratios and trigger levels substantially greater than the noise level.

This estimate of the variance was obtained with the assumption that individual Randomdec sample time histories were uncorrelated to one another. In practice, this is not generally the case. Sample time histories are typically acquired each time the random process crosses the specified trigger level. For reasonable trigger levels (such as on the order of the rms level of the random process), data acquisition will be initiated many times within the time frame of the decay length of $R_X(\tau)$. Thus each Randomdec sample may overlap many others, and the assumption of uncorrelated samples will not be valid. For a finite number of samples, correlation between samples will in general increase the variance of the estimate. Therefore, there is probably not much gained by triggering a new sample before data acquisition of the most recent one has been terminated. Users of Randomdec indicate that hundreds of samples of the highly overlapping type are required for convergence. It is suggested that convergence could be obtained with many fewer samples if overlapping were not allowed. This would not likely reduce the total data length required, but would cut down on the number of necessary computations. Cole [3] conducted Monte Carlo simulations and reports values of the variance for uncorrelated samples from the output of a single degree of freedom oscillator excited by band limited white noise. His values agree with the predictions of equation (46).

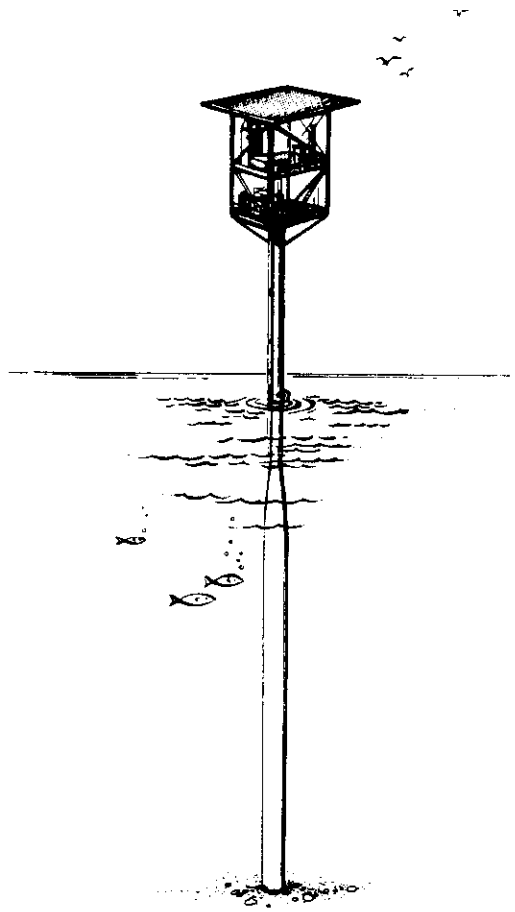

Fig. 1 Single caisson production platform

An Application to an Offshore Structure

In March of 1980, authors Vandiver and Cook made acceleration response records on a single cylinder petroleum production platform depicted in Fig. 1. This structure stands in 90 ft of water, is 4 ft in dia at the waterline and extends to 76 ft above the water at the helicopter deck. It is very active dynamically with a lowest natural period of 3.28 s. Horizontal accelerations were recorded at several locations on the structure.

Randomdec and other more conventional analysis procedures have been applied to these data. Some of these results are presented here.

Figure 2 is an auto-correlation function computed from an acceleration time history of a location near the top of the structure. The maximum lag is 80 s and the total record length was 80 min, yielding a ratio of total record length to maximum lag of 60, a measure of the variance. The magnitude of this auto-correlation function has been normalized to force it to the same scale as the Randomdec signatures to be presented later. The recording was low pass filtered at 15 Hz to remove generator noise. No other filtering was employed. The data were very noise free and were clearly dominated by the response of the lowest bending natural mode of the structure. The auto-correlation function looks

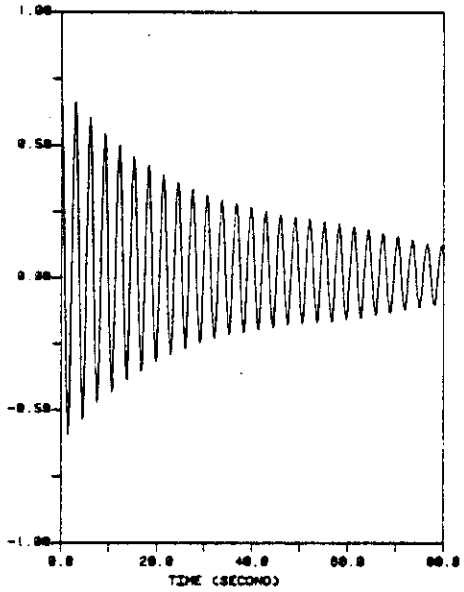

Fig. 2 Auto-correlation function computed from acceleration response

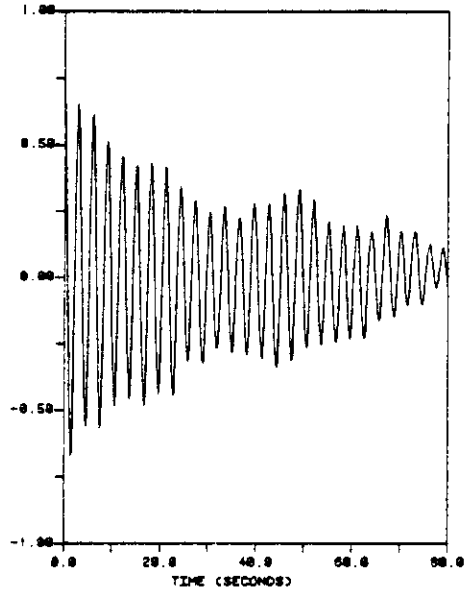

Fig. 3 Randomdec signature with 40 averages

exactly as one would expect from a single degree of freedom oscillator excited by white noise.

A simple waveform averaging program was written for use on a GenRad Time Series Analysis system which was based on a Digital Equipment Corporation PDP 11/34 minicomputer.

The Randomdec signatures were obtained by the following sampling procedure. The programmer specified the trigger level for the sample and selected positive or negative slope. After each trigger, a sample 80 s long was acquired. The sample was stored and when the trigger conditions were next satisfied, a new sample was begun. In this way, two sequential samples could be considered to be essentially statistically independent, as can be tested by checking the value of the auto-correlation function at lags of 80 s and greater.

With this triggering procedure, a maximum of 60 samples could be obtained from the total record for any specified trigger level and either + or − slope. Two sampling runs were made on the data. The trigger level was the same for each run, but the slope was plus for one and minus for the other. In the first case, 50 samples were obtained; in the second, 43 samples were the result. The trigger level was set at approximately the rms level of the record.

Figure 3 shows the result of the ensemble average of 40 samples, 20 each with positive and negative slope. The result is clearly a long way from convergence to the shape of the auto-correlation function. Figure 4 shows the result of 86 averages, 43 of positive and 43 of negative slope. The result is considerably improved over the previous one, which had only 40 averages, although still a crude approximation to the shape of the auto-correlation function. Without requiring additional data, the only way to improve this result would be to obtain many highly correlated samples, for example, by triggering a new sample every time the trigger level is crossed with either positive or negative slope. This is in fact advocated in the Randomdec literature. Such techniques would be difficult to implement in our present software, and were not attempted.

Comparisons of the computed modal damping ratios using the auto-correlation data in Fig. 2 and the Randomdec signature from Fig. 4 are of interest. Logarithmic decrement calculations over 20 cycles from each figure yield the following estimates for the modal damping ratio:

$\xi_1 = 0.010$	Auto-correlation
$\xi_1 = 0.016$	Randomdec
$\xi_1 = 0.014 \pm 0.0027$	MEM

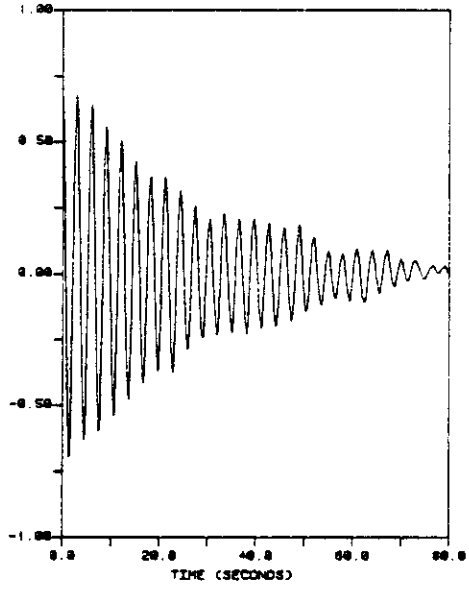

Fig. 4 Randomdec signature with 86 averages

The MEM estimate refers to a technique described in reference [11], which uses the maximum entropy method (MEM) of spectral analysis to obtain an estimate of the damping ratio. That method also provides an estimate of the 95 percent confidence bounds on the estimated damping as previously shown. Of the three techniques, the authors place the most confidence in the MEM results.

Conclusions

The relationship between the auto-correlation of a random process and the most popular form of the Randomdec signature has been established. For a Gaussian random process, the Randomdec signature reduces to the product of the correlation function and the trigger level. For this case, the variance of the estimated Randomdec signature is also found.

Because of the numerical simplicity of the Randomdec

method, it provides a potentially useful way of obtaining the correlation function. In doing so, the shape of the auto-correlation function is obtained at the sacrifice of the knowledge of the mean square value of the process. This is adequate for many purposes.

Acknowledgments

This research was sponsored by the Branch of Marine Oil and Gas Operations of the United States Geological Survey.

References

1 Cole, H. A., Jr., "Failure Detection of a Space Shuttle Wing Flutter Model by Random Decrement," NASA TMX-62, 041, May 1971.

2 Cole, H. A., Jr., "Method and Apparatus for Measuring the Damping Characteristics of a Structure," United States Patent No. 3, 620, 069, Nov. 16, 1971.

3 Cole, H. A., Jr., "On-Line Failure Detection and Damping Measurement of Aerospace Structures by Random Decrement Signatures," NASA CR-2205, Mar. 1973.

4 Cole, H. A., Jr., "On-the-line Analysis of Random Vibrations," AIAA Paper No. 68-288, AIAA/ASME Ninth Structures, Structural Dynamics and Materials Conference, Palm Springs, Calif., 1968.

5 Chang, C. S., "Study of Dynamic Characteristics of Aero-Elastic Systems Utilizing Randomdec Signatures," NASA CR-132563, 1975.

6 Ibrahim, S. R., "Random Decrement Technique for Modal Identification of Structures," *The AIAA Journal of Spacecraft and Rockets*, Vol. 14, No. 11, 1977.

7 Caldwell, D. W., "The Measurement of Damping and the Detection of Damage in Linear and Nonlinear Systems by the Random Decrement Technique," Ph.D. thesis, University of Maryland Dept. of Mechanical Engineering, 1978.

8 Ibrahim, S. R., and Mikulcik, E. C., "A Method for the Direct Identification of Vibration Parameters from Free Responses," *Shock and Vibration Bulletin*, Bulletin 47, 1977.

9 Caughey, T. K., and Stumpf, H. J., "Transient Response of a Dynamic System under Random Excitation," *Journal of Applied Mechanics*, Dec. 1961, pp. 563-566.

10 Crandall, S. H., and Mark, W. D., *Random Vibration in Mechanical Systems*, Academic Press, New York and London, 1963.

11 Campbell, R. B., and Vandiver, J. K., "The Determination of Modal Damping Ratios from Maximum Entropy Spectral Estimates," ASME Paper No. 80-WA/DSC-29, presented at the ASME Winter Annual Meeting, Chicago, Nov. 1980.

Printed in U.S.A.